**Departamento de Farmacia y Tecnología Farmacéutica y Parasitología**

**Programa de Doctorado en Biomedicina y Farmacia**

# "Impact of Undernourishment on the Pharmacokinetics of Erlotinib and Gefitinib in Rats."

Memoria que, para optar al
Grado de Doctor en Farmacia, presenta:

**Alejandro Pérez Pitarch**

Directores:

Matilde Merino Sanjuán, Virginia Merino Sanjuán, Amparo Nácher Alonso

Burjasot (Valencia), Marzo de 2017

# Departamento de Farmacia y Tecnología Farmacéutica y Parasitología

## Programa de Doctorado en Biomedicina y Farmacia

Las Dras. Matilde Merino Sanjuán, Virginia Merino Sanjuán y Amparo Nácher Alonso, Catedrática y Profesoras Titulares respectivamente, del Área de Farmacia y Tecnología Farmacéutica de la Universidad de Valencia,

Certifican que:

El trabajo de Tesis Doctoral realizado por Alejandro Pérez Pitarch y que lleva por título "Impact of Undernourishment on the Pharmacokinetics of Erlotinib and Gefitinib in Rats", ha sido realizado bajo la dirección compartida de las mismas y reúne todos los requisitos necesarios para su presentación, juicio y calificación.

Lo que suscriben, en Valencia, a 10 de Marzo de 2017.

Matilde Merino Sanjuán Virginia Merino Sanjuán Amparo Nácher Alonso

Este proyecto ha sido subvencionado por “L’ajuda per a Accions Especials d’Investigació – 2014” de la Universitat de València (nº Ref. UV-INV-AE14-269177).

Los resultados obtenidos en esta Tesis Doctoral han dado lugar a los siguientes trabajos publicados o enviados para su publicación:

- Pérez-Pitarch A, Nácher A, Merino V, Catalán-Latorre A, Jiménez-Torres NV, Merino-Sanjuán M. Impact of nutritional status on the pharmacokinetics of erlotinib in rats. Biopharmaceutics Drug Disposition. Sept 2015. Vol. 36, Issue 6, pages 373–384. Doi: 10.1002/bdd.1948
- Pérez-Pitarch A, Guglieri-López B, Nácher A, Merino V, Merino-Sanjuán M. Levofloxacin effect on erlotinib absorption. Evaluation of the interaction in undernutrition situations through population pharmacokinetic analysis in rats. Biopharmaceutics Drug Disposition. 2017 Jan 18. Epub ahead of print. Doi: 10.1002/bdd.2065
- Pérez-Pitarch A, Guglieri-López B, Nácher A, Merino V, Merino-Sanjuán M. Impact of Under-Nutrition on the Pharmacokinetics and Pharmacodynamics of Anti-Cancer Drugs: A Literature Review. Nutrition and Cancer. In press. Doi: 10.1080/01635581.2017.1299878.
- Pérez Pitarch A, Higueras L, Lozoya-Agulló I, Merino V, Nácher A, Merino-Sanjuán, M.Impact of undernourishment on the pharmacokinetics of gefitinib: from rats to humans. Enviado para su revision a la revista Biopharmaceutics Drug Disposition.
- Pérez-Pitarch A, Guglieri-López B, Catalán-Latorre A, Nácher A, Merino V, Merino-Sanjuán M. A simple, sensitive and rapid method for the determination of erlotinib (OSI-774) in rat plasma by high-performance liquid chromatography: application to pharmacokinetic studies. Enviado para su revisión a la revista Current Pharmaceutical Analysis.

**“Life is and will ever remain an equation incapable of solution, but it contains certain known factors”.**

Nikola Tesla

*Las personas con las que he compartido estos años han sido determinantes en el camino hasta la lectura de esta tesis*

Recuerdo mis primeras clases de farmacocinética. La pasión por la profesión que Víctor Jiménez transmitía en sus clases fue suficiente para que tras una de sus clases le dijese que me quería dedicar a la farmacocinética. Gracias a él empezó mi camino hacia la lectura de esta tesis.

En este trayecto he trabajado y conocido a mucha gente a la que tengo tanto que agradecer. En primer lugar me gustaría agradecer a mis directoras Matilde, Virginia y Amparo su dedicación a este proyecto. Ellas han sido los pilares básicos de esta tesis en todo momento y a ellas les debo mi inicio en la investigación. Recuerdo con mucho cariño aquella tarde en la que por primera vez obtuve los datos de una curva de concentraciones plasmáticas de erlotinib en plasma de rata. Bajé al laboratorio de prácticas donde estaba Mati, y con un par de operaciones me demostró como la teoría de las clases se plasmaba en lo que ocurría en el interior de aquella rata. Después de esa primera rata vinieron muchas más... y con ellas muchas operaciones quirúrgicas en las que también recibí muchísimo apoyo de Virginia y Amparo, siempre dispuestas a remangarse la bata para ayudarme a operar. Sé que habéis dedicado mucho tiempo durante todo el proceso, que habéis tenido mucha paciencia y habéis hecho un gran esfuerzo para finalizar con éxito esta tesis. De corazón, muchas gracias.

También quiero expresar lo agradecido que estoy a todos aquellos con los que he compartido horas de laboratorio. La primera tú, Ana, que me diste el relevo en el proyecto de la desnutrición y que compartiste todo lo que sabías conmigo sin ningún reparo. Porque tuviste mucha paciencia para ensañarme a usar el HPLC, a canular ratas y a hacer “dolus” sin esperar nada a cambio... porque eres así. Muchas gracias. También a mis compañeros/amigos de laboratorio Isa y Javi… hemos vivido en paralelo nuestras tesis. Contigo Isa he compartido laboratorio y también trabajo… tu ayuda con los “dolus” ha sido muy importante para acabar esta tesis. Y contigo Javi, ya son muchos años de amistad y trabajo.. y espero que sean muchos más.

Agradecer también a Carmina, José, Juana y Pilar por vuestra amistad y ayuda este tiempo que hemos compartido en el departamento. A Carmina y a José os debo una buena por todas esas “unidosis” de comida de rata con las que me ayudasteis. También a Inma y al personal del animalario que siempre se mostraron dispuestos a

ayudarme y a colaborar, y quienes en más de una ocasión me echaron una mano con las extracciones de sangre para las analíticas. Gracias a todos.

Y a mis compañeros y amigos de la Farmacia del Hospital Clínico. Me gustaría dar las gracias a todos los adjuntos, residentes y personal auxiliar, técnico y de enfermería con los que he compartido estos cuatro años. Me llevo un gran recuerdo de todos. Me llevo un recuerdo especial de mis buenos amigos de la segunda reunión de cada mañana Rafa, Francis, Pablo, Bea y Álvaro, y de mis R-mayores Pablo, María José y Manu. Me gustaría dar las gracias a mi tutor, Rafa, por todo el tiempo que me ha dedicado, y por transmitirme su entusiasmo (que admiro) por investigar y publicar. También agradecer a mi Jefe, Manu, todo lo que me ha enseñado y todas las oportunidades que me ha dado para formarme profesionalmente. Muchas gracias a todos.

Now in English for my international colleagues and friends.

There was an important change in my career during these last years. Probably the most important factor, or at least a crucial factor, was the Pharmacometrics Summer School at Uppsala. I would like to acknowledge Prof. Mats Karlsson and his team for organizing such a great course. This was not only a great opportunity to learn about pharmacometrics but also to meet other PhD students from all around the world. Thanks to Michael, Mohammed, Pieter, Gopi, Cheto, Elodie, Snehal, Nivea, Alex, Jia, Yupang, Shuangmin, Ally, Nacho, Abhisheak, Iris, Johannna, Andrezej, Jens… and all others for that really special weeks we shared at Uppsala. I'm sure we will meet again… pharmacometrics world is quite small.

I would also like to thank the Pharmacometrics team at Boehringer Ingelheim for the opportunity they gave me to learn from them. You taught me so many things and opened my eyes regarding which direction I wanted my proffessional career to take. I arrived there and found great work colleagues, and when returned to Spain I felt I left behind some very good friends who I hope to meet again soon.

Then came my stay at Amsterdam. I would like to thank sincerely Prof. Dr. Alwin Huitema, who gave me the opportunity to participate in really interesting projects. It was a great opportunity for me to face new challenges. And also, thank him for sharing his knowledge with me; I learned new things in every meeting we had. I would also like to thank all the people who I met at the NKI, and specially to my friends of Room 5: Julie, Rose, Aurelia, Huixin and Remy. Thanks to all of you; I felt really confortable working there and hope to see you soon.

Por último en español para los más cercanos a mi.

Esta tesis es el fruto de la educación y de la motivación que mis padres me han brindado. Siempre habéis sido mi modelo a seguir. Un modelo en el que las metas se alcanzan gracias al esfuerzo diario. Esta tesis os la dedico a vosotros que me lo habéis dado todo. Como no, también a ti Edu. Porque tu forma de ser me recuerda a diario que el espíritu de trabajo constante es lo que nos permite alcanzar cualquier meta. Que me has hecho tener presente a diario que no importa que día sea; fin de semana, Navidad o día de partido del Valencia… lo primero es lo primero. Y también a mis abuelos, porque al igual que mis padres, han sido un ejemplo de esfuerzo durante toda la vida. Qué mejor momento para recordar la frase “estudia xiquet” que tantas veces dijo el abuelo. A mi familia, que os lo debo todo, no solo esta tesis.

Y dedicártela a ti Bea, porque durante estos años hemos compartido tantas cosas inolvidables y porque te quiero. Juntos hemos formado un gran equipo, tanto dentro como fuera del trabajo. Soy muy afortunado por haberte tenido ahí apoyándome en cada paso. Ahora nuestras Tesis marcan el fin una preciosa etapa y el principio de nuestro matrimonio. Volviendo a la frase que abre esta sección de dedicatorias; seguro que la aventura en la que nos embarcamos ahora va a ser muy especial… porque que la voy a vivir contigo. Gracias cariño.

# Table of Contents

# List of abbreviations

| | |
|---|---|
| 5-FU | 5-fluorouracil |
| AED | Animal equivalent dose |
| ALAT | Alanine aminotransferase |
| ASAT | Aspartate aminotransferase |
| AUC | Area under the concentration-time curve |
| BCRP | Breast cancer resistance protein |
| BMI | Body mass index |
| BSV | Between subject variability |
| CI | Confidence interval |
| CL | Central compartment clearance |
| CV | Coefficient of variation |
| df | Degrees of freedom |
| DHFR | Dihydrofolate reductase |
| DN | Desnutridas |
| EGFR | Epidermal growth factor receptor |
| f | Bioavailability |
| fr | Correction fraction |
| HED | Human equivalent dose |
| HER | Human epidermal growth factor receptor |
| HPLC | High performance liquid chromatography |
| IOV | Inter-occasion variability |
| ISV | Inter-study variability |
| IV | Intravenous |

| | |
|---|---|
| ka | Absorption rate constant |
| Km | Michaelis Menten constant |
| LC-MS/MS | Liquid chromatography-tandem mass spectrometry |
| MOFV | Minimum objective function value |
| MRP | Multidrug resistance protein |
| MTX | Methotrexate |
| NN | Normonutridas |
| NSCLC | Non-small cell lung cancer |
| OATP | Organic anion-transporting polypeptide |
| PEM | Protein-energy malnutrition |
| PD | Pharmacodynamics |
| PK | Pharmacokinetics |
| PsN | Perl speaks NONMEM |
| Q | Inter-compartmental clearance |
| RSE | Relative estimation error |
| RT-qPCR | Reverse transcription quantitative real-time polymerase chain reaction |
| sd | Standard deviation |
| $t_{1/2}$ | Half-life |
| TK | Tyrosine kinase |
| TKI | Tyrosine kinase inhibitor |
| $T_{max}$ | Time since drug administration until maximum drug concentration is reached |
| UDP | Uridine 5'-diphospho-glucuronosyltransferase |

| | |
|---|---|
| UN | Under-nourished |
| Vc | Central compartment volume of distribution |
| Vd | Volume of distribution |
| Vp | Peripheral compartment volume of distribution |
| $V_t$ | Intestinal perfusion solution remaining volume at time t |
| Vmax | Maximum process velocity |
| WN | Well-nourished |

Resumen

# Resumen

Resumen

## 1. Introducción

La malnutrición se define como el desequilibrio entre el aporte de nutrientes y energía y los requerimientos del organismo necesarios para mantener el correcto crecimiento y funcionamiento. El estado de desnutrición (en el que los requerimientos nutricionales superan a los aportes de nutrientes) está altamente relacionado con ciertos estados patológicos, entre ellos el cáncer.

La etiología de la desnutrición en los pacientes con cáncer es multifactorial y compleja. Las alteraciones nutricionales en el paciente onco-hematológico pueden ocurrir como resultado de cambios metabólicos, bloqueo físico del tracto digestivo o problemas psicológicos. Además, algunos tratamientos empleados en pacientes con cáncer incrementan el riesgo de desnutrición como resultado de sus efectos adversos. El grado de desnutrición que desarrollan los pacientes con cáncer depende en gran medida del tipo de cáncer, el estadio de la enfermedad y el tratamiento seleccionado para su abordaje (3).

Los cambios fisiopatológicos resultantes de la desnutrición conllevan alteraciones funcionales en todos los sistemas del organismo. Entre otras muchas consecuencias de la desnutrición, existe evidencia científica del potencial impacto que puede tener sobre el comportamiento farmacocinético de los fármacos (23).

Teniendo en cuenta los aspectos indicados en los párrafos anteriores, que el estado nutricional tiene especial relevancia en el estado funcional de los pacientes con cáncer y que los fármacos antineoplásicos presentan, en la mayoría de casos, estrechos intervalos terapéuticos, es importante profundizar en los estudios que permitan conocer el impacto que tiene la desnutrición sobre la farmacocinética

de los fármacos empleados en el tratamiento del cáncer. En este sentido, los estudios clínicos encaminados a evaluar la influencia de este estado fisiopatológico sobre la farmacocinética de los medicamentos presentan dificultades éticas y técnicas de gran importancia. Por ello, el estudio de este problema a nivel pre-clínico puede ser una aproximación útil, soslayando las dificultades e inconvenientes que presentan los estudios clínicos. En esta línea se ha desarrollado el trabajo de la Tesis Doctoral que se presenta, en el que utilizando un modelo animal de desnutrición desarrollado por Merino-Sanjuán y colaboradores (80), que permite evaluar el efecto de la desnutrición sobre la farmacocinética de los medicamentos en un ambiente controlado, se ha evaluado la farmacocinética de dos fármacos antineoplásicos de administración por vía oral.

Hasta el momento, existe evidencia científica sobre la relación entre el estado nutricional y el comportamiento farmacocinético de fármacos antineoplásicos clásicos, en general administrados por vía intravenosa, pero la información disponible referente a las terapias más novedosas es escasa (23). Ante esta necesidad, este proyecto se ha centrado en evaluar el efecto de la desnutrición sobre la farmacocinética de dos fármacos inhibidores de tirosina-quinasa, ampliamente utilizados en la actualidad en la práctica clínica: erlotinib y gefitinib. Como ya se ha indicado, estos fármacos se administran por vía oral y, por tanto, la concentración de fármaco que se alcanza en la circulación sistémica está expuesta a fuentes de variabilidad adicionales a las que afectan a los fármacos antineoplásicos administrados por vía intravenosa. Este hecho, añadido a que la utilización de estos fármacos se prolonga durante largos periodos de tiempo, hace que el tema

desarrollado en esta Memoria sea de elevado interés sanitario, ya que las alteraciones en el estado nutricional de los pacientes podrían explicar parte de la variabilidad farmacocinética de los fármacos utilizados y su conocimiento podría contribuir a aumentar el estándar de seguridad en el manejo de estos medicamentos.

## Objetivos

Evaluar el impacto de la desnutrición sobre la farmacocinética de erlotinib y gefitinib en ratas.

Para alcanzar este objetivo general, se han definido los siguientes objetivos parciales:

- Evaluar el impacto de la desnutrición sobre marcadores analíticos y moleculares en ratas.
- Analizar el impacto de la desnutrición sobre la absorción intestinal de los fármacos seleccionados mediante estudios de perfusión intestinal *in situ*.
- Determinar el impacto de la desnutrición sobre la farmacocinética de erlotinib y gefitinib tras la administración *in vivo* de los fármacos por vía intravenosa y por vía oral.

## 2. Material y métodos

### 2.1 Población de estudio y fármacos estudiados

Los ensayos se han realizado en ratas Wistar macho de acuerdo con la directiva 2010/63/EU del 22 de septiembre de 2010 respecto a la protección de los animales de experimentación. Antes de iniciar el estudio, el Comité Ético de Experimentación Animal de la Universidad de Valencia aprobó los protocolos de experimentación (A1326906234491).

Los fármacos evaluados en los estudios *in situ* e *in vivo* fueron erlotinib y gefitinib. Todos los animales incluidos en el estudio se sometieron a un protocolo nutricional (80). Para ello, los animales se distribuyeron de forma aleatoria en dos grupos. Durante un periodo de adaptación de 23-26 días, un grupo se alimentó con una dieta estándar (20g / 60.2 kcal; 14% proteínas) (animales normonutridos (NN)) y el segundo grupo (animales desnutridos (DN)) fue alimentado con una dieta baja en proteínas y energía (10 g / 38 kcal; 5% proteínas).

### 2.2 Procedimientos de experimentación

Para la ejecución de los ensayos experimentales se utilizaron los procedimientos que se describen a continuación. En todos ellos, los animales se anestesiaron previamente utilizando pentobarbital sódico (30 mg/kg) por vía intraperitoneal, seguido de la administración subcutánea de butorfanol tartrato (0.5 mg/kg) como analgésico y antiinflamatorio.

### 2.2.1 Evaluación de las alteraciones bioquímicas y moleculares

Las alteraciones bioquímicas y moleculares asociadas a la desnutrición se evaluaron utilizando muestras sangre y de tejidos intestinal y hepático. Para ello, tras la anestesia de los animales (NN y DN), se extrajeron las muestras de tejido intestinal y hepático y se determinó el mRNA de moléculas determinantes en el proceso farmacocinético (transportadores y enzimas implicados en el transporte y metabolismo de fármacos). El mRNA se cuantificó mediante el método de la transcripción inversa a cDNA y la subsecuente cuantificación mediante qRT-PCR empleando el kit Revert Aid (Thermo Fisher Scientific, Waltham MA, Fermentas).

Asimismo, se extrajeron muestras de sangre, se determinaron los parámetros bioquímicos y se realizó el hemograma. Para ello, las muestras sanguíneas se separaron en dos alícuotas. A partir de una de ellas se realizó el recuento de elementos formes de la sangre, se determinó la concentración de hemoglobina y se determinó el hematocrito y el volumen corpuscular medio de los eritrocitos. Por otra parte, en la segunda alícuota se realizó el proteinograma y se determinaron las concentraciones de alanina aminotransferasa (ALAT), aspartato aminotransferasa (ASAT), proteínas totales y alfa glicoproteína ácida.

### 2.2.2 Estudio de la absorción intestinal de los fármacos.

Los ensayos de absorción intestinal se realizaron en los segmentos proximal y distal del intestino delgado utilizando el método de perfusión *in situ* propuesto por Doluisio y colaboradores (90). Las ratas fueron intervenidas quirúrgicamente para implantar cánulas

intestinales de modo que los tramos intestinales seleccionados quedasen aislados como compartimentos independientes. Así, a través de las cánulas implantadas, se llevó a cabo la perfusión intestinal de las soluciones de fármaco y la posterior toma de muestra del líquido perfundido. Se perfundieron 5 mL de la solución ensayada en cada tramo intestinal y, posteriormente, se tomaron muestras de 200 µL cada 5 minutos durante un tiempo total de 30 minutos.

En estos ensayos se administraron los fármacos investigados en forma de solución a distintas concentraciones, en presencia o ausencia de potenciales inhibidores de los sistemas de transporte intestinal. Las disoluciones ensayadas para cada fármaco estudiado se indican a continuación:

- Erlotinib: 8 y 20 µg/mL en presencia o ausencia de levofloxacino (600 µg/mL).
- Gefitinib: 40 µg/mL en presencia o ausencia de azida sódica (6500 µg/mL) y 8 µg/mL en ausencia de azida sódica.

### 2.2.3 Ensayos farmacocinético.

El análisis farmacocinético de erlotinib y gefitinib se realizó tras la administración de los fármacos *in vivo* por vía intravenosa y por vía oral una vez canulada la vena yugular de los animales. La intervención quirúrgica consistió en la inserción de 3.4 cm de cánula de silicona a través de la vena yugular en dirección al corazón y en la exteriorización del extremo opuesto de la cánula, que fue conducido subcutáneamente hasta la base dorsal del cuello donde se exteriorizó. La cánula implantada permitió la administración intravenosa de los fármacos seleccionados y la toma de muestras de sangre durante los ensayos. Por

otra parte, la administración oral de los fármacos se llevó a cabo empleando un sonda gástrica que se introdujo a través de la boca hasta alcanzar el estómago.

En estos ensayos, erlotinib y gefitinib fueron administrados en diferentes sistemas dispersos. Los animales NN o DN fueron de nuevo aleatorizados para recibir los fármacos por diferentes vías de administración (intravenosa u oral). A continuación, se detallan los sistemas empleados, las vías de administración y las dosis empleadas para cada fármaco:

- Erlotinib se administró en forma de solución tanto por vía intravenosa como por vía oral y en forma de suspensión por vía oral (dosis = 3,34 mg).
- Gefitinib se administró en forma de solución por vía intravenosa (dosis = 0,495 mg) y en forma de suspensión por vía oral (dosis = 6,5 mg).

## 2.3 Métodos analíticos

La cuantificación de los fármacos ensayados en las matrices biológicas se realizó mediante cromatografía líquida de alta resolución (HPLC) utilizando un detector UV/VIS. La longitud de onda seleccionada para cuantificar erlotinib en ambas matrices biológicas ensayadas, plasma y líquido intestinal, fue 345 nm. Para cuantificar gefitinib en las muestras de líquido intestinal, la longitud de onda fue de 330 nm. Por último, para cuantificar gefitinib en muestras de plasma se empleó un espectrómetro de masas equipado con un electrospray como fuente de ionización.

## 2.4 Análisis farmacocinético

El análisis farmacocinético de los datos experimentales obtenidos en los ensayos *in situ* e *in vivo* se realizó utilizando el procedimiento de modelado no lineal de efectos mixtos empleando el software NONMEM versión 7.3. Los modelos estudiados se ajustaron a los pares de valores de concentración plasmática-tiempo obtenidos en los ensayos *in vivo* y a los pares de valores de concentración de fármaco en lumen-tiempo obtenidos en los ensayos *in situ*.

En el análisis farmacocinético se desarrollaron modelos estructurales, estadísticos y de covariables. Con el objetivo de desarrollar modelos estructurales que describiesen el proceso de absorción de los fármacos en los ensayos de perfusión intestinal se consideraron modelos mecanicistas constituidos por dos compartimentos, en representación del lumen intestinal y del interior del enterocito. En estos modelos se consideraron cinéticas de primer orden y orden mixto para describir los procesos de absorción (desde el lumen al enterocito) y de secreción (desde el enterocito al lumen). En aquellas situaciones en las que los modelos mecanicistas no describieron de manera satisfactoria las observaciones, para describir el comportamiento de los pares de valores experimentales se utilizó el modelo de Weibull.

Los modelos estructurales considerados para describir los datos obtenidos en los ensayos farmacocinéticos *in vivo* se desarrollaron de manera secuencial. En primer lugar se probaron modelos mono- y bi-compartimentales para describir los datos obtenidos tras la administración de los fármacos por vía intravenosa, considerando eliminación lineal de los fármacos desde el compartimento central.

Posteriormente se incorporaron los datos obtenidos tras la administración del fármaco por vía oral y se desarrollaron los modelos de absorción sobre los modelos seleccionados en el paso anterior.

Los modelos estadísticos empleados consistieron en la incorporación de variabilidad interindividual para los parámetros farmacocinéticos y de variabilidad residual (discrepancia entre las predicciones y las observaciones). La variabilidad interindividual se modeló de acuerdo con el modelo exponencial. En cuanto a la variabilidad residual, se probaron los modelos de variabilidad aditiva, proporcional y exponencial.

Los modelos de covariables se desarrollaron con el objetivo de evaluar la influencia de covariables sobre los procesos de absorción y secreción intestinal (ensayos *in situ*) y sobre los procesos de LADME (ensayos *in vivo*). Para construir estos modelos se utilizó el método de modelado de covariables por pasos implementado en PsN (Perl Speaks NONMEM), estableciendo un nivel de significación de 0.05 y de 0.01 en la inclusión y exclusión de la covariable en el modelo. En los modelos de absorción intestinal se evaluaron como covariables el estado nutricional de los animales, la presencia o ausencia de potenciales inhibidores y la concentración de la solución perfundida. En los estudios *in vivo*, las covariables analizadas fueron el estado nutricional, el peso (como factor de escalado alométrico), los valores de albúmina sérica y el sistema disperso empleado para la administración del fármaco.

El modelo final se validó mediante comprobación visual de la capacidad predictiva (VPC) y mediante la técnica de re-muestreo y re-estimación (bootstrap).

## 2.5 Ejercicios de simulación

Por último, mediante ejercicios de simulación farmacocinética, el modelo mecanicista de absorción intestinal seleccionado, obtenido en los animales de experimentación, se utilizó para explorar el proceso de absorción intestinal, en la misma especie animal, a diferentes concentraciones de fármaco en el lumen intestinal y bajo distintas condiciones. Para ello, las simulaciones se realizaron teniendo en cuenta la matriz de varianza-covarianza obtenida en el modelo final. A partir de los resultados de las simulaciones, se calculó la constante de absorción efectiva dividiendo la velocidad neta de absorción por la concentración de fármaco en el lumen intestinal. La importancia de cada una de las covariables se analizó mediante la representación gráfica de la velocidad efectiva de absorción para distintos subgrupos frente a las concentraciones de fármaco en el lumen intestinal.

Por otra parte, los modelos seleccionados para los dos fármacos ensayados, a partir de los ensayos farmacocinéticos *in vivo*, se emplearon para extrapolar los resultados a una población simulada de pacientes normo (n = 1000) y desnutridos (n = 1000). Para ello, se tuvo en cuenta la dosis diaria habitual empleada en pacientes oncológicos (erlotinib = 150 mg; gefitinib = 250 mg). Este ejercicio se realizó a partir de los resultados obtenidos en los animales de experimentación utilizando el método de escalado alométrico. La distribución de pesos y de otras covariables requeridas para simular pacientes normo- y desnutridos se obtuvieron del estudio publicado por Piskorz y colaboradores (99). Las simulaciones tuvieron en cuenta las variabilidades interindividuales y residuales del modelo final. Todas las

simulaciones se ejecutaron utilizando el software estadístico R empleando los paquetes “MASS” y “deSolve”.

## 3. Resultados

Al finalizar el periodo de adaptación, las ratas se clasificaron en función de su estado nutricional, como normonutridas y desnutridas con grados leve, moderado y severo de desnutrición. La mayoría de las ratas en el grupo de desnutridas desarrollaron desnutrición leve o moderada y solo una desarrolló desnutrición severa.

En el ensayo para la evaluación del impacto de la desnutrición sobre marcadores moleculares y analíticos se incluyeron un total de 14 ratas (7 ratas NN y 7 ratas DN). Los resultados se muestran en la Figuras 3.4-3.5 y la Tabla 3.12 del texto, que se reproducen de nuevo a continuación para facilitar la lectura de este resumen.

Resumen

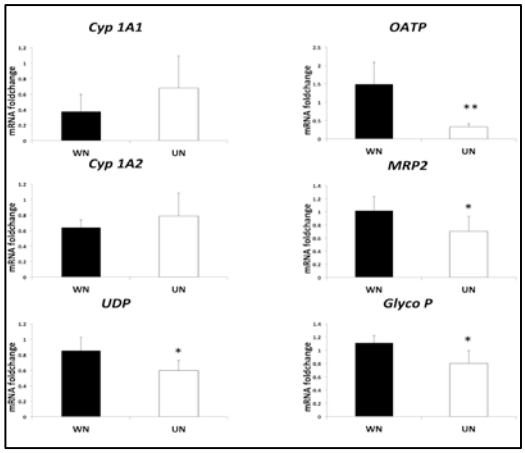


*Figura 3.4. Resultados de los análisis qRT-PCR para enzimas metabólicas y transportadores hepáticos en ratas normo- (WN) y desnutridas (UN). Significación estadística: * = p < 0.05; ** = p < 0.01.*

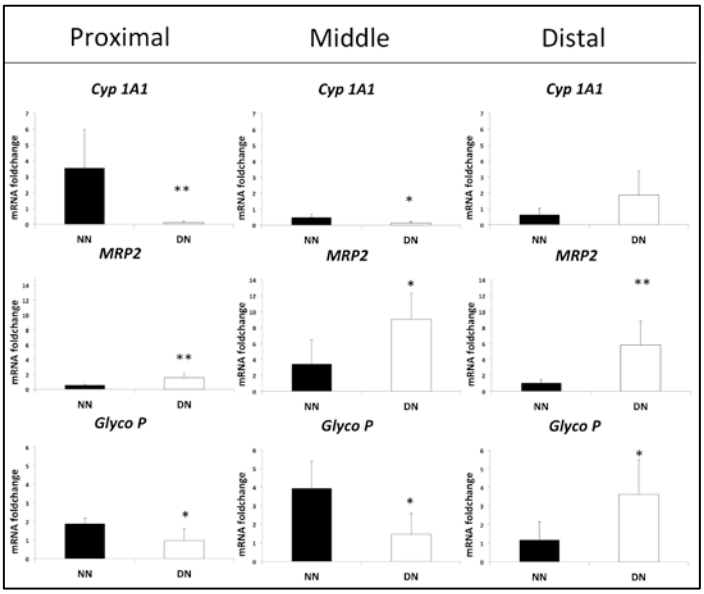


*Figura 3.5. Resultados de los análisis qRT-PCR para enzimas metabolicas y transportadores en los tramos proximal, medio y distal del intestino en ratas normo- (WN) y desnutridas (UN). Significación estadística: * = p < 0.05; ** = p < 0.01.*

*Tabla 3.12. Resultados de hemograma, parámetros bioquímicos, peso total, peso hepático y peso hepático relativo al peso total obtenidos en las ratas normo- y desnutridas al final del periodo de adaptación.*

| Parámetros | Ratas NN[(a)] (n = 7) | Ratas DN[(a)] (n = 7) | p valor |
|---|---|---|---|
| Hemograma | | | |
| Eritrocitos ($10^6$/μL) | 7.4 (1.8) | 4.7 (0.8) | 0.003 |
| Leucocitos ($10^3$/μL) | 3.09 (1.1) | 1.79 (0.6) | 0.012 |
| Plaquetas ($10^3$/μL) | 507.8 (445.1) | 69.3 (40.5) | 0.032 |
| Concentración de hemoglobina (g/dL) | 13.3 (2.7) | 8.6 (1.4) | <0.001 |
| Hematocrito (%) | 41.6 (7.8) | 29.1 (6.1) | 0.004 |
| Volumen corpuscular medio (fL) | 57.6 (6.0) | 60.6 (4.8) | 0.297 |
| Analítica bioquímica | | | |
| ALAT/GPT (U/L) | 42.0 (18.1) | 69.4 (11.8) | 0.006 |
| ASAT/GOT (U/L) | 143.0 (77.9) | 282.7 (77.9) | <0.001 |
| Concentración total de proteínas (g/L) | 61.1 (11.0) | 46.3 (3.9) | 0.006 |
| Concentración de alfa-glicoproteína ácida (mg/dL) | 14.6 (2.7) | 17.9 (2.1) | 0.025 |
| Bandas electroforéticas | | | |
| Albúmina (%) | 51.6 (7.09) | 43.9 (1.3 | 0.015 |
| Alpha-1 (%) | 8.1 (0.5) | 9.8 (0.8) | <0.001 |
| Alpha-2 (%) | 14.6 (1.2) | 16.2 (0.54) | <0.001 |
| Beta (%) | 21.6 (0.5) | 24.9 (1.4) | 0.15 |
| Gamma (%) | 4.0 (0.5) | 5.2 (0.5) | 0.001 |
| Peso total (g) | 290.2 (14.8) | 193.8 (13.6) | <0.001 |
| Peso hepático (g) | 10.2 (0.93) | 6.2 (0.4) | <0.001 |
| Peso hepático/Peso total | 0.036 (0.001) | 0.032 (0.001) | <0.001 |

[(a)] Media (desviación estándar). NN: normonutridas; DN: desnutridas; n: número de ratas; ALAT/GPT: alanina aminotransferasa; ASAT/GOT: aspartato aminotransferasa; fL: fentolitro.

## 3.1 Ensayo de absorción intestinal de erlotinib

En los ensayos de perfusión intestinal de erlotinib se incluyeron un total de 40 ratas (20 NN y 20 DN). El modelo que mejor describió los datos obtenidos en los dos tramos de intestino delgado consistió en

la combinación de un proceso de absorción pasiva y uno de secreción mediada por transportadores, utilizando un parámetro para corregir la fracción de dosis administrada que queda adsorbida en la pared intestinal y otros factores intestinales que pueden contribuir a la dilución inicial de la muestra perfundida (factor de corrección, *fr*). De esta forma se corrige la fracción de la dosis administrada que no queda disponible para su absorción debido a fenómenos de adsorción y/o de metabolismo rápido.

En ausencia de levofloxacino la constante de Michaelis-Menten (Km) que rige el proceso de transporte mediado de secreción se fijó a cero y no se estimó, mientras que en presencia de levofloxacino se estimó el valor de este parámetro.

El modelo de absorción intestinal de erlotinib seleccionado evidenció que en estados de desnutrición tiene lugar una disminución estadísticamente significativa de la capacidad máxima de secreción (representada en el modelo como velocidad máxima de secreción). Este comportamiento farmacocinético se observó en ambos tramos intestinales, donde la velocidad máxima de secreción disminuyó en ratas DN, en relación a los valores obtenidos en ratas NN, un 63% y un 72% en los tramos inicial y final, respectivamente. Los principales resultados se muestran en las Tablas 3.17 y 3.18, que de nuevo se reproducen a continuación para facilitar la lectura del texto.

*Tabla 3.17. Estimas de los parámetros y resultados del análisis bootstrap para el modelo de absorción de **erlotinib** en el intestino proximal.*

| Parámetro | Estima | EER (%) | Resultados del bootstrap | |
|---|---|---|---|---|
| | | | Mediana | IC 95% |
| Parámetros de efecto fijo | | | | |
| ka ($min^{-1}$) | 0.159 | 12 | 0.162 | 0.131-0.269 |
| $Vmax_s$ (μg/min) | 0.209 | 24 | 0.221 | 0.142-0.379 |
| $Km_s$ (μg/mL) | 0 (FIX) | - | - | - |
| *fr* | 0.861 | 6 | 0.873 | 0.790-0.990 |
| Desnutrición sobre $Vmax_s$ | -0.634 | 16 | -0.644 | (-0.792)-(-0.269) |
| $Km_s$ Levofloxacino (μg/mL) | 6.49 | 45 | 5.89 | 0.17-104.25 |
| Variabilidad interindividual | | | | |
| $\omega^2$ ka | 0.256 | 17 | 0.233 | 0.104-0.436 |
| $\omega^2$ $Vmax_s$ | 0.213 | 32 | 0.262 | 0.148-0.673 |
| Error residual | | | | |
| $\varepsilon_{exp}$ | 0.0197 | 12 | 0.0209 | 0.0123-0.0572 |

*EER: Error estándar relativo; IC: intervalo de confianza; ka: constante de velocidad de absorción (ka =9.54 $h^{-1}$); $Vmax_s$: velocidad máxima de secreción; $Km_s$: concentración de erlotinib a la que la secreción ocurre a la mitad de la velocidad de máxima en ausencia de levofloxacino; fr: parámetro de corrección; $Km_s$ Levofloxacino: concentración de erlotinib a la que la secreción ocurre a la mitad de la velocidad de máxima en presencia de levofloxacino; $\omega^2$: varianza interindividual; $\varepsilon_{exp}$: variabilidad residual exponencial.*

*Tabla 3.18. Estimas de los parámetros y resultados del análisis bootstrap para el modelo de absorción de **erlotinib** en el intestino distal.*

| Parámetro | Estima | EER (%) | Resultados del bootstrap | |
|---|---|---|---|---|
| | | | Mediana | IC 95% |
| Parámetros de efecto fijo | | | | |
| ka ($min^{-1}$) | 0.138 | 12 | 0.140 | 0.112-0.180 |
| $Vmax_s$ (μg/min) | 0.423 | 29 | 0.443 | 0.250-0.711 |
| $Km_s$ (μg/mL) | 0 (FIX) | - | - | - |
| *fr* | 0.978 | 1 | 0.971 | 0.929-0.997 |
| Desnutrición sobre $Vmax_s$ | -0.715 | 13 | -0.731 | (-0.835)-(-0.492) |
| $Km_s$ Levofloxacino (μg/mL) | 4.70 | 56 | 4.75 | 1.31-18.00 |
| Variabilidad interindividual | | | | |
| $\omega^2$ ka | 0.284 | 19 | 0.259 | 0.134-0.537 |
| $\omega^2$ $Vmax_s$ | 0.116 | 24 | 0.107 | 0.014-0.238 |
| Error residual | | | | |
| $\varepsilon_{exp}$ | 0.0146 | 20 | 0.0156 | 0.0069-0.0319 |

*EER: Error estándar relativo; IC: intervalo de confianza; ka: constante de velocidad de absorción (ka =8.28 $h^{-1}$); $Vmax_s$: velocidad máxima de secreción; $Km_s$: concentración de erlotinib a la que la secreción ocurre a la mitad de la velocidad de máxima en ausencia de levofloxacino; fr: parámetro de corrección; $Km_s$ Levofloxacino: concentración de erlotinib a la que la secreción ocurre a la mitad de la velocidad de máxima en presencia de levofloxacino; $\omega^2$: varianza interindividual; $\varepsilon_{exp}$: variabilidad residual exponencial.*

Resumen

Los gráficos para la comprobación de la capacidad predictiva (VPC) (Figura 3.10), que se reproducen a continuación, así como los resultados del análisis de re-muestreo y reestimación (bootstrap) (Tabla 3.18) muestran la validez del modelo seleccionado.

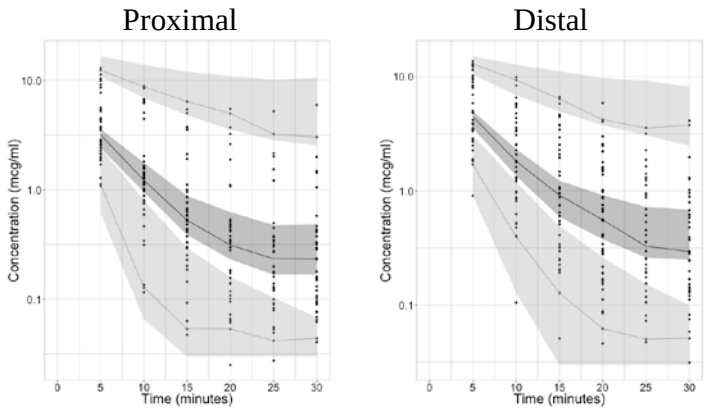


*Figura 3.10. Gráficos para la comprobación de la capacidad predictiva para los modelos de absorción intestinal de* ***erlotinib****. Izquierda: intestino proximal; Derecha: intestino distal; Puntos: concentraciones observadas; Líneas sólidas: percentiles 2,5, 50 y 97,5 de las observaciones; Áreas sombreadas: intervalos de confianza del 95% de los percentiles 2,5 y 97,5 (gris claro) y 50 (gris oscuro) de las concentraciones simuladas.*

Los resultados del ejercicio de simulación del proceso de absorción de erlotinib bajo distintas condiciones se muestran en la figura siguiente (Figura 3.11).

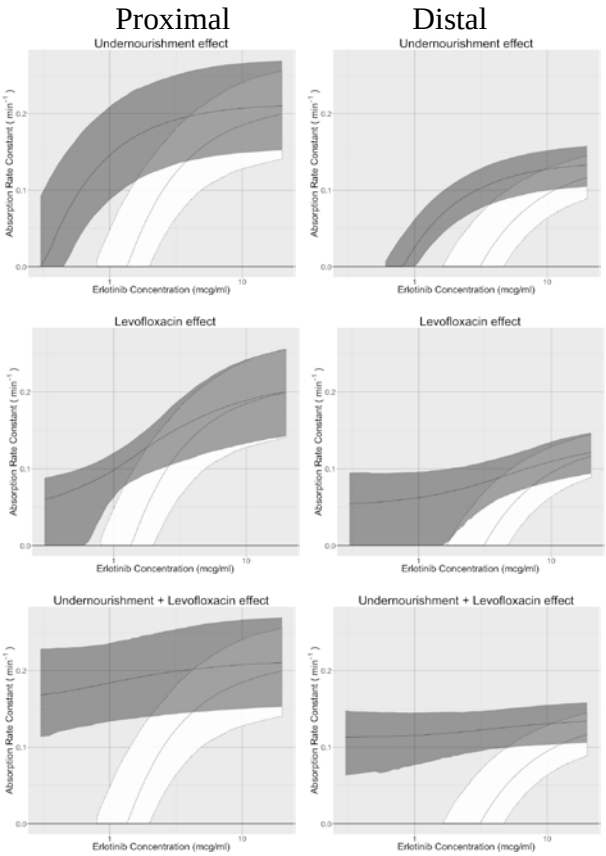


*Figura 3.11. Simulaciones para la evaluación del efecto de las covariables sobre el proceso de absorción de **erlotinib** en intestino proximal (izquierda) e intestino distal (derecha). Las gráficas representan la constante de velocidad de absorción efectiva frente a la concentración de erlotinib en el lumen intestinal. Blanco: normonutridas sin levofloxacino (todos los paneles); Gris oscuro: desnutridas sin levofloxacino (paneles superiores), normonutridas con levofloxacino (paneles medios), desnutridas con levofloxacino (paneles inferiores).*

## 3.2 Ensayo de absorción intestinal de gefitinib

En los ensayos de perfusión intestinal para gefitinib se incluyeron un total de 48 ratas (24 normonutridas y 24 desnutridas).

Los pares de valores concentración-tiempo obtenidos en los ensayos de perfusión intestinal *in situ* para gefitinib fueron evaluados

mediante modelos mecanicistas considerando procesos de absorción y secreción lineales y no-lineales. Los modelos desarrollados no fueron completamente satisfactorios y por ello los datos se evaluaron empleando el modelo de Weibull.

El modelo de Weibull seleccionado constaba de los siguientes parámetros: $\alpha$, parámetro de escalado; $\beta$, parámetro de forma; *fr*, parámetro de corrección. En este modelo se identificó la concentración inicial de fármaco perfundida como covariable predictora de *fr*. El valor del parámetro *fr* fue 1 en aquellas ratas que recibieron gefitinib a la concentración de 8 µg/mL, mientras que el valor de este parámetro fue inferior a la unidad cuando los animales recibieron el fármaco a la concentración de 40 µg/mL, siendo este menor en el tramo distal que en el proximal. Por otra parte, el estado nutricional de los animales y el empleo de azida sódica no demostraron alterar el perfil de absorción de gefitinib. Los resultados del modelo final se muestran en la tabla que se reproduce a continuación (Tabla 3.22).

*Tabla 3.22. Estimas del modelo final y resultados del bootstrap para el ensayo de perfusión intestinal in situ para* ***gefitinib****.*

| Parámetro | Estima | EER (%) | Resultados del bootstrap Mediana | IC 95% |
|---|---|---|---|---|
| Parámetros de efecto fijo | | | | |
| $\alpha$ ($h^{-1}$) | 2.40 | 5.6 | 3.27 | 2.34 – 4.52 |
| $\beta$ | 0.78 | 2.1 | 0.86 | 0.75 – 0.95 |
| $fr_{40}$ – proximal | 0.61 | 7.7 | 0.54 | 0.46 – 0.66 |
| $fr_{40}$ – distal | 0.51 | 8.7 | 0.48 | 0.38 – 0.59 |
| Variabilidad interindividual | | | | |
| $\omega^2 \beta_{proximal}$ | 0.0069 | 13.2 | 0.0057 | 0.0031 – 0.0090 |
| $\omega^2 \beta_{distal}$ | 0.0049 | 13.7 | 0.0040 | 0.0017 – 0.0071 |
| Error residual | | | | |
| $\varepsilon_{exp}$ | 0.051 | 15.1 | 0.047 | 0.032 – 0.072 |

*EER: error estándar relativo; IC: intervalo de confianza; α: factor de escalado; β: parámetro de forma; $fr_{40}$ – proximal: factor de corrección para la administración de la solución de 40 µg/mL en el tramo proximal.; $fr_{40}$ – distal: actor de corrección para la administración de la solución de 40 µg/mL en el tramo distal; $\omega^2$: varianza interindividual; $\varepsilon_{exp}$: variabilidad residual exponencial.*

Los gráficos de la comprobación de la capacidad predictiva (VPC) (Figura 3.16) y los resultados del análisis de re-muestreo y reestimación (bootstrap) (Tabla 3.22) muestran la validez del modelo seleccionado.

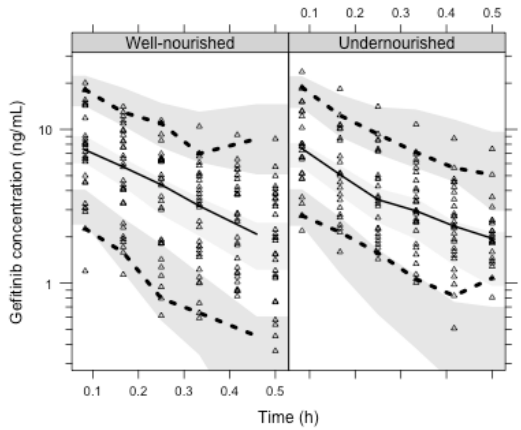


*Figura 3.16. Gráficos para la comprobación de la capacidad predictiva del modelo de absorción intestinal de **gefitinib** en animales normo- y desnutridos. Puntos: concentraciones observadas; Líneas sólidas: percentiles 2,5, 50 y 97,5 de las observaciones; Áreas sombreadas: intervalos de confianza del 95% de los percentiles 2,5 y 97,5 (gris claro) y 50 (gris oscuro) de las concentraciones simuladas.*

## 3.3 Ensayo farmacocinético de erlotinib

En los ensayos de administración intravenosa y oral utilizados para el estudio de la farmacocinética de erlotinib se incluyeron un total de 42 ratas (19 normonutridas y 23 desnutridas).

Se seleccionó un modelo bi-compartimental para describir la fase de disposición de erlotinib. En este modelo se identificó el estado nutricional como covariable predictora del aclaramiento del fármaco. Se observó un aclaramiento un 5% inferior en ratas desnutridas frente al observado en ratas normonutridas. En cuanto al proceso de absorción, se evidenció que la constante de velocidad de absorción

intestinal estaba influenciada por el estado nutricional y por las características de la formulación (solución o suspensión) administrada. Por otra parte, se estimó que la biodisponibilidad oral de la solución administrada era del 100%, mientras que al administrar erlotinib en suspensión la biodisponibilidad sólo fue incompleta en ratas normonutridas (f= 87,2%) . Los resultados del modelo final se muestran en la tabla siguiente (Tabla 3.26).

*Tabla 3.26. Estimas de los parámetros farmacocinéticos y resultados del Bootstrap del modelo final para el ensayo in vivo de* ***erlotinib****.*

| Parámetro farmacocinético | | Modelo final | | Resultados del bootstrap | |
|---|---|---|---|---|---|
| | | Estima | EER (%) | Mediana | IC 95% |
| Parámetros de efecto fijo | | | | | |
| CL (L/h) | | 9.9 | 8.1 | 9.8 | 8.62-11.5 |
| $FCL_{DN}$ | | -0.0511 | 12.6 | -0.0499 | -0.0681-(-0.0103) |
| Vc (L) | | 21.6 | 49.1 | 20.8 | 8.1-62.6 |
| Vp (L) | | 108.0 | 12.1 | 105.3 | 74.6-132.4 |
| Q (L/h) | | 36.4 | 17.9 | 33.4 | 20.5-47.3 |
| $k_a$ ($h^{-1}$) | $NN_{sol}$ | 0.417 | 18.1 | 0.408 | 0.238-0.555 |
| | $DN_{sol}$ | 0.200 | 24.5 | 0.187 | 0.082-0.310 |
| | $NN_{susp}$ and $DN_{susp}$ | 0.147 | 18.7 | 0.310 | 0.098-0.209 |
| f | $NN_{sol}$, and $DN_{sol}$ and $DN_{susp}$ | 1 (FIX) | - | - | - |
| | $NN_{susp}$ | 0.872 | 12.0 | 0.860 | 0.685-0.988 |
| Variabilidad interindividual | | | | | |
| $\omega^2$ CL (%) | | 38.6 | 12.5 | 37.4 | 28.6-49.0 |
| $\omega^2$ Vp (%) | | 110.0 | 29.8 | 106.0 | 1.1-191.0 |
| $\omega^2$ ka (%) | | 50.4 | 40.6 | 50.5 | 0.504-86.6 |
| Variabilidad residual | | | | | |
| $\varepsilon_{exp}$ (%) | | 38.1 | 15.8 | 37.4 | 31.4-43.8 |

*EER: Error estándar relativo; IC: Intervalo de; CL: Aclaramiento; $FCL_{DN}$: Factor que cuantifica en relación con los animales normonutridos el cambio del aclaramiento en ratas desnutridas expresado como fracción; Vc: Volumen de distribución del compartimento central; Vp: Volumen de distribución del compartimento periférico; Q: Aclaramiento intercompartimental; ka: Constante de velocidad de absorción; f: Biodisponibilidad; NN: normonutridas; DN: desnutridas; $\omega^2$: Variabilidad interindividual; $\varepsilon_{exp}$: Variabilidad residual exponencial.*

Los gráficos para la comprobación de la capacidad predictiva (VPC) (Figura 3.18) y los resultados del análisis de re-muestreo y reestimación (bootstrap) (Tabla 3.26) muestran la validez del modelo seleccionado.

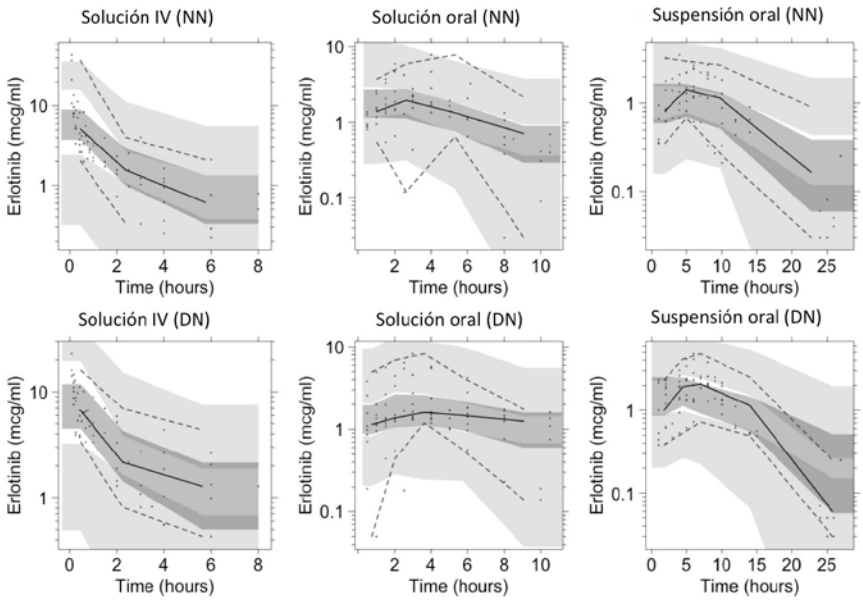


*Figura 3.18. Gráficos para la comprobación visual de la capacidad predictiva del modelo farmacocinético seleccionado para el* ***erlotinib****. Puntos: concentraciones observadas; líneas sólidas: percentil 50 de las observaciones; líneas discontinuas: percentiles 2.5 y 97.5 de las observaciones; Áreas sombreadas: intervalo de confianza del 95% para el percentil 50 (gris oscuro) y los percentiles 2.5 y 97.5 (gris claro) de los datos simulados. NN: normonutridas. DN: desnutridas.*

El ejercicio de simulación de una población de pacientes normo (n = 1000) y desnutridos (n = 1000) teniendo en cuenta que la pauta posológica de administración de erlotinib es de 150 mg cada 24 horas ha proporcionado los resultados que se reproducen en la Figura 3.19 y se describen numéricamente a continuación:

- La concentración mínima que se alcanza en estado estacionario para individuos normo- y desnutridos es de 299,7 (IC 95%: 36,5

– 1118,8) ng/mL y de 370,2 (IC 95%: 46,5 – 1330,2) ng/mL, respectivamente.

- El área bajo la curva de concentraciones plasmáticas frente al tiempo para individuos normo- y desnutridos alcanza un valor de 12919,3 (IC 95%: 4629,4 – 36986,1) ng/mL·h y de 15375,7 (IC 95%: 5513,9 – 44471,6) ng/mL·h, respectivamente.

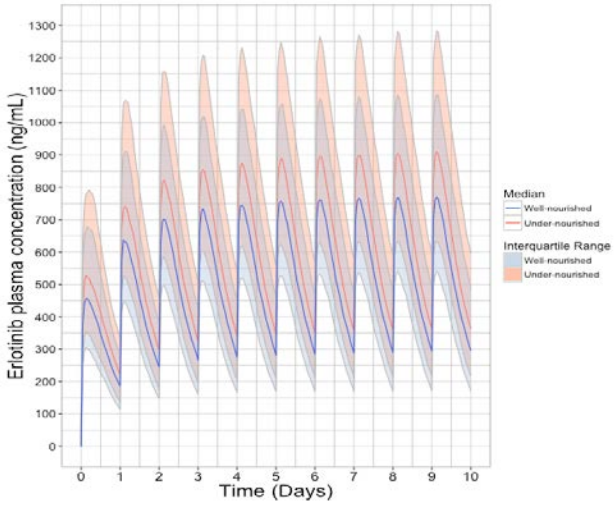


o

*Figura 3.19. Perfiles simulados de concentración plasmática-tiempo de **erlotinib** administrado por vía oral a la dosis de 150 mg cada 24 horas en pacientes normo-(azul) y desnutridos (salmón).*

## 3.4 Ensayo farmacocinético de gefitinib

En los ensayos de administración intravenosa y oral para el estudio de la farmacocinética de gefitinib se incluyeron un total de 21 ratas (11 NN y 10 DN).

Se seleccionó un modelo bi-compartimental para describir la disposición de gefitinib. En cuanto al modelo de absorción, se utilizó un compartimento de tránsito entre el compartimento de administración

y el compartimento central. En este modelo se evidenció que la biodisponibilidad oral de gefitinib tras su administración oral en forma de suspensión es mayor en ratas DN en comparación con la biodisponibilidad en ratas NN. Los principales resultados del modelo se muestran en la siguiente tabla (Tabla 3.31).

*Tabla 3.31. Estimas de los parámetros farmacocinéticos y resultados del Bootstrap del modelo final para el ensayo in vivo de **gefitinib**.*

| Parámetro | Estima | EER (%) | Resultados del Bootstrap | |
|---|---|---|---|---|
| | | | Mediana | IC 95% |
| Parámetros de efecto fijo | | | | |
| Vc (L) | 22.8 | 50.9 | 26.7 | 12.5 – 77.6 |
| Vp (L) | 366 | 28.7 | 397 | 258 - 601 |
| CL (L $h^{-1}$) | 14.1 | 21.0 | 14.0 | 9.08 – 19.7 |
| Q (L $h^{-1}$) | 19.5 | 38.3 | 21.6 | 12.1 - 40.8 |
| Desnutrición sobre Vc | 0.321 | 89.1 | 0.326 | -0.247 – 0.975 |
| ka ($h^{-1}$) | 0.198 | 30.5 | 0.207 | 0.115 – 0.410 |
| f normonutrición | 0.446 | 33.6 | 0.472 | 0.160 – 0.759 |
| f desnutrición | 0.681 | 23.2 | 0.683 | 0.373 – 0.961 |
| Variabilidad interindividual | | | | |
| $\omega^2$ CL | 0.168 | 59.1 | 0.160 | 0.0227 – 0.469 |
| $\omega^2$ ka | 0.442 | 59.0 | 0.443 | 0.0401 – 0.966 |
| Variabilidad residual | | | | |
| $\varepsilon_{exp}$ | 0.163 | 18.1 | 0.153 | 0.108 – 0.217 |

*EER: Error estándar relativo, IC: intervalo de confianza; ka: constante de velocidad de absorción; Vc: Volumen de distribución del compartimento central; Vp: volumen de distribución del compartimento periférico; CL: aclaramiento; Q: aclaramiento inter-compartimental; Desnutrición sobren Vc: efecto de la desnutrición sobre el volumen de distribución del compartimento central; f: biodisponibilidad; $\omega^2$: variabilidad interindividual; $\varepsilon_{exp}$: variabilidad residual exponencial.*

Los gráficos para la comprobación de la capacidad predictiva (VPC) (Figuras 3.22-3.23) y los resultados del análisis de re-muestreo y reestimación (bootstrap) (Tabla 3.31) justifican la selección del modelo.

Resumen

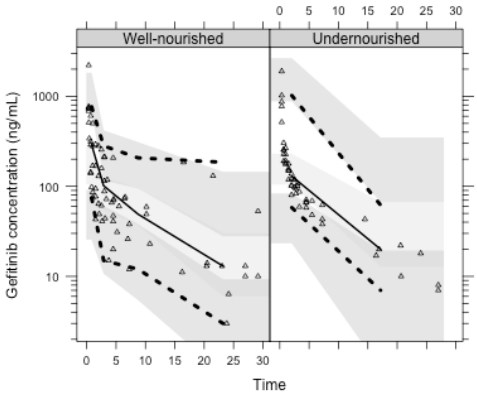


*Figura 3.22. Comprobación visual de la capacidad predictiva para el modelo de **gefitinib** tras la administración intravenosa. Triángulos: concentraciones observadas; Líneas sólidas: percentil 50 de las observaciones; Líneas discontinuas: percentiles 2.5 y 97.5 de las observaciones; Áreas sombreadas: intervalo de confianza del percentil 50 (gris claro) y de los percentiles 2.5 y 97.5 (gris oscuro) de los valores simulados.*

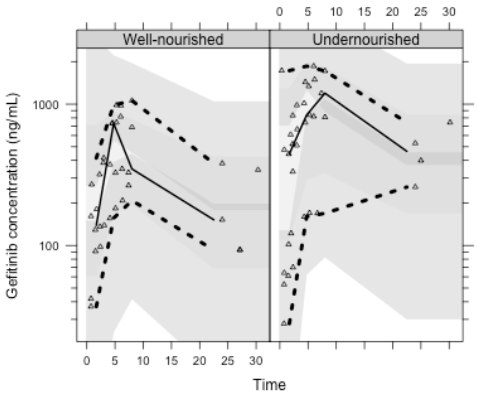


*Figura 3.23. Comprobación visual de la capacidad predictiva para el modelo de **gefitinib** tras la administración oral. Triángulos: concentraciones observadas; Líneas sólidas: percentil 50 de las observaciones; Líneas discontinuas: percentiles 2.5 y 97.5 de las observaciones; Áreas sombreadas: intervalo de confianza del percentil 50 (gris claro) y de los percentiles 2.5 y 97.5 (gris oscuro) de los valores simulados.*

Los resultados del ejercicio de simulación realizado para una población de pacientes normo- (n = 1000) y desnutridos (n = 1000) teniendo en cuenta que la pauta de administración de gefitinib es de

250 mg cada 24 horas se muestran en la Figura 3.24 y se describen a continuación:

- La concentración mínima en estado estacionario para individuos normo- y desnutridos es de 215,8 (IC 95%: 54,8 – 811,8) ng/mL y 333,7 (IC 95%: 81,4 – 1268,7) ng/mL, respectivamente.
- El área bajo la curva de concentraciones plasmáticas frente al tiempo para individuos normo- y desnutridos es de 7509,8 (IC 95%: 2436,3 – 24155,5) ng/mL·h y 11357,5 (IC 95%: 3825,2 – 37336,4) ng/mL·h, respectivamente.

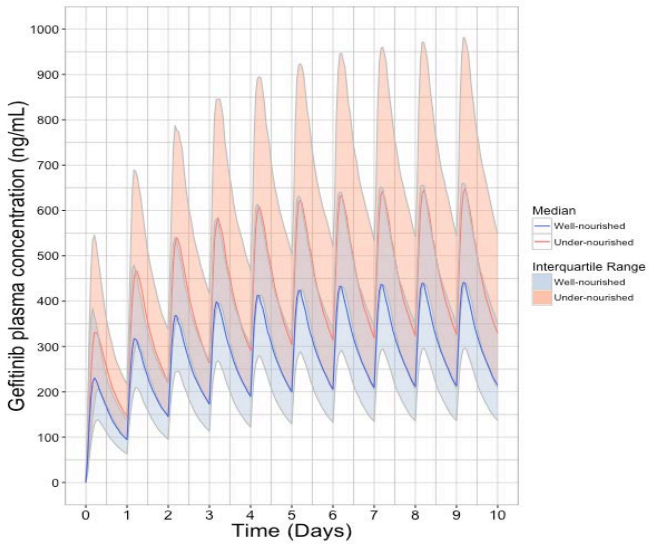


*Figura 3.24. Perfiles simulados de concentración plasmática-tiempo de **gefitinib** administrado por vía oral a la dosis de 250 mg cada 24 horas en pacientes normo-(azul) y desnutridos (salmón).*

# 4. Discusión

## 4.1 Población de estudio

La especie animal seleccionada para llevar a cabo esta investigación fue la rata Wistar. Esta especie animal tiene importantes similitudes fisiológicas y anatómicas con la especie humana que favorecen su uso en estudios de investigación pre-clínica (102).

El estado nutricional se evaluó en un total de 165 ratas Wistar. Todas las ratas del grupo de normonutridas manifestaron un estado de normonutrición al final del periodo de adaptación. En el grupo de desnutridas, solo una rata desarrolló desnutrición severa y el grado de desnutrición del resto de los animales fue leve (79.8%) y moderado (19.0%).

## 4.2 Evaluación del impacto de la desnutrición sobre marcadores moleculares y analíticos

En esta Tesis, para evaluar el impacto de la desnutrición sobre los marcadores moleculares y analíticos, se ha realizado la determinación del mRNA de enzimas involucradas en los procesos de metabolismo y secreción de fármacos a nivel intestinal y hepático. Sin embargo, los estudios especializados en este tema indican que al evaluar los resultados de expresión génica es importante tener en cuenta la existencia de mecanismos compensatorios, que pueden aumentar la síntesis de mRNA en aquellas situaciones en las que la disponibilidad de aminoácidos está disminuida (por ejemplo, la desnutrición). Por tanto, la disminución de la expresión de mRNA en estados de desnutrición se puede interpretar como una disminución de la síntesis

de proteínas, pero el aumento de mRNA no necesariamente implica un aumento de la síntesis de proteínas puesto que puede ser el resultado del desarrollo de algún mecanismo compensatorio como respuesta fisiológica al estado carencial.

Los resultados obtenidos en los marcadores moleculares a nivel hepático indican que los niveles de mRNA de las enzimas OATP, MRP2, P-gp y UDP son significativamente más bajos en ratas desnutridas que en ratas normonutridas y ponen de manifiesto el potencial riesgo de alteraciones farmacocinéticas en estados de desnutrición cuando estas enzimas intervienen en los procesos de secreción o de biotransformación metabólica de los fármacos. Por otra parte, en las muestras de tejido hepático, los niveles de mRNA de las enzimas metabólicas CYP1A1 y CYP1A2 en ratas desnutridas tienden a ser ligeramente superiores a los obtenidos en ratas normonutridas aunque las diferencias no alcanzaron significación estadística.

El análisis de marcadores moleculares también se llevó a cabo en muestras de tejido intestinal procedente de los tramos proximal, medio y distal. En los resultados obtenidos se observó que en el estado de desnutrición los niveles de mRNA de glicoproteína-P a lo largo del intestino se ven alterados de manera irregular, mientras que los niveles de la enzima MRP2 se incrementan en todos los tramos intestinales evaluados. El balance final de la expresión de ambas enzimas secretoras podría justificar los cambios que se objetivan en la biodisponibilidad de los fármacos administrados por vía oral. En cuanto al efecto de la desnutrición sobre la expresión del marcador metabólico intestinal CYP1A1 en estados de desnutrición, indicar que ha mostrado un patrón irregular (en los tramos proximal y medio se objetiva una

reducción estadísticamente significativa, mientras que en el tramo distal aumentó, sin alcanzar su incremento significación estadística). Estos resultados indican que la absorción de los fármacos en estados de desnutrición se modificará, en mayor o menor medida, dependiendo de los sistemas enzimáticos implicados en el proceso.

Los hemogramas realizados indican que el valor de los parámetros evaluados es inferior en ratas desnutridas. Las restricciones dietéticas pueden causar alteraciones severas a nivel de la medula ósea hematopoyética, tales como hipocelularidad y necrosis (105). Los resultados obtenidos evidencian que estas alteraciones pueden tener un impacto potencial sobre la distribución de fármacos (sobre todo para aquellos fármacos que se unen en elevada proporción a elementos formes de la sangre). Además, contribuyen a explicar, al menos en parte, el incremento del riesgo de efectos adversos hematológicos desencadenados por fármacos antineoplásicos en pacientes con cáncer que sufren desnutrición (55).

Así mismo, los resultados de los parámetros bioquímicos evidenciaron una disminución de albúmina sérica. Por el contrario, se observó un aumento de alfa-glicoproteína ácida y de los niveles de ALAT y ASAT en animales desnutridos. Este aumento, junto con la reducción de la concentración de albúmina plasmática y del peso del hígado en los animales desnutridos, son indicios de que la desnutrición ocasiona en los animales un daño hepático considerable. Tanto las alteraciones en médula ósea como las producidas en el hígado han sido descritas previamente en humanos (99, 106); por tanto, los resultados obtenidos en este estudio, además de aportar información sobre el deterioro funcional ocasionado por el estado nutricional, confirman la

idoneidad del modelo animal empleado para evaluar, en estudios preclínicos, la farmacocinética de medicamentos bajo la influencia del estado nutricional .

Por todo lo expuesto, se puede afirmar que la respuesta del organismo destinada a compensar el aporte inadecuado de energía y proteínas es complejo. Por ello, las alteraciones farmacocinéticas en estados de desnutrición son difíciles de predecir, muy variables y dependientes del fármaco administrado.

### 4.3 Ensayos de absorción intestinal *in situ*

La idoneidad de los ensayos de perfusión intestinal en ratas reside en la elevada correlación entre los resultados obtenidos en esta especie y los obtenidos en humanos para muchos fármacos (110). Además, se trata de un método que permite el estudio de los mecanismos implicados en el proceso de absorción de los fármacos así como la valoración de las interacciones entre fármacos o entre fármacos y nutrientes.

El uso simultáneo de levofloxacino y fármacos inhibidores de tirosina-quinasa es habitual en la práctica clínica, ya que el levofloxacino es un antibiótico de uso frecuente en múltiples infecciones respiratorias y urinarias. Esta combinación de fármacos puede tener relevancia clínica, hasta el momento no considerada, ya que estudios recientes han descrito una interacción a nivel de la glicoproteína-P intestinal entre levofloxacino y otros fármacos inhibidores de tirosina quinasa, tales como imatinib, dasatinib y sunitinib (113). Por esta razón, en este proyecto se ha evaluado el

efecto inhibidor de levofloxacino sobre la secreción intestinal de erlotinib.

Sin embargo, hasta el momento no se ha descrito que gefitinib sea sustrato de proteínas de resistencia a fármacos. Por ello, para evaluar la pérdida de linealidad en el proceso de absorción intestinal de gefitinib se ha perfundido el fármaco a dos concentraciones en solución libre, y se ha evaluado el efecto de la presencia de la azida sódica en la solución de mayor concentración. La azida sódica es un inhibidor metabólico inespecífico capaz de inhibir todos los procesos que requieren la participación de energía por interrumpir la producción de energía mediada por ATP (117).

### 4.3.1 Absorción intestinal de erlotinib

El modelo seleccionado para explicar el proceso de absorción intestinal de erlotinib incorpora un proceso de absorción pasiva y un proceso de secreción mediada por transportadores regido por la ecuación de Michaelis-Menten.

Dada la baja solubilidad de erlotinib y la limitación analítica para cuantificar con fiabilidad concentraciones muy bajas del fármaco, el ámbito de concentraciones de fármaco estudiadas fue limitado. Esta podría ser la razón por la que no fue posible estimar el valor de la constante de Michaelis-Menten (Km) que caracteriza el proceso de secreción intestinal de erlotinib en ausencia de levofloxacino. Finalmente, para permitir una mayor estabilidad del modelo, el valor de Km se fijó a cero. Sin embargo, el valor de este parámetro se pudo estimar cuando se evaluaron en conjunto los datos experimentales

obtenidos tras la perfusión del fármaco en solución libre y los obtenidos tras la perfusión del fármaco en presencia de levofloxacino.

El modelo seleccionado apunta a la participación de algún proceso de secreción activa en la absorción de erlotinib, que de acuerdo con la bibliografía consultada está mediado por la glicoproteína-P (116). En el estudio realizado en esta Tesis, el valor de la velocidad máxima del proceso de secreción fue mayor en el tramo distal que en el tramo proximal. Estos resultados concuerdan con el modelo ADAM (advanced dissolution, absorption and metabolism) que considera que la expresión de glicoproteína-P aumenta desde el yeyuno hasta el íleon (121) y corroboran la robustez del modelo desarrollado. Sin embargo los resultados obtenidos en los qRT-PCR muestran para mRNA de glicoproteína-P una tendencia ascendente para los tramos proximal y medio, pero no para el tramo distal en ratas NN. Este resultado podría atribuirse, al menos en parte, al tamaño de la muestra utilizando para estos estudios (n = 7) y a la gran variabilidad en las cuantificaciones de mRNA.

Asimismo, los modelos desarrollados muestran que el valor estimado de ka en el tramo proximal es ligeramente superior al estimado en el tramo distal. Este resultado, junto a la menor capacidad de secreción de erlotinib en el tramo proximal en comparación con el tramo distal, indican que el tramo proximal del intestino presenta condiciones más favorables para la absorción de erlotinib.

Por otra parte, el modelo desarrollado ha demostrado que, en relación con los valores obtenidos en animales normonutridos, la capacidad de secreción intestinal de erlotinib en estado de desnutrición es un 63% y 72% menor en los tramos proximal y distal,

respectivamente. Estos resultados concuerdan con la menor expresión de glicoproteína-P intestinal determinada en animales desnutridos.

Por otra parte, los modelos desarrollados para evaluar la influencia de levofloxacino sobre el proceso de absorción intestinal de erlotinib, indican que el antibiótico ejerce una inhibición sobre el proceso de secreción de erlotinib, tal y como ya se ha demostrado para otros fármacos inhibidores de la tirosina-quinasa (113). La implicación clínica de esta interacción puede resultar tanto en una mayor velocidad de absorción como en una mayor biodisponibilidad en magnitud, lo que en principio podría dar lugar a una mayor exposición al antineoplásico cuando ambos fármacos se administraran simultáneamente, siendo esta interacción de mayor magnitud en pacientes desnutridos.

El ejercicio de simulación realizado (Figura 3.11) indica que en ratas normonutridas y en ausencia de levofloxacino, la absorción efectiva de erlotinib en el tramo inicial del intestino delgado ocurre cuando la concentración de fármaco en lumen es superior a 1 μg/mL mientras que en el tramo distal del intestino delgado se requiere un incremento aproximado de 5 veces de la concentración de fármaco en lumen para que la absorción del fármaco sea efectiva. Este hecho puede explicarse teniendo en cuenta que en estas condiciones el proceso de secreción activa se satura y prevalece la difusión pasiva del antineoplásico desde el lumen intestinal hacia el torrente circulatorio. Por el contrario, en ratas desnutridas, puesto que está reducida la capacidad de los sistemas enzimáticos implicados en la secreción intestinal del fármaco, la absorción efectiva de erlotinib en presencia de levofloxacino ocurre cuando el antineoplásico se encuentra en lumen intestinal a concentraciones inferiores. Estos resultados indican que el

tramo inicial del intestino delgado puede ser el lugar preferente de absorción del erlotinib y podría explicar, en parte, la biodisponibilidad incompleta de este fármaco cuando se administra por vía oral en forma de comprimidos (84).

### 4.3.2 Absorción intestinal de gefitinib

Para explicar el proceso de absorción intestinal de gefitinib se seleccionó el modelo de Weibull debido a que los modelos mecanicistas fueron incapaces de describir de manera completamente satisfactoria los perfiles observados tras la administración de las soluciones de estudio. La selección de este modelo permitió estimar parámetros que describían de manera satisfactoria las concentraciones observadas, permitiendo así evaluar el efecto de la desnutrición, de la adición de azida sódica, de la concentración de la solución perfundida y del tramo intestinal estudiado sobre los parámetros del modelo.

El modelo de Weibull converge en un cinética de orden 1 cuando $\beta=1$. Sin embargo, el valor estimado para este parámetro fue inferior a la unidad ($\beta=0.78$). Esto indica que la cinética de desaparición de gefitinib del lumen intestinal se desvía ligeramente de la cinética lineal, observándose una pequeña reducción de la constante de velocidad de absorción efectiva con el tiempo. Esta ligera desviación respecto a un modelo lineal puede deberse, entre otras causas, a procesos de adsorción y desorción del fármaco sobre la mucosa intestinal.

Los resultados obtenidos indican que el proceso de absorción del gefitinib no se ve influenciado por la desnutrición ni por la presencia de azida sódica. El hecho de que la presencia de azida sódica no tenga ninguna influencia sobre los perfiles de absorción del fármaco indica

que el proceso de absorción de gefitinib está, probablemente, gobernado por un mecanismo de difusión. No obstante, la falta de convergencia en el modelo de absorción definido por una cinética de orden uno hace sospechar de la posible existencia de procesos de adsorción y desorción. Por otra parte, los resultados obtenidos en este estudio indican que el proceso de absorción de gefitinib no se modifica de forma significativa en estados de desnutrición, lo que pone de manifiesto que las alteraciones fisiológicas que causa la desnutrición (alteración en los sistemas de transporte y/o daño morfológico de la membrana absorbente) no tienen un impacto significativo sobre el proceso de absorción de este fármaco.

El modelo desarrollado también objetivó un valor del parámetro de corrección *fr* inferior en aquellas ratas que recibieron gefitinib 40 μg/mL en comparación con aquellas que recibieron gefitinib 8 μg/mL. Así mismo, el valor de *fr* al administrar gefitinib 40 μg/mL fue menor en el tramo distal que en el tramo proximal. Estos resultados pudieron deberse, entre otros motivos, a procesos de adsorción del fármaco a la mucosa intestinal dependiente de la concentración de gefitinib y del pH del tramo intestinal estudiado.

## 4.4 Ensayos farmacocinéticos

### 4.4.1 Erlotinib

El modelo seleccionado para describir los datos obtenidos tras la administración de erlotinib por vía intravenosa y oral fue un modelo bi-compartimental. El modelo seleccionado permitió identificar las covariables predictoras del comportamiento farmacocinético y demostró que el aclaramiento de erlotinib se reduce un 5 % en estados

de desnutrición. Esta disminución puede ser resultado de variaciones en el metabolismo ya que estudios previos realizados en roedores han demostrado que la desnutrición está asociada a una inhibición del citocromo P450 (104).

Por otra parte, el modelo seleccionado indica que el proceso de absorción oral es dependiente del estado nutricional y del tipo de sistema disperso empleado para la administración del fármaco por vía oral (la velocidad de absorción del erlotinib administrado en forma de suspensión es más lenta que cuando se administra en solución). Este comportamiento confirma que debido a la baja solubilidad del fármaco el proceso de liberación del mismo desde el sistema que lo contiene (en el que se incluye la disolución del fármaco en los fluidos intestinales) constituye un factor limitativo en el proceso de absorción.

Por otra parte, la constante de velocidad de absorción del erlotinib tras la administración del fármaco por vía oral en solución a ratas desnutridas fue un 52% menor que en ratas normonutridas. Este resultado podría atribuirse a los cambios en la solubilidad de erlotinib en ratas desnutridas, ya que los estados de desnutrición se asocian a una reducción en la secreción de ácido gástrico (123,124) y este hecho puede alterar el grado de ionización del erlotinib y, como consecuencia, su solubilidad en el lumen intestinal.

Es interesante resaltar que en el ensayo de absorción intestinal *in situ* del erlotinib no se evidenció esta disminución de la velocidad de absorción en ratas desnutridas frente a ratas normonutridas. Este hallazgo posiblemente se deba a que en el ensayo *in situ* el fármaco se deposita directamente en el tramo intestinal objeto de ensayo y por no

pasar previamente por el estómago no está expuesto a los cambios de secreción de ácido.

Por otra parte, el modelo mostró que tras la administración del fármaco en forma de suspensión la constante de velocidad de absorción en ratas normo- y desnutridas es la misma. Este resultado indica de nuevo que en las condiciones ensayadas, el único factor que condiciona el proceso de absorción del fármaco administrado por vía oral en forma de suspensión es la liberación del mismo desde la formulación que lo contiene.

El modelo seleccionado también pone de manifiesto la influencia tanto del tipo de sistema disperso empleado para la administración del fármaco como del estado nutricional de las ratas sobre la biodisponibilidad de erlotinib. En efecto, tras la administración del fármaco en forma de solución, la biodisponibilidad fue completa, del mismo modo que lo fue cuando el fármaco se administró en suspensión en ratas desnutridas. En cambio, tras la administración de la suspensión de fármaco a las ratas normonutridas la biodisponibilidad del fármaco fue próxima al 87% (Tabla 3.26). La biodisponibilidad completa tras la administración de la solución puede explicarse por la saturación de los sistemas enzimáticos de secreción debido a la elevada concentración de fármaco que contiene (preparada con ayuda de co-solventes). Por el contrario, la administración de erlotinib en suspensión (sin co-solventes) expone al epitelio intestinal a concentraciones de fármaco más bajas que podrían ser insuficientes para saturar los sistemas enzimáticos de secreción, contribuyendo a reducir la biodisponibilidad en ratas normonutridas. De forma global, la menor capacidad de secreción del epitelio intestinal de las ratas desnutridas que recibieron

erlotinib en suspensión, así como el daño de la mucosa intestinal asociado a la desnutrición, pueden ser los factores que favorecen el incremento de la biodisponibilidad observada en animales desnutridos que reciben erlotinib en suspensión.

Las alteraciones que origina la desnutrición en la membrana absorbente conllevan cambios en la longitud del intestino, en el espesor de las capas muscular, submucosa y mucosa del intestino, así como disminución, aplanamiento y acortamiento de las vellosidades del borde de cepillo, hipoplasia de criptas y menor densidad de proyecciones digitiformes (129). Asimismo, el estado de desnutrición se asocia a cambios en la motilidad intestinal, que podría estar reducida en animales desnutridos como resultado de las alteraciones en las secreciones gástricas (130) permitiendo, de este modo, un aumento del tiempo de residencia del fármaco en el intestino delgado y facilitando así que se absorbiera una mayor fracción de la dosis administrada.

### 4.4.2 Gefitinib

El modelo seleccionado para describir los datos obtenidos tras las administración por vía intravenosa y oral de gefitinib fue un modelo bi-compartimental utilizando un compartimento de tránsito entre el compartimento de absorción y el compartimento central. Este modelo permitió la evaluación de covariables predictoras del comportamiento farmacocinético de gefitinib.

En este estudio se ha evidenciado que la desnutrición incrementa el volumen de distribución del compartimento central en un 30%. El gefitinib se une en más del 90% a proteínas plasmáticas (principalmente a albumina y a alfa-1-glicoproteína ácida, sin

conocerse en qué proporción a cada una de ellas) por lo que el mecanismo subyacente de este comportamiento podría relacionarse con la disminución de la concentración total de proteínas en plasma que se produce en estado de desnutrición.

Como se ha indicado, para caracterizar la absorción intestinal de gefitinib se utilizó un compartimento de tránsito que permite modelar la existencia de un periodo de latencia previo a la absorción del fármaco. Este periodo de latencia en la absorción del fármaco puede atribuirse a la combinación de distintos procesos, entre ellos la disgregación del fármaco, su liberación y disolución, su tránsito a través del intestino y su difusión a través del contenido del lumen intestinal hasta alcanzar la membrana apical de las células columnares absorbentes.

El modelo seleccionado para describir la farmacocinética de gefitinib ha permitido determinar que en ratas desnutridas la biodisponibilidad del fármaco es, en términos relativos, aproximadamente un 50% superior a la observada en ratas normonutridas. Este resultado podría deberse, entre otras causas, a la disminución del peristaltismo intestinal y a la menor expresión del sistema CYP1A1 en los tramos inicial y medio del intestino delgado observadas en estados de desnutrición calórico-proteica. Estos cambios se manifiestan sobre la biodisponibilidad en magnitud del fármaco estimada en los ensayos *in vivo*. En cambio, la técnica experimental empleada en los ensayos *in situ* no permite evidenciarlos. En este punto cabe resaltar que en estados de desnutrición las alteraciones en la expresión de CYP1A1 solo se producen a nivel intestinal y no a nivel hepático, lo que justifica que el aclaramiento del fármaco no se encuentre alterado en los animales desnutridos.

## 4.5 Ejercicios de simulación

Los ejercicios de simulación realizados para escalar los resultados obtenidos en los modelos seleccionados a una población de humanos han permitido realizar predicciones de las concentraciones plasmáticas de los fármacos en pacientes, clasificados como normo- y desnutridos, sometidos a tratamiento farmacológico con erlotinib y gefitinib a las dosis terapéuticas (150 mg / 24 horas y 250 mg / 24 horas para erlotinib y gefitinib, respectivamente).

Para erlotinib, los resultados obtenidos en las simulaciones indican que el área bajo la curva de concentración plasmática frente al tiempo en los pacientes desnutridos simulados es un 20% superior a la esperada en pacientes normonutridos simulados.

Para el gefitinib, este ejercicio también apunta a que los pacientes desnutridos tratados con el fármaco estarían expuestos a valores de concentración plasmática superiores que los pacientes normonutridos. En este caso el área bajo la curva de concentración plasmática frente al tiempo en pacientes desnutridos sería un 50% superior a la esperada en pacientes normonutridos. Al comparar los resultados obtenidos en estas simulaciones con los obtenidos en dos ensayos clínicos en Fase II llevados a cabo con este fármaco en pacientes con cáncer (136) se podría confirmar la validez del escalado alométrico incorporado al modelo seleccionado. Esta decisión está avalada si se tiene en cuenta que la concentración plasmática mínima en estado estacionario determinada en los ensayos clínicos fue de 261 ng/mL (IC 95%: 88-774 ng/mL) (136). Es de esperar que la población de pacientes que participaron en los ensayos clínicos estuviera formada por pacientes normo- y desnutridos. En consecuencia, los resultados obtenidos en el

ejercicio de simulación realizado en esta Tesis concuerdan con los publicados previamente, ya que la concentración plasmática mínima en estado estacionario predicha para los individuos simulados normo- y desnutridos, tras recibir la misma pauta de administración que la utilizada en los ensayos clínicos, alcanzan el valor de 215 ng/mL y 334 ng/mL, respectivamente, coincidiendo el valor de la concentración mínima obtenido en el ensayo clínico con el valor medio de estos.

## 5. Conclusiones

El trabajo desarrollado ha permitido obtener las siguientes conclusiones:

1. El estado de desnutrición provoca alteraciones significativas en los niveles de mRNA de las enzimas metabólicas (Cyp1A1, Cyp1A2 y UDP) y transportadoras (OATP, MRP2 y Glicoproteína P) intestinales y hepáticas. En hígado se reducen los niveles de todas las enzimas evaluadas excepto de los citocromos. Sin embargo, en intestino delgado la influencia de la desnutrición sobre los niveles de mRNA no sigue un único patrón y el resultado final depende del tramo intestinal y de la enzima estudiada.
2. Las alteraciones observadas en las enzimas hepáticas alanina-aminotransferasa y aspartato-aminotransferasa así como la reducción de la concentración plasmática de albúmina confirman el daño hepático asociado a la desnutrición. Asimismo, la reducción en el recuento de elementos formes de la sangre corrobora la alteración medular provocada por la desnutrición calórico-proteica .

3. La incorporación de erlotinib al organismo desde el lumen intestinal se rige por un proceso de difusión pasiva y un proceso activo de secreción. Este último es sensible al estado nutricional y susceptible de inhibirse en presencia de levofloxacino.
4. El proceso de absorción intestinal de gefitinib se describe mediante un mecanismo de difusión pasiva que no se modifica por la presencia de azida sódica en la disolución de perfusión. Además, en las condiciones ensayadas *in situ* no se evidencian alteraciones en el proceso debidas al estado nutricional de los animales.
5. El modelo bi-compartimental es el que mejor describe la evolución temporal de las concentraciones plasmáticas de erlotinib y de gefitinib.
6. En estado de desnutrición el aclaramiento de erlotinib se reduce un 5%. La biodisponibilidad en velocidad y en magnitud del fármaco es dependiente del estado nutricional y del sistema de administración utilizado. La constante de velocidad de absorción cuando se administra en solución es un 52 % inferior en ratas desnutridas. La biodisponibilidad en magnitud es incompleta únicamente cuando se administra en suspensión a los animales normonutridos. Con estos resultados se predice un incremento del 20% en el área bajo la curva de concentración plasmática tiempo de erlotinib en pacientes desnutridos simulados.
7. Los parámetros farmacocinéticos del gefitinib volumen de distribución y biodisponibilidad en magnitud incrementan en estado de desnutrición calórico-proteica en un 30 y un 50 %,

respectivamente. Este resultado se reproduce en el ejercicio de simulación, en el cual se evidencia que, en relación con pacientes normonutridos, la concentración mínima en estado estacionario y el área bajo la curva de concentración plasmática-tiempo en pacientes desnutridos simulados incrementa un 50%.

8. El mecanismo de respuesta del organismo destinado a compensar las deficiencias calórico-proteicas es complejo. Las alteraciones farmacocinéticas en estados de desnutrición son difíciles de predecir, muy variables y dependientes del fármaco y de la vía de administración utilizada, ya que todos los procesos del LADME son sensibles a estos cambios.

# 1 Introduction and Objectives

## 1.1 Under-nutrition

Malnutrition is defined as the imbalance between supply of nutrients and energy and the demand for them to ensure maintenance, growth and functionality of the body (1). In this context, it can refer to individuals who are either over- or under-nourished.

Under-nutrition is considered to be either protein-energy wasting, commonly known as protein-energy malnutrition (PEM), and/or due to specific nutrient deficiencies. PEM has two main forms: marasmus and kwashiorkor. Marasmus is a severe deficiency of calories and protein, mainly occurring in infants and very young children. As a result of marasmus, weight loss and dehydration take place. The most extreme form of marasmus (and under-nutrition) is starvation, which results from a lack of essential nutrients for a long period of time. On the other side, kwashiorkor is a severe deficiency of protein and calories, with a more severe imbalance of proteins when compared with marasmus. This condition is less common than marasmus. Kwashiorkor tends to occur in certain areas of the world where foods used to feed babies are deficient in protein, such as rice, sweet potatoes, and green bananas. But this is not only restricted to babies: anyone can develop kwashiorkor if their diet consists mainly of carbohydrates. People who suffer kwashiorkor tend to retain fluid, making them swollen. In cases of severe kwashiorkor, the abdomen may even protrude (2).

### 1.1.1 Etiology of under-nutrition

Under-nutrition is associated with many disorders and circumstances, such as poverty and social isolation. Risk is also greater

at certain times of life: infancy, adolescence, pregnancy, breastfeeding, and elderly people.

**Infants and children** are particularly susceptible to under-nutrition because of the high demand for energy and essential nutrients during high growth-rate stages. During **adolescence**, nutritional requirements increase because of an even higher growth rate. Furthermore, adolescents have a high risk of suffering anorexia nervosa, particularly adolescent girls.

Under certain physiological situation, requirements for nutrients can increase in **adults**; this is the case of pregnancy and breastfeeding. During these periods of time, anaemia among other nutritional disorders can occur.

Even in those people with normal diets and without disease, the process of **aging** can lead to a progressive loss of lean body mass (sarcopenia). As life progresses, food intake commonly decreases, especially in men. Undernourishment due to aging has many causes, including increased release and activity of cholecystokinin (responsible of satiation), increased leptin and diminished taste and smell, which can reduce the eating pleasure. Under-nutrition in the elderly can also be due other causes (i.e. loneliness, inability to shop or cook, dementia, certain chronic disorders, treatment with certain drugs). But also dental problems limit the possibility of chewing food correctly and thus, digesting foods. Swallowing difficulties are also common.

Certain **health problems** (specially chronic disorders) are also related to under-nutrition. Disorders such as diabetes can affect the gastrointestinal tract. Intestinal resections and certain other gastrointestinal surgical procedures tend to impair absorption of fat-

soluble vitamins, vitamin B12, Ca, and iron. Malabsorption can be a consequence of gluten enteropathy, pancreatic insufficiency or other disorders. Liver disorders cause an impaired storage of certain vitamins and alter metabolism of proteins. Renal insufficiency predisposes to protein, iron, and vitamin D deficiencies. Patients with cancer or depression and many with AIDS consume inadequate amounts of food. Infections, trauma, hyperthyroidism, extensive burns, prolonged fever and again cancer can increase metabolic demands. Any condition that increases cytokines may lead to muscle loss, lipolysis, low albumin levels, and anorexia. Under this setting, cancer patients are known to be a group of patients particularly susceptible of suffering undernourishment. In the following section the etiology of undernourishment in cancer patients will be discussed in more depth.

#### *1.1.1.1 Etiology of under-nutrition in cancer patients*

Nutritional deterioration is highly correlated to cancer and its treatment. The degree of under-nutrition that takes place is dependent on cancer type, stage and treatment selection. The aetiology of cancer-induced undernourishment is multifactorial, complex and highly influenced by inter-individual variability. Deterioration of nutritional status can occur at any point after cancer diagnosis or start of treatment. These changes may occur as a result of metabolic changes, mechanical blockages or abnormalities, treatment side effects or psychosocial issues (3).

Certain factors, such as dysphagia, nausea, xerostomia and changes in taste and smell, may directly lead to diminished food intake. Other factors may have an indirect influence on food intake by

**Comentario**
incluido dent
qué separado

Alejandro: lo
lo cambio?

affecting appetite. Patients suffering pain, fatigue and psychological problems may experience a decrease in food intake. Additionally, tumour-related mechanisms such as obstruction of the gastrointestinal tract can cause dysphagia, which usually has an early effect on weight. But not only disease-related mechanisms contribute to weight loss. A variety of metabolic and endocrine changes, and activation of catabolic pathways also account for weight loss.

Pro-inflammatory cytokines (secreted by either immune cells or tumours) play a central role. Cytokines have three major effects: 1) alteration of macronutrient metabolism, 2) depression of appetite, and 3) initiation of an acute phase protein response. This acute phase protein response is energy-intensive with high requirements for essential amino acids. The need for amino acids drives the loss of muscle. Along with the acute phase protein response, changes in intermediary metabolism also occur, most notably, in protein metabolism (3)

### 1.1.2 Pathophysiology of under-nutrition and its relation with pharmacokinetic alterations

Pathophysiology of undernourishment condition will mainly depend on its nature, severity and duration. Inadequate energy intake leads to various physiological adaptations such as growth restriction, loss of fat, of muscle and of visceral mass and to metabolic rate reduction. Physiopathological changes resulting from under-nutrition cause functional alterations in every organ system of the body, as shown in Table 1.1.

*Table 1.1 Physiopathological alterations caused by under-nutrition.*

| Organs system | Effects of under-nutrition |
|---|---|
| Gastrointestinal tract | Villous atrophy along with loss of enzymes (such as disaccharidases), crypt hypoplasia, and altered intestinal permeability results in absorption alterations. Pancreatic atrophy is also common. Fatty infiltration of the liver takes place and protein synthesis, glycogenesis, and drug metabolism are decreased. |
| Cardiovascular system | Reduction in cardiac muscle mass takes place and the decrease in cardiac output results on reduced renal perfusion and glomerular filtration rate. |
| Respiratory system | Decreased functionality of diaphragmatic and respiratory muscles reduces expectoration capacity and worsens respiratory tract infections. |
| Endocrine system | Most endocrine functions are supressed by under-nutrition:<br>• T3 and T4 are reduced<br>• Gonadotropins are supressed<br>• Insuline secretion is reduced (but insulin sensitivity rises): Hypoglycaemias may indicate terminal phase. |
| Immune system | Cellular immunity is affected mainly because of the atrophy of thymus, lymph nodes and tonsils. Phagocytosis is impaired and IgA secretion is reduced. Immune system alterations increase the susceptibility to infections. |
| Nervous system | Reduction in the number of neurons, synapses, dendritic arborisations and myelinisation. All these alterations result in decreased brain size along with delayed global function, motor function and memory. Furthermore, psychological consequences such as apathy, depression and anxiety have been reported. |

#### *1.1.2.1* Pathophysiological changes that affect drug pharmacokinetics in protein-energy malnutrition.

The pharmacokinetic (PK) behaviour of a drug depends on patient-related factors as well as on the drug's chemical properties. In this sense, patients' characteristics have important relevance on treatment schedule

selection; some patient-related factors (such as renal function, sex or age) are commonly used to reduce uncontrolled inter-individual PK variability, to predict the PK behaviour in populations, and are thus employed in dose individualization. Inter-individual variability is commonly be related to genetic differences as well as variations in the functional status of cancer patients (4). Under-nutrition has the potential to play an important role in cancer patients' functional status and as a consequence, it should be investigated as a potential factor affecting PK behaviour of anti-cancer drugs.

Many of the physiological systems altered in patients with PEM influence, either directly or indirectly, the disposition of commonly used drugs. The following section briefly reviews those aspects of physiological systems that are influenced by PEM and consequently cause PK alterations.

**Changes in gastrointestinal system**

Diarrhoea and vomiting are common problems of PEM. As a consequence, oral drugs may not be retained, and moreover, the transit time through the bowel may be decreased. Furthermore, PEM is associated with villous atrophy of the jejunal mucosa and this may impair drug absorption (5, 6). Nevertheless, an impaired barrier function has also been associated with increased drug absorption for several drugs (7, 8).

**Changes in cardiovascular system**

Patients with severe PEM have a smaller and thinner heart and a lower stroke volume (9). Renal failure also adversely affects the heart and thus, the circulation is overloaded more easily than usual and there

is higher risk of oedema. Furthermore, decreased blood flow can result in alterations of drug elimination if perfusion of elimination organs is modified.

**Body fluid distribution**

Body fluid compartments are altered by many factors such as nutritional status and disease. The increased total body water is associated with a proportional rise in extracellular fluid; this is seen particularly in patients with oedema (10, 11).

Contrarily, there is a significant reduction in adipose mass as well as lean body mass which can alter the apparent volume of distribution of drugs. The distribution of lipid-soluble drugs into adipose tissue is known to be reduced in PEM. A major clinical implication of such reduction is that the concentration of the lipid-soluble drug would increase at the target tissues, thus increasing its pharmacodynamics (PD) actions (12).

**Plasma proteins**

Following absorption and entry of drugs into the vascular system, drug molecules frequently bind to plasma proteins. In general, acidic drugs bind to albumin and basic drugs bind to α1-acid glycoprotein (13). Hypoproteinaemia is a common feature of PEM (14, 15). Under this setting, plasma albumin and fractions of the glycoproteins responsible for binding drugs are decreased (16-18). As a result of this decreased protein binding, in theory, there may be a substantial increase in the plasma free-drug fractions of highly protein-bound drugs and patients with PEM may experience variations in their response to drug treatment or be at risk of increased drug toxicity (19).

## Changes in renal function

Renal function is a very important determinant of the PK action of many drugs, but the effects of malnutrition on renal function have not been studied extensively. Despite lack of evidence of established renal damage in patients with PEM, the oedema observed in marasmic-kwashiorkor and kwashiorkor patients has been attributed to the inability of the kidneys to adequately excrete excess fluid and sodium (20), as well as to the presence of hypoproteinaemia (21). The impact of malnutrition on glomerular filtration rate is most relevant for patients receiving drugs primarily excreted by the kidneys, such as penicillin and aminoglycosides. Another example is the PK of methotrexate, which has been studied in undernourished and well-nourished patients with cancer. This drug is primarily excreted by the kidneys and its elimination half-life was evidenced to be more prolonged in the malnourished than well-nourished patients (22).

## Changes in hepatic function

The liver is very sensitive to lack of dietary proteins and calories, and a spectrum of changes in the liver both in animals and in humans has been described. Electron microscopic studies demonstrate a decrease in mitochondria, ribosomal proteins and endoplasmic reticulum. Hepatic alterations can result in modifications of biotransformation, hepatic and biliary excretion, entero-hepatic circulation and first-pass metabolism resulting in PK alterations (19).

## 1.2 The influence of under-nutrition on the pharmacokinetics and pharmacodynamics of anticancer agents

The evidenced role of under-nutrition in cancer treatment-outcomes suggests the need of considering nutritional status when evaluating anti-cancer treatments. The relationship between nutritional status and PK of anticancer drugs was first reviewed by Murry et al. (23) in 1998, and since then, many studies have expanded the knowledge about this phenomenon. But the quantification of nutritional status' impact on PK behaviour of anticancer drugs cannot be fully applied to patient care without the understanding of PD repercussions. In order to merge the available data and offer a global view of this phenomenon, the following section reviews in a drug-by-drug basis the under-nutrition-related PK and PD aspects of those anti-cancer treatments for which evidence is available in the literature (main aspects are summarised in Table 1.2).

*Table 1.2. Clearance characteristics of antineoplastic drugs and undernourishment's influence on them.*

| Drug | Clearance characteristics | Impact of under-nutrition on drug clearance |
|---|---|---|
| 5-Fluorouracil | • Hepatic metabolism (primary route): The rate-limiting step of 5-FU catabolism is dihydropyrimidine dehydrogenase conversion of 5-FU to dihydrofluorouracil.<br>• Renal excretion (24). | • Significantly lower in low-protein fed rats(25, 26). |
| Methotrexate | • Hepatic metabolism<br>• Bile excretion: ABCC2 (MRP-2) and ABCB1 (P-gp)<br>• Renal excretion (primary route) (27) | • Decreased in animal models and humans (22, 28-32).<br>• Biliary excretion of MTX is a carrier-mediated process sensitive to nutritional status of the host (30). |
| Anthracyclines | • Hepatic metabolism<br>• Bile excretion<br>• Renal excretion: ABCB1 (P-gp), ABCC1, ABCC2 (MRP-2), ABCG2, RALBP1 (33) | • Decreased in animal models as shown in most of the preclinical studies (34-37).<br>• Transformation of the drug into its aglycone metabolites seems to be decreased.<br>• Urinary excretion of aglycone metabolites seems to increase (37). |
| Vinca alkaloids | • Hepatic metabolism: CYP3A4, CYP3A5<br>• Bile excretion (80% approximately in humans): ABCC2 (MRP-2) and ABCB1 (P-gp) (38) | • Decreased clearance in malnourished patients (39). |
| Etoposide | • Hepatic metabolism: CYP3A4, CYP3A5 (40)<br>• Bile excretion: almost exclusively dependent on ABCC2 (MRP-2) (41). | • Decreased clearance in protein-calorie malnourished rats.<br>• Biliary excretion of etoposide did not seem to change in undernourishment status (42). |

**5-fluorouracil**

The literature review regarding the relationship between nutritional status and PK/PD of 5-fluorouracil (5-FU) reveals a lack of consensus between pre-clinical controlled studies and uncontrolled clinical studies. Several studies carried out in rats have found protein depletion to cause an increase in the toxicity of 5-FU. Torosian et al. (43) described a higher incidence of 5-FU-related leukopenia in under-nourished rats than that found in well-nourished ones, and a higher incidence and longer duration of diarrhoea in the undernourished group receiving high doses of 5-FU. Similarly, Davis LE et al. (26) concluded that 5-FU drug clearance was significantly lower in the low-protein fed rats and that drug accumulation caused an increased toxicity, with diarrhoea, weight loss and leukopenia. Borrelli et al. (44) studied the underlying mechanism by which under-nutrition enhances leukopenia in mice receiving 5-FU. Their experiment concluded that PEM leads to the depletion of progenitor hematopoietic populations and changes in cellular development. Regarding gastrointestinal toxicity, the study by Motawi et al. (25) evaluated the metabolism and toxicity of 5-FU in rat stomach. Their results indicated that protein malnutrition exacerbates the gastric toxicity for 5-FU by reducing its catabolism and drug clearance in rat stomach.

On the other hand, studies in humans do not reach a consensus about the effect of nutrition on PK/PD of 5-FU. Published study designs with this objective are highly variable. Fleming et al. (45) conducted a clinical study in 187 patients with head and neck cancer and studied the correlation between analytical parameters (albumin, transferrin and

prealbumin levels) and clearance of 5-FU, concluding that relations were no statistically significant. Nevertheless, the evaluation of nutritional status through unique laboratory parameters is not considered an optimal system. Even though no gold standard has been defined with consensus, scoring systems of under-nutrition have evolved and several screening tools have been developed to identify under-nutrition with high sensitivity and specificity (46). In 2002, Gusella et al. (47) studied the relationships between body composition parameters and 5-FU pharmacokinetics. Interestingly, the stepwise multiple regression analysis revealed a better correlation between PK parameters and bioelectrical impedance analysis related parameters (body cell mass, total body water and fat free mass) than with the anthropometric parameters employed for adjusting 5-FU doses (body surface area and total body weight). Supporting these results, in a study published in 2010 by Hasenberg et al. (48) regarding 5-FU-related toxicity, lower incidence of chemotherapy-associated side effects along with better quality of life was described in patients receiving supplemental parenteral nutrition.

**Methotrexate**

The literature review has revealed a profound consensus within the results from preclinical and clinical studies regarding the PK/PD behaviour of MTX in undernourishment status. Among published preclinical studies carried out in rats, protein deprived diets have shown to be related with increased MTX exposure mainly due to decreased drug clearance (28-30, 32). The impact of malnutrition on PD of MTX (toxicity and efficacy) has been studied in depth. Torosian (49) studied in a group of rats with subcutaneous mammary tumour implants the

effect of a protein-depleted diet on dihydrofolate reductase (DHFR) activity of both tumour and host cells. Protein depletion reduced enzyme activity in bone marrow and tumours to 50% and 85%, respectively, respect to levels found in animals receiving standard diet. On the other hand, enzymatic levels were unchanged in liver and increased in gastrointestinal mucosa (136%) when protein depletion took place compared with standard diet administration. Grossie et al. (50) carried out a similar study and concluded that DHFR levels in bone marrow and liver were lower in malnourished rats than in controls. These results could explain in part the increased myelosupression and hepatic toxicity from MTX in malnourished animals, but other mechanisms must be implicated to account for increased gastrointestinal toxicity. In another study by Torosian et al. (51), improved nutritional status by enteral nutrition reduced the mortality and morbidity associated with MTX in tumour bearing rats and equivalent tumour response was observed in norm and malnourished rats. These results contrast with those obtained by Daly et al. (52), who studied tumour growth in experimental animals receiving MTX. Tumour growth in the group of rats receiving a protein-free diet reached a plateau during the study and MTX did not significantly affect tumour growth patterns. Accordingly, Reynolds et al. (53) reported a similar phenomenon, concluding that dietary protein depletion inhibited both tumour growth and tumour response to MTX.

Most of the clinical results are in accordance with those obtained in preclinical studies. PK studies in patients have revealed a significant prolongation of biological half-life and a reduction of drug clearance in undernourishment status (22, 31). Regarding clinical PD of MTX, undernourishment is an adverse prognostic factor. Undernourished

patients have a worse clinical performance as compared with well-nourished patients because of the diminished bone marrow reserve in malnourishment and thus, making necessary to employ suboptimal doses in maintenance chemotherapy (54). Israëls et al. (55) recently reported results from clinical study in which malnutrition at diagnosis was found to be associated with a significantly higher rate of profound neutropenia (the analysis took into account possible confounders). All the patients with profound neutropenia, prolonged neutropenia and treatment related deaths were malnourished at diagnosis. According to the researchers, chemotherapeutic regimens have to be adapted to patients' nutritional status to avoid unacceptable morbidity and mortality.

**Anthracyclines**

The consequences of under-nutrition on the PK and PD of several anthracylines have been revealed in animals but the consequences of this condition in the clinical setting remain unexplored. In 1992, Cusak et al. (34) concluded that protein depletion significantly decreased doxorubicin clearance and therefore increased the area under the plasma concentration-time curve (AUC). Kim et al. (37) proved that in under PEM conditions the transformation of the drug into its aglycone metabolites was decreased. The overall consequence of PEM was a higher AUC.

PK/PD studies soon proved that anthracyclines caused dose-dependent cardiotoxicity, but it was not until 2012 when Demerdash et al. (35) concluded that the prolonged exposure of the heart to these drugs and malnutrition enhanced anthracycline cardiotoxicity, and thus suggested the need of dose adjustment in nutritionally deprived patients.

The underlying mechanism by which undernourishment influences the PK/PD of these drugs has not been fully elucidated, but it is known that both, nutritional deficiency and anthracycline administration are cardiotoxic (56). This fact could account for the additive/synergistic damage on heart tissue that takes place when these two situations coexist.

The only evidence available supporting the translation of these preclinical results to the clinical setting was published by Prado et al. (57). A population PK analysis of epirubicin was undertaken to test effects of body composition on epirubicin clearance and AUC. Lean body mass predicted 18% of the variability in epirubicin clearance. Furthermore, their investigation pointed towards a relation between liver attenuation (a surrogate marker of fat infiltration obtained through image tests) and AUC. The authors concluded that dose normalization to lean body mass could better individualize treatment than normalizing to body surface area. Nevertheless, this analysis does not isolate the influence of under-nutrition on the PK of anthracyclines in patients, but supports, at least in part, the evidence generated in preclinical studies.

**Vinca alkaloids**

According to literature, vincristine clearance is affected by nutritional status. Israels T. et al. reported a significantly lower vincristine clearance (2.2 versus 2.6 mL/min, $p = 0.001$) and thus higher AUC values (3.8 versus 3.5 μg/mL·min, $p = 0.003$) in malnourished Malawian patients than in a comparable patient population with better nutritional status in the UK (39). Given the narrow therapeutic index of vincristine, increased exposure can result in severe toxicity. Gomber et

al. (58) reported increased neurotoxicity in undernourished patients included in a retrospective study carried out in a paediatric cancer population: all the patients in their study who developed neurotoxicity were severely malnourished. Nevertheless, increased toxicity may be related, not only to increased drug exposure, but also to the neurotoxicity predisposition of undernourished patients (59, 60).

**Etoposide**

Several authors have described altered PK and PD of etoposide in nutritional deficiency states. Suh et al. (42) evidenced that etoposide clearance in protein-calorie malnourished rats was significantly lower as compared to control rats, resulting in a 28% increase of AUC. This effect was attributed to the decrease in protein expression and/or mRNA level of CYP3A1/2 compared with controls. Interestingly, biliary excretion of etoposide did not seem to change compared with controls. These results were consistent with previous reports: P-glycoprotein (P-gp) hepatic expression is known to be decreased in protein-calorie malnutrition but hepatobiliary output of etoposide is almost entirely dependent on multidrug resistance protein (MRP) and not P-gp. On the other side, absorption rate proved to be significantly lower in undernourished rats when compared with the control group after oral administration of the drug. The mechanism behind this behaviour might be a reduction in the microvilli in the small intestine of undernourished rats.

Regarding etoposide PD in nutritional deficient states, Spronck et al. (61) evidenced that bone marrow cells in rats fed a niacin depleted diet and receiving etoposide are capable of undergoing apoptosis, but the

proportion of cells committed to die is significantly reduced when compared to a control group fed with normal diet. This results point to the potential decrease of treatment effectiveness in patients with a deficiency of this amino acid in their food intake. Furthermore, their investigations suggested the possibility of an increased risk of secondary treatment-related malignancies when patients have a deficient niacin intake. Nevertheless, clinical studies have not investigated these interactions.

**New anti-cancer agents**

Most of the scientific literature regarding the impact of undernourishment on the PK/PD of antineoplastic agents was produced in studies employing drugs that have been used for decades in the onco/haematological clinical setting. The nutritional status-PK/PD relationship has been studied in depth for classical anticancer drugs (cytotoxic agents), but this relationship remains unexplored for modern therapies involving targeted drugs. Furthermore, not only new action mechanisms have been developed but also alternative administration routes, other than parenteral, are now employed for a wide range of anti-cancer drugs (cytotoxic agents and targeted therapies). The administration of drugs outside the central compartment introduces a new source of PK variability that plays an important role in therapeutic outcomes. In particular, high variability in drug exposure has been observed for orally administered tyrosine kinase inhibitors as a result of a highly variable absorption process. For these drugs, factors such as changes in gastric/intestinal pH, gastric/intestinal motility (due to disease or concomitant medication), and enzymatic and transporter

activity in the intestinal wall play an important role in inter-individual variability (62). Since most anticancer drugs have a narrow therapeutic window and are dosed at or close to the maximum tolerated dose, a wide variability in the exposure can have a negative impact on treatment outcome (63). Understanding the influence of nutritional status on the absorption process can be crucial in clinical practice. Nevertheless, this PK aspect of new anti-cancer drugs has not been considered in any clinical study.

Not only new administration routes and new action mechanisms have modified the setting described by Murry et al. in 1998 when they reviewed the impact of nutrition on PKs of anti-neoplastic agents. Monoclonal antibodies and derivatives have been used in the treatment of various malignancies over the last years. The PK properties of macromolecules differ markedly from those of non-antibody-type drugs, and these properties can have important clinical implications. PK differences are mainly due to target-mediated drug disposition: distribution and clearance are mainly affected by neonatal Fc receptor (FcRn) expression and distribution across body tissues. Interestingly, alterations of Fc receptor expression have been described to occur in protein malnutrition (64). Considering the up-regulation of FcRn expression induced by TNF-α and IL-1β during inflammation, alterations in the PKs of monoclonal antibodies can be expected in malnourishment status (65). Park S. et al. studied the relationship between the nutritional status of diffuse large B-cell lymphoma patients treated with rituximab and the survival outcome, and found that most of the nutritional parameters showed a significant association with survival (66). The up-regulation of FcRn due to inflammation, and the

consequent increase of antibody clearance, could be a plausible explanation to the results of their analysis. Taking into account the amount of new monoclonal antibodies ready for market launching, the described relationship will probably require further investigation.

## 1.3 Approaches for the evaluation of the impact of undernourishment on drug pharmacokinetics

Conducting clinical studies in patients in order to quantify the influence of under-nutrition on the PK of drugs has technical difficulties that are difficult to overcome. The first aspect that has to be dealt-with in studies designed for this purpose is the way in which nutritional status is going to be evaluated. Secondly, in order to thoroughly investigate the PK processes being affected by undernourishment, full PK profiles have to be obtained, implying intensive blood sampling schedules which most of the time will be very difficult or impossible to obtain, especially if studies are carried out after drug development and commercialization.

Concerning the first aspect, in order to evaluate the impact of nutritional status on drug PK it is necessary to evaluate nutritional status and to identify under-nutrition. To achieve this, nutrition-screening tools represent the best evaluation system. The selection of the optimum nutrition-screening tool depends on the population being evaluated, the resources available and the purpose for which screening is being conducted.

Seltzer et al. (67) first introduced the concept of nutrition-screening more than 30 years ago. Since then, it has become increasingly

complicated to define nutritional status of patients. In this first approach to screen nutritional status, the authors used albumin and total lymphocyte count to identify patients on hospital admission who required a nutritional intervention (67). By doing this, they could instantly assess nutritional status of patients in a similar way to what we now call nutritional screening.

Potosnak et al. (68) then complemented this first approach with laboratory data and information about appetite and weight change over time. After this, many initiatives were started to develop nutritional screening tools and by 1994 the American Dietetic Association recommended more than 60 nutrition screening-criteria. Nevertheless, until now no consensus has been reached on the best screening tool to identify hospitalised patients at risk of malnutrition (69).

Although many nutritional screening and assessment tools are available for their use in the clinical setting (46), few have been validated in the inpatient oncology population. This population has a particular nutritional condition (70). These patients may be unwell or suffering from treatment side effects, which compromise nutritional status. For this reason, regular nutritional screening in the inpatient setting is recommended (71). A nutrition support program for cancer patients must count with a nutrition assessment to identify patients at greatest risk, determine the level of deficit and establish the appropriate nutrition intervention. This approach may lead to improvements in nutritional status, quality of life, patient satisfaction and treatment outcomes (72).

The ESPEN recommends the following nutritional screening tools: the Malnutrition Universal Screening Tool (MUST), the Nutritional Risk

Screening (NRS- 2002), and the Mini Nutritional Assessment® method (MNA) (73). Other of the most commonly used screening tools are: the Screening Tool for the Nutritional Control (CONUT), the Subjective Global Assessment (SGA) and the scored Patient-Generated Subjective Global Assessment (PG-SGA).

The **MUST** is a system designed to detect adults who are at risk for malnutrition or who are malnourished on the basis of knowledge about the association between impaired nutritional status, body composition, and physical function (70). Three independent criteria are used by MUST to determine the overall risk for malnutrition: current weight status using body mass index (BMI), unintentional weight loss, and acute disease effect. It is the preferred screening tool for patients in the community by ESPEN, which is the setting for which it was primarily developed. Nevertheless, the MUST seems not to be the tool of choice in cancer patients because it lacks sensitivity and specificity for this population (70).

The ESPEN recommends the **NRS-2002** as the preferred screening tool for hospitalized patients (mixed population). It contains all the components of the MUST and, in addition, a grading of severity of disease as a reflection of increased nutritional requirements. According to a study by Kyle et al. (74), the NRS-2002 was associated with higher sensitivity and specificity and higher positive and negative predictive values than the MUST. The NRS-2002 is a better screening tool than MUST in the hospital setting, but it has not been well-validated in cancer patients.

The **MNA®** is a rapid and efficient nutrition assessment tool developed to assess nutritional status of elderly patients or otherwise

frail individuals in nursing homes and hospitals (75). The full MNA includes 18 items grouped into four sections: anthropometric assessment, general assessment, short dietary assessment, and subjective assessment. On the other hand, the MNA-short form (MNA-SF) uses six strongly correlated items: food intake, involuntary weight loss, mobility, acute illness, neuropsychological problems and BMI. Although the MNA and the MNA-SF tools have been used in oncology patients, there is limited evaluation in the oncology population (76). The sensitivity of the MNA in analysing an unintentional weight loss was merely 33%, and the positive predictive value in oncology patients was limited at 59% (76).

The **CONUT** screening tool was developed by Uribarri et al.(77) and takes into account serum albumin, total cholesterol level and total lymphocyte count. The high sensitivity and specificity of the tool confirm CONUT as an efficient and valid screening method for early detection of hospital malnutrition. Nevertheless, this tool has not been validated in cancer patients.

The **SGA** was developed by Detsky et al. (78) using a questionnaire that contains medical history and clinical findings items (weight loss, changes in dietary intake, gastrointestinal symptoms, presence of symptoms that can influence nutritional intake, functional capacity, a physical examination, and the clinicians' overall judgment of the patient's nutritional status). The SGA is an assessment tool rather than a screening tool. Years later in 1994, the SGA was adapted by Ottery (79) to more specifically meet the needs of the cancer patient, with increases in the gastrointestinal symptom section to include the nutritionally determinant symptoms found in the oncology population

(PG-SGA). The **PG-SGA** is the most studied and most commonly accepted system for an accurate nutritional assessment of oncology patients and is therefore considered the “gold standard” in oncology patients (70). Nevertheless, this methodology is not a screening tool but an assessment tool, and the required information for its use makes it difficult to implement in the clinical setting.

Given that there is no validated tool for nutritional status screening in cancer patients (PG-SGA is an assessment tool and not a screening tool), the design of studies aiming to evaluate the impact of undernourishment on PK becomes even more challenging when considering anti-cancer drugs. Furthermore, intensive blood sampling is required in order to perform a thorough investigation to detect which PK processes are altered in undernourishment status. In the setting of PK studies in clinical trials, intensive blood samplings are possible. Nevertheless, such trials do not evaluate nutritional status and thus, evaluation of the influence of under-nutrition on pharmacokinetic parameters is not possible.

In this context, preclinical studies can be a highly informative approach to evaluate the effect of undernourishment on PK, overcoming the previously described problems encountered in the clinical setting. The development of animal models permits researchers carry out this kind of investigations. The **animal model of under-nutrition** developed by Merino et al. is a fit for purpose tool which permits the evaluation of the impact of under-nutrition on the PK of drugs in a controlled setting where confounding factors are minimized and the investigated phenomenon is isolated for its analysis (80).

This model was developed through an experiment consisting of 2 study groups: well-nourished (WN) rats on a regular diet and undernourished (UN) rats on a protein-calorie restricted diet. Assessment of the nutritional status of rats was carried out using serum albumin and total serum cholesterol levels as biochemical parameters and weight as a biometrical parameter. Serum albumin is an indicator of protein reserves and cholesterol is a caloric depletion parameter. Animals were considered undernourished when their serum albumin level was under 2.3 g/dL and their body weight was under 240 g. Both parameters were used to classify the animals according to three different degrees of under-nutrition: mild, moderate and severe. The authors assigned scores based on the CONUT screening tool. Statistically significant differences in serum albumin and body weight ($p < 0.05$) between WN and UN animals were detected from week 3 until the last day of the adaptation period. Total serum cholesterol in both groups was similar at the end of the adaptation period and statistical differences were obtained only at the end of the experience. The authors concluded that total serum cholesterol did not reflect the nutritional state of the animals. Consequently, the degree of nutritional undernourishment was evaluated using a total score based only on serum albumin level and body weight.

## 1.4 Investigated drugs: Erlotinib and Gefitinib

As discussed previously, the relationship between nutritional status and PK/PD has been studied for classical anticancer drugs (cytotoxic agents), but this relationship remains unexplored for modern therapies involving targeted drugs and new administration routes. The

administration of drugs outside the central compartment introduces a new source of PK variability (drug absorption) that plays an important role in therapeutic outcomes. Understanding the influence of nutritional status on this process can be crucial in clinical practice. Nevertheless, this PK aspect of new therapies has not been considered.

For this reason, this thesis focuses on 2 novel orally administered targeted-drugs: erlotinib (trade name Tarceva) and gefitinib (trade name Iressa).

### 1.4.1 Erlotinib and gefitinib

The identification of mutations driving malignancies has had a significant impact on the treatment approach for many cancers. An illustrative example of how this new knowledge has improved treatment outcomes is non-small cell lung cancer (NSCLC). In this population, the understanding of molecular alterations has lead to the identification of subgroups of patients, such as those whose tumours have an epidermal growth factor receptor (EGFR) mutation, an anaplastic lymphoma kinase (ALK) mutation or a proto-oncogen tyrosine-protein kinase (ROS-1) mutation, and subsequently to the individualization of treatment selection.

EGFR is a trans-membrane glycoprotein, which belongs to a family of structurally related receptor tyrosine kinases (TK) that play a critical role in many cell-signalling pathways that influence cell division, apoptosis, motility and adhesion (Figure 1.1). Binding of a specific set of ligands to the receptor promotes EGFR dimerization and the autophosphorylation of the receptors on tyrosine residues. Upon autophosphorylation of the receptor, several signal transduction

pathways downstream of EGFR become activated. The Ras/Raf mitogen-activated protein kinase pathway and the phosphoinositol 3'-kinase/Akt pathway are two major signalling routes for the human epidermal growth factor receptor (HER) family. Signal transduction finally results in nuclear gene activation. EGFR and its ligands are involved in autocrine growth loops in a number of tumor types, including NSCLC (81).

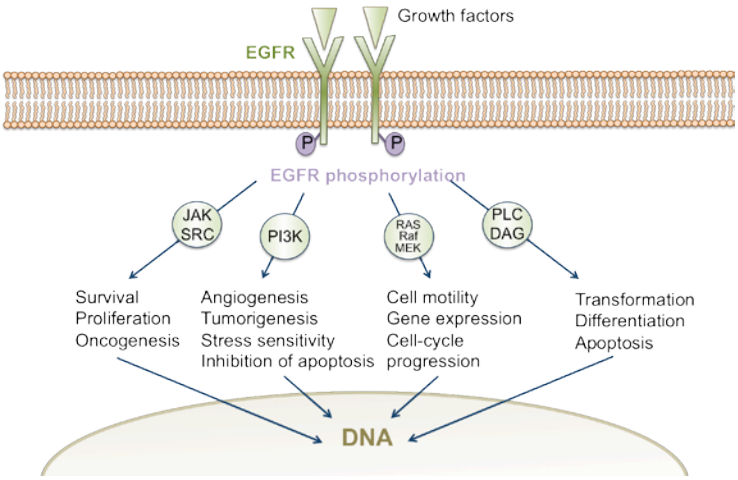


*Figure 1.1 Epidermal growth factor receptor signalling pathways.*

The EGFR family comprises four trans-membrane TK growth factor receptors: EGFR itself (ErbB1) (EGFR/HER1), ErbB2 (HER2/neu), ErbB3 (HER3), and ErbB4 (HER4) (81). Erlotinib and gefitinib were the two first-generation tyrosine kinase inhibitors (TKI). Both of them are orally available, potent, reversible, and selective inhibitors of the EGFR (ErbB1) tyrosine kinase capable of causing arrest in the G1 cell cycle phase.

For tumours expressing EGFR mutations, there is strong evidence that EGFR TKIs, such as gefitinib and erlotinib, significantly prolong

progression free survival (PFS) compared with platinum based chemotherapy. Studies on the efficacy of EGFR-TKIs have been on-going for more than a decade now. With time, correlations have been reported between treatment outcomes and clinical factors such as histology of tumours, gender, smoking status and ethnicity, as well as somatic mutations in the tyrosine kinase domain of the EGFR which are now known to be a predictor of response to erlotinib and gefitinib.

In the following sections, the development programs leading to erlotinib and geftinib commercialization will be overviewed, physicochemical characteristics of erlotinib and gefitinib will be briefly discussed and then their main pharmacokinetic characteristics will be summarised.

**Development programs**

The program leading to the discovery of erlotinib was initiated in the early 1990s. In 1997 in vitro testing of erlotinib demonstrated its potential as a specific and potent inhibitor of EGFR (82). After this, *in vivo* experiments demonstrated the efficacy of EGFR inhibition when tested against tumour xenograft models. Furthermore, erlotinib demonstrated adequate oral bioavailability and PK properties that made it suitable for clinical development. Phase I studies in healthy subjects and cancer patients assessed the safety and PK of erlotinib at various dose levels. The results of these first trials suggested a fixed daily oral dose of 150 mg as the recommended dose for Phase II studies. Treatment efficacy was then evaluated in humans in a Phase II study, which included patients with NSCLC who had progressed despite platinum-based chemotherapy. The outcome of the trial was a 12.3%

objective response rate and a median overall survival (OS) of 8.4 months (83). Subsequently, two Phase III trials of erlotinib in first-line NSCLC with combination chemotherapy were initiated. In addition, a Phase III study of erlotinib as single agent in patients with NSCLC after failure of at least one prior chemotherapy regimen was conducted. In this last Phase III trial, a significantly longer OS and PFS was observed for erlotinib compared to best supportive care (84).

Erlotinib was finally formulated and commercialized as film-coated tablets. The recommended daily dose of erlotinib is 150 and 100 mg for NSCLC and pancreatic caner, respectively. When dose adjustment is necessary, the dose is usually reduced in 50 mg steps. For this to be possible, three strength levels are available: 25 mg, 100 mg and 150 mg.

Regarding gefitinib, its antiproliferative activity in preclinical studies, alone or in combination with cytotoxic drugs, was investigated in human ovarian, breast, and colon cancer cell lines, which express EGFR and transforming growth factor alpha. Gefitinib inhibited colony-forming ability in a concentration-dependent manner. In Phase I trials gefitinib proved to have a favourable tolerability and patients with NSCLC had a good response. By the time the Phase III study (INTEREST) had already been initiated, EGFR mutations where first observed in NSCLC patients. This study did not select patients based on EGFR mutational status and failed to prove clinical benefit in global study population. Nevertheless, the subgroup analysis evidenced that those patients with EGFR mutation had a significantly better response than those treated with docetaxel. Consequently the IPASS study was then designed to evidence the clinical benefit of gefitinib for those

patients with EGFR mutation. Iressa was finally approved for a biomarker-targeted population (EGFR+).

Gefitinib was finally formulated as film-coated tablets. The recommended daily dose of gefitinib is 250 mg for NSCLC. Patients with poorly tolerated diarrhoea or skin adverse reactions may be successfully managed by providing a brief (up to 14 days) therapy interruption followed by reinstatement of the 250 mg dose.

**Physicochemical characteristics**

Gefitinib and erlotinib are both 4-Anilinoquinazolines. Summarised physicochemical characteristics for both drugs are presented in Table 1.3.

Erlotinib hydrochloride is a white to pale yellow crystalline, non-hygroscopic powder and sparingly soluble in organic solvents, water and aqueous buffer with the chemical name N-(3-ethynylphenyl)- 6,7-bis(2-methoxyethoxy)-4 quinazolinamine, monohydrochloride (Figure 1.2). It is an anhydrous crystalline solid with three known polymorphic forms and has a non-chiral molecular structure (84). Erlotinib hydrochloride presents and increased solubility at at pH<5 and maximal solubility of 0.4 mg/mL at pH 2.

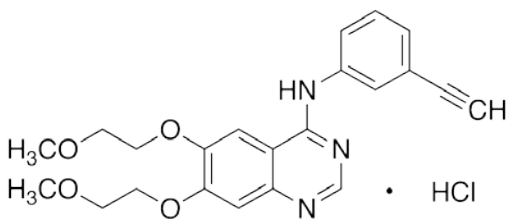


*Figure 1.2. Chemical structure of N-(3-ethynylphenyl)- 6,7-bis(2-methoxyethoxy)-4 quinazolinamine, monohydrochloride.*

Similarly, gefitinib is a white, crystalline, non-hygroscopic powder. The solubility of gefitinib in aqueous solution is pH dependent. At pH 3 it is sparingly soluble, while it is practically insoluble at pH 7. Gefitinib is freely soluble in glacial acetic acid and in dimethylsulfoxide, soluble in pyridine, sparingly soluble in tetrahydrofuran and slightly soluble in methanol, ethanol (99.5%), ethyl acetate, propan-2-ol and acetonitrile. Its chemical name is N-(3-chloro-4-fluorophenyl)-7-methoxy-6-(3-morpholinopropoxy)quinazolin-4-amine (Figure 1.3). Gefitinib doesn't contain asymmetric carbon atoms (85).

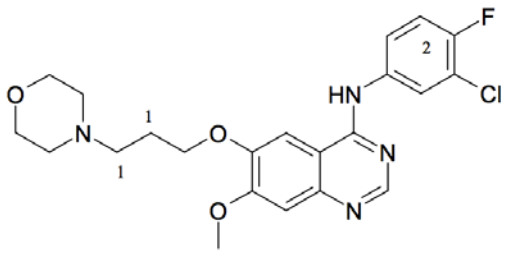


*Figure 1.3. Chemical structure of N-(3-chloro-4-fluorophenyl)-7-methoxy-6-(3 morpholinopropoxy)quinazolin-4-amine*

*Table 1.3. Physicochemical properties of gefitinib and erlotinib.*

| Physicochemical properties | Gefitinib | Erlotinib |
|---|---|---|
| pKa values | 5.4 and 7.2 | 5.4 |
| Aqueous solubility | Sparingly soluble at pH 1. Practically insoluble above pH 7 (sharp solubility dropt between 4 and 6) | Increased solubility at at pH < 5. Maximal solubility of 0.4 mg/mL occurs at pH 2. |

## Pharmacokinetic characteristics

TKIs erlotinib and gefitinib present substantial differences when compared with traditional cytotoxic chemotherapeutic agents. Firstly, these drugs are orally administered. For orally administered drugs, pharmacological action is dependent on adequate intestinal absorption and distribution before elimination via metabolic and excretory pathways. Secondly, traditional cytotoxic chemotherapeutic agents are administered according to patient's body surface area, whereas TKIs are orally given on a daily basis at fixed doses. PK characteristics of these drugs (summarized in Table 1.4) should be understood in order to optimize pharmacotherapy.

*Table 1.4. Pharmacokinetic properties of gefitinib and erlotinib.*

| Pharmacokinetic properties | Gefitinib | Erlotinib |
|---|---|---|
| Usual starting dose (mg/day) | 250 | 150 |
| $t_{max}$ (h) | 3–7 | 4 |
| Vd/f (L) | 1700 | 232 |
| Protein binding (%) | ~90 | ~95 |
| $t_{1/2}$ (h) | 48–72 | 36 |
| f (%) | ~60 | ~76 |
| CL/f (L/h) | 46 | 4.5 |
| Metabolism | Extensive | Extensive |
| Renal excretion | 4% | ~9% |
| Accumulation | 1.5 to ~4-fold | 1.5 to 5.4-fold |
| Gastric pH effect | Reduces absorption | Reduces absorption |
| Food effect | Not relevant | AUC ↑34–66% |
| Age effect | None reported | None reported |
| Weight effect | None reported | None reported |
| Gender effect | None reported | None reported |
| Race Effect | None reported | None reported |
| Potential drug interactions | CYP enzymes | CYP enzymes |

*$t_{max}$: time to reach maximum plasma concentration since drug administration; Vd: volume of distribution; f: bioavailability; $t_{1/2}$: elimination half life; CL: Clearance.*

Molecular PK determinants of erlotinib and gefitinib can play an important role in therapeutic outcomes. Patients receiving TKIs are at great risk of over- or under exposure because of PK modifications

involving molecular kinetic determinants (drug metabolizing enzymes and drug transporters). Table 1.5 summarises the main molecular PK determinants for erlotinib and gefitinib reported in the review by Scholler et al. (86).

*Table 1.5 Known interactions of erlotinib and gefitinib as substrates of human pharmacokinetic determinants (enzymes and drug transporters)*

| Pharmacokinetic determinant | Erlotinib | Gefitinib |
|---|---|---|
| CYP3A4 | Yes | Yes |
| CYP3A5 | - | Yes |
| CYP2D6 | No | Yes |
| CYP1A1 | Yes | Yes |
| CYP1A2 | Yes | No |
| CYP2C8 | No | - |
| CYP2C9 | No | No |
| CYP2C19 | - | No |
| P-gp | Yes | No |
| MRP | No | - |
| BCRP | Yes | Conflicting |

*P-gp: P-glycoprotein; MRP: Multidrug resistance protein; BCRP: Breast cancer resistance protein.*

**Pharmacokinetics-pharmacodynamics relationship**

These TKIs inhibit the adenosine triphosphate-binding site of TK receptors in malignant cells, thereby inhibiting the autophosphorylation of the tyrosine residues, and thus prohibit activation of proteins involved

in the angiogenesis and tumour proliferation signalling. Given that a exposure–response relationship has been identified for several tyrosine kinase inhibitors for several therapeutic indications, the individualization of dosing schedules based on individual pharmacokinetic parameters can result in improved therapeutic outcomes.

In preclinical studies for **erlotinib**, much information has been generated regarding exposure-response relationship (87). In one of the first preclinical studies, erlotinib displayed activity and sensitivity at concentrations of 215 ng/mL when tested on NSCLC cell lines. Some years later, results generated in several preclinical experiments were summarized, and a concentration of 500 ng/mL was suggested to be the target trough concentration in humans to achieve the necessary EFGR inhibition in order to cause a relevant anti-proliferative effect (87). Accordingly, in the clinical study presented by Perez-Pitarch et al., where response was evaluated as time to progression through a time to event model, and exposure was based on simulated erlotinib concentrations, erlotinib concetrations of 116 ng/mL caused 50% of the maximum response, and concentrations of 500 ng/mL where associated to approximately 80% of the maximum response (Figure 1.4) (88).

Regarding exposure-safety relationship, consistent evidence can be found in the literature. Plasma concentrations have been correlated with skin toxicity. A study carried out in NSCLC patients suggested that those patients with trough concentrations above 1,810 ng/mL were expected to develop grade 3 skin-toxicity (87).

Even though a definitive pharmacokinetic target has not been established yet, considering the available evidence, some hospitals

already carry out therapeutic drug monitoring for erlotinib plasma concentrations in daily clinical practice.

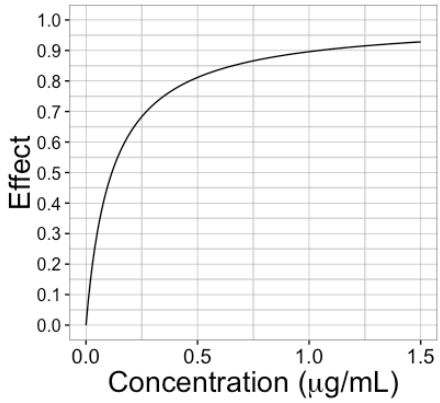


*Figure 1.4. Exposure-response relationship curve for erlotinib (88).*

A few studies explored the exposure–response relationship for **gefitinib** (87). Zhao et al. showed that in patients with advanced NSCLC, 10 % with mutated EGFR and 90 % with wild type EGFR, a $C_{trough}$ > 200 ng/mL was associated with significantly longer median OS (14.6 vs. 4.7 months, p = 0.009) and a higher incidence of rash (85.7 vs. 42.9 %, p = 0.043) than in patients with a $C_{trough}$ < 200 ng/mL. In patients with wild-type EGFR, a $C_{trough}$ > 200 ng/mL predicted higher median OS (16.8 vs. 4.1 months, p = 0.002).

There is no definitive exposure–response relationship established for gefitinib in EGFR-mutated NSCLC patients. However, based on the available evidence, a $C_{trough}$ of 200 ng/mL may be used for therapeutic drug monitoring in patients with NSCLC.

## 1.5 Pharmacokinetic modelling

### 1.5.1 Introduction to pharmacokinetic modelling

Modelling methods have evolved and population-modelling methods have been incorporated into pharmaceutical research to provide a framework for quantitating and explaining drug exposure and response. Population modelling methods have enabled to identify and describe relationships between a subject characteristics and observed drug exposure or response. Population pharmacokinetics, upon which nonlinear mixed effects models were developed, is the study of the pharmacokinetics of a drug in a population of subjects taking into account the different levels of variability (between-subject, within-subject, inter-occasion, residual, etc.).

In the field of pharmacokinetics, experimental data require the fit of non-linear equations capable of describing the relationship between drug concentrations and time. The complexity of underlying models composed of systems, organs and tissues through which drugs distribute, cannot be fully described by mathematical equations and thus, assumptions are required to simplify the process. Pharmacokinetic models are based on the “compartmentalization” of the body, assuming that a compartment represents a region of the body in which the drug is kinetically homogeneous. Models describing pharmacokinetics in mammals in general have a central compartment representing plasma and in some occasions with one or more peripheral compartments linked to the central compartment by rate constants (Figure 1.5). More

complex models can be built, but in order to design physiologically-based PK models, tissue and plasma concentrations are required. On the other hand, models built with fewer compartments can be generally informed by blood or plasma concentrations alone, and are probably sufficiently robust for most pharmacokinetic analysis purposes.

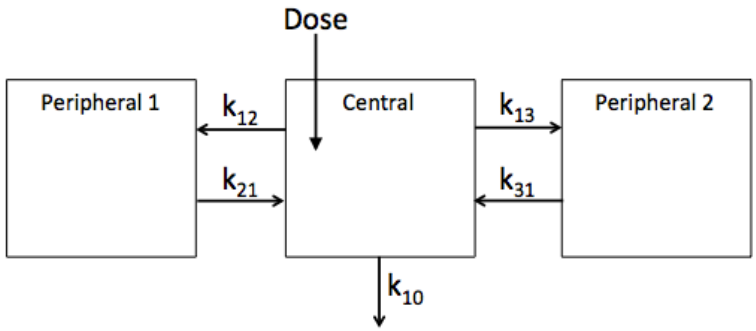


*Figure 1.5. Schematic representation of 3-compartment model composed of a central compartment and 2 peripheral compartments linked to the central compartment by rate constants k12, k21, k13 and k31.*

In order to describe pharmacokinetic models, nonlinear functions (algebraic or differential) are designed to describe the time course of drug concentrations. Simple pharmacokinetic models (such a one-compartment model) can be described with algebraic equations, but certain analyses require more complex pharmacokinetic systems that cannot be stated with algebraic equations. This problem can be overcome employing systems of differential equations. The pharmacokinetic model described in Figure 1.5 can be written as the following system of differential equations:

$$\frac{dC}{dt} = -C \cdot k_{12} - C \cdot k_{13} + P1 \cdot k_{21} + P2 \cdot k_{31} - C \cdot k_{10} \quad \textit{Equation 1.1}$$

$$\frac{dP1}{dt} = C \cdot k_{12} - P1 \cdot k_{21} \qquad \textit{Equation 1.2}$$

$$\frac{dP2}{dt} = C \cdot k_{13} - P2 \cdot k_{31} \qquad \textit{Equation 1.3}$$

where $\frac{dC}{dt}$, $\frac{dP1}{dt}$ and $\frac{dP2}{dt}$ represent the instantaneous variation rates of drug concentrations in the central, peripheral 1 and peripheral 2 compartments respectively; C, P1 and P2 represent drug concentrations in the central, peripheral 1 and peripheral 2 compartments; $k_{12}$, $k_{21}$, $k_{13}$, and $k_{31}$ represent the first order rate constants linking peripheral compartments with the central compartment and; $k_{10}$ represents the first order elimination rate constant governing drug elimination from the central compartment. In pharmacokinetic models, differential equations describe the rate of change of drug concentration in each compartment. This approach can deal with more complex structural models, but numerical methods needed to solve systems of differential equations can be computationally intensive.

### 1.5.2 Structural, statistical and covariate models

Nonlinear mixed effects models consist of two main components: the structural model (mean response for the population) and the statistical or variance model. Non-linear mixed effects models may or may not include a covariate model.

**Structural model**

The first step during the model building procedure is to develop the structural model describing how the mean response profile changes over time:

$$Y = f(t;\beta) + \varepsilon \qquad \textit{Equation 1.4}$$

where *t* is time, β is a vector of estimable regression parameters and ε is the residual error. The regression function *f* depends on β in a nonlinear manner and can be designed as algebraic or differential equations as described previously in this section. If previous studies have described a structural model for the process that is going to be evaluated, the model selection can start from that one. If there is no previous information of which structural model to use, the first step would be to try a variety of base models (one-, two, three-compartments) and choose the best model using a combination of selection criteria such as minimum objective function value (MOFV), graphical examination using residual plots, etc.

**Statistical model**

In a population analysis, there are usually two sources of variability: between-subject variability (BSV), and residual variability (RV). BSV refers to the variance of a parameter across different individuals in the population. RV refers to the unexplained variability in the observed data after controlling other sources of variability.

Certain parameters in models are not expected to be constant across individuals. In the clinical setting it is often obvious that patients do not respond in the same way to treatments, and this happens due to pharmacokinetic and/or pharmacodynamic BSV variability. Hence, a model may consist of some parameters that are fixed across all individuals and some parameters that are allowed to vary across individuals. In pharmacokinetic studies in which variability across individuals is going to be estimated, an exponential model is often

chosen since pharmacokinetic model parameters must be constrained to be greater than zero.

All the variability that is not explained by the model and that is model misspecifications, assay errors, dosing history errors, etc., is lumped into RV. This is called the residual variance model.

**Covariates model**

In pharmacokinetic studies, a covariate is defined as any variable that is specific to an individual and may influence the pharmacokinetics of a drug. Covariates can be classified as intrinsic factors, such as age, weight, height, and race, or extrinsic factors, such as dose, degree of compliance, smoking status, and presence of concomitant medications.

One of the most important reasons for using a population approach when modelling pharmacokinetic data is that covariates can be built into the model through their associations with model parameters. For example, if volume of distribution depends on the weight of subjects, then weight can be introduced into the model. By building this covariate into the model, BSV and RV are reduced. When covariates are identified and their influence on pharmacokinetic parameters is sufficiently high to cause a big reduction on BSV, models can even be used to individualize dosing schedules based on patients' characteristics.

## 1.6 Objectives

The main objective of this thesis was to evaluate the impact of undernourishment on the pharmacokinetics of erlotinib and gefitinib in rats.

In order to achieve this general objective, the following partial objectives were defined:

- To evaluate the impact of undernourishment on analytical and molecular biomarkers.
- To analyse the impact of undernourishment on erlotinib and gefitinib absorption in rats through *in-situ* intestinal perfusion studies.
- To determine the impact of undernourishment on the pharmacokinetics of erlotinib and gefitinib in rats through *in vivo* pharmacokinetic studies.

# 2 Materials and Methods

## 2.1 Study design

Experiments were performed in male Wistar rats in accordance with 2010/63/EU directive of 22 September 2010 regarding the protection of animals used for scientific experimentation. The Ethics Committee for Animal Experimentation of the University of Valencia approved the experimental protocols (code A1326906234491 and 2016/VSC/PEA/00101; Appendix 7.1).

The research investigation was divided into 3 main experiments (as shown in Figure 2.1):

- Evaluation of analytical and molecular alterations associated with undernourishment
- *In situ* intestinal perfusion studies
- *In vivo* PK studies

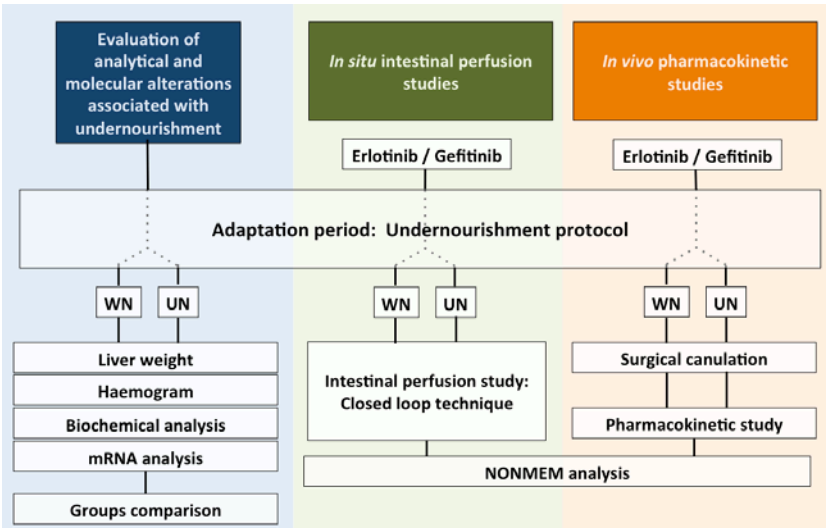


*Figure 2.1. Schematic representation of study-design. WN: well-nourished group, UN: undernourished group.*

In all experiments, rats were randomised into well-nourished (WN) and undernourished (UN) groups. Rats underwent an adaptation period under a nutritional protocol described in the following sections (80). *In situ* intestinal perfusion studies and *in vivo* PK studies were performed for 2 drugs: erlotinib and gefitinib.

In the *in situ* intestinal perfusion studies and *in vivo* PK studies for erlotinib and gefitinib, rats were randomized to different groups in which they received different drug dispersion systems through different administrations routes. Dose, administration route and additives employed for *in situ* and *in vivo* assays are shown in Tables 2.1 and 2.2, respectively. Each rat received a single dose of the investigated drug.

*Table 2.1. Groups for the in situ intestinal perfusion studies.*

| Investigated drug | | Additive compound | | Nutritional status | |
|---|---|---|---|---|---|
| Name | Concentration (μg/mL) | Name | Concentration (μg/mL) | WN (n) | UN (n) |
| Erlotinib | 20 | - | - | 5 | 5 |
| | 20 | Levofloxacin | 600 | 5 | 5 |
| | 8 | - | - | 5 | 5 |
| | 8 | Levofloxacin | 600 | 5 | 5 |
| Gefitinib | 40 | - | - | 9 | 9 |
| | 8 | - | - | 7 | 7 |
| | 40 | Sodium azide | 6500 | 8 | 8 |

*WN: well-nourished group; UN: undernourished group; n: rats per group.*

*Table 2.2. Groups for the in vivo pharmacokinetic studies*

| Investigated drug | Administration route | Dose (mg) | Nutritional status | |
|---|---|---|---|---|
| | | | WN (n) | UN (n) |
| Erlotinib | Intravenous (solution) | 3.34 | 4 | 5 |
| | Oral (solution) | 3.34 | 7 | 9 |
| | Oral (suspension) | 3.34 | 8 | 9 |
| Gefitinib | Intravenous (solution) | 0.495 | 7 | 5 |
| | Oral (suspension) | 6.5 | 4 | 5 |

*WN: well-nourished group; UN: undernourished group; n: rats per group.*

## 2.2 Assayed drugs

Erlotinib and gefitinib were administered in different drug dispersion systems. In the following section, used drug preparations are described.

### 2.2.1 Erlotinib

In order to perform the *in situ* intestinal perfusion studies, erlotinib hydrochloride (Apollo scientific Ltd.) and levofloxacin hydrochloride (Normon Laboratories, Madrid, Spain) were dissolved in saline solution to obtain solutions of different erlotinib concentrations in absence or presence of levofloxacin. Assayed erlotinib concentrations were 8 μg/mL and 20 μg/mL, and the assayed levofloxacin concentration was 600 μg/mL. All solutions were buffered to pH 6.4 by addition of 1% (V/V) Sørensen phosphate buffer solution in order to reproduce intestinal lumen pH conditions and had 1% (V/V) dimethyl sulfoxide in order to facilitate solubility of erlotinib and ensure that no precipitation took place during *in situ* assays.

In order to perform the *in vivo* PK study, Tarceva® film-coated tablets containing 100 mg of erlotinib were used (Roche Farma S.A, Madrid, Spain). Erlotinib solution was prepared by combining finely pulverised tablets and a mixture containing 20% propylene glycol, 30% ethanol and 50% bi-distilled water. Solutions at 3.34 mg/mL were then prepared for intravenous (IV) and oral administration. In addition, an oral suspension system at 3.34 mg/mL was prepared by dispersing the required amount of pulverised tablet using water as a solvent. Each rat received 1mL of the corresponding drug preparation. The selected dose of erlotinib (3.34 mg) was based on an allometric transposition of the dose used in humans as calculated by:

$$AED = HED \times RCN \qquad \textit{Equation 2.1}$$

where AED is the animal equivalent dose in mg/Kg, HED is the human equivalent dose in mg/Kg and RCN is the interspecies conversion number, for rats RCN = 6.2 (89).

### 2.2.2 Gefitinib

In order to perform the intestinal perfusion studies, different solutions of gefitinib in presence or in absence of sodium azide were prepared. Assayed gefitinib concentrations were 8 μg/mL and 40 μg/mL in free solutions. Additionally, a gefitinib solution (40 μg/mL) with sodium azide (6500 μg/mL) was assayed. All solutions were buffered to pH 5.0 by addition of 1% (V/V) Sørensen phosphate buffer solution and had 1% (V/V) dimethyl sulfoxide in order to facilitate solubility of gefitinib and ensure that no precipitation took place during *in situ* assays.

On the other hand, in order to perform the *in vivo* pharmacokinetic study for gefitinib, different drug dispersion systems were assayed for IV and oral administration: the IV administration consisted in a single bolus injection of 1.5 mL solution at 0.33 mg/mL gefitinib (dose = 0.495 mg) in an aqueous 10% (w/w) hydroxypropyl-β-cyclodextrin (CAVASOL® W7-HP, Wacker Ibérica, Barcelona, Spain) solution; the oral dispersion system consisted in a 6.5 mg/mL aqueous suspension (dose = 6.5 mg). The selected dose of gefitinib for IV administration was limited by its solubility whereas for oral administration it was based on an allometric transposition of the dose used in humans calculated as described in Equation 2.1 (89).

## 2.3 Undernutrition protocol

Adult male Wistar rats proceeding from controlled colonies were employed. All the animals were housed in individual cages at the same temperature (22-23ºC), humidity (50-60%) and under 12-hour light/darkness cycles.

In order to provoke the adequate protein energy malnutrition (PEM), a malnutrition protocol developed and published by Merino-Sanjuán et al. was employed (80).

Animals were randomly distributed into two trial groups: WN and UN. Both groups had free access to drinking water and restricted access to food. The WN group was fed a normal daily requirement diet for rats (20 g/60.2 kcal; 14% protein) and the UN group was fed a low

protein-calorie diet (10 g/38 kcal; 5% protein) (Harlan Laboratories, Santa Perpetua de Mogoda, Spain).

All rats received the assigned diet for a period of 23-26 days. At the end of the adaptation period, body weight and serum albumin were measured using commercial kits (Química Clínica Aplicada S.A, Amposta, Spain). Weight and serum albumin levels were used as inclusion criteria and to assess nutritional status. Rats were classified into different nutritional status levels according to a score system developed by Merino-Sanjuán et al. based on a human nutritional status screening-tool (80).

## 2.4 Surgical procedures

Three different surgical procedures were employed in this research project: blood and tissue samples extraction, intestinal cannulation for *in situ* intestinal perfusion studies and jugular cannulation for *in vivo* pharmacokinetic studies.

Prior to surgical interventions, anaesthesia was induced. The anaesthetic sodium pentobarbital was administered (dose 30 mg/kg) by intra-peritoneal route. The anaesthesia was prepared by diluting 1:9 sodium pentobarbital 20% (W/V) (Eutanax®, Laboratorios Normon S.A., Madrid, Spain) in physiologic saline (Simple sodium chloride. Braun S.A). Once the anaesthesia had been induced, the analgesic and anti-inflammatory butorphanol tartrate (Torbugesic®, Fort Dodge, S.A., Girona, Spain) was administered subcutaneously (0.5 mg/kg).

### 2.4.1 Blood and tissue sampling

In order to obtain blood and tissue samples, the following surgical procedure was performed. The abdomen was opened and the intestine was washed with phosphate buffer saline at pH 7.4 (Gibco). Thereafter, intestine was rapidly excised and divided into three segments (proximal, middle and distal intestine), which were then clamped and frozen in liquid nitrogen. Rats were then exsanguinated by cardiac puncture and blood samples were collected in citrate or heparin tubes. Samples were stored at -80° C until analysis. Finally, the liver was carefully extracted and weighted, clamped and frozen in liquid nitrogen for posterior analysis.

### 2.4.2 Intestinal cannulation

Intestinal absorption was evaluated by an *in situ* "closed loop" perfusion method based on the Doluisio-technique (90). In order to carry out these assays, the proximal and distal segments, corresponding to the first and last third of the small intestine, were cannulated. The objective of the surgical procedure was to obtain closed loops (isolated compartments) in which drug solutions were going to be administered and sampled from (Figure 2.2).

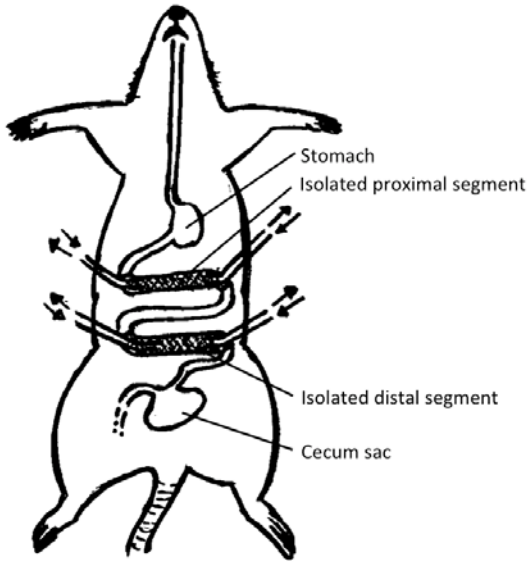


*Figure 2.2. Schematic representation of perfusion method based on the Doluisio-technique showing isolation of intestinal segments.*

An incision was made in the abdominal midline of the animal. The bile duct was ligated in order to avoid drug enterohepatic circulation and presence of bile salts in the lumen of proximal segment. For the first segment, two small incisions were practiced, the first one at the beginning of the duodenum and the second one, at a distance of 33 cm from the first incision. Surgical ligature to a catheter was placed at the first incision. The catheter was connected to a glass syringe using a three-way stopcock valve. The intestinal lumen was cleaned and conditioned with isotonic saline (pH 6.4) with 1% Sørensen phosphate buffer (V/V) at 37 °C until mucosa was free of chime-traces. Subsequently, air was pumped through the intestine to completely remove the residual washing liquid and to avoid excessive dilution of the drug solution. Another catheter was introduced at the second

incision and connected to another valve and syringe. Analogously, in order to isolate the distal small intestine segment, an oblique incision was made at the end of the ileum portion just before the cecum sac and the second one at a distance of 33 cm from this incision. Then, surgery was performed as described above and this segment was cleaned with isotonic saline (pH 7.4) with 1% Sørensen phosphate buffer (V/V) at 37°C. Next, intestine was carefully placed back into the peritoneal cavity and covered with a cotton pad saturated with isotonic saline at 37°C to avoid losses of liquid and heat that could alter the mesenteric blood flow.

### 2.4.3 Jugular cannulation

In order to perform the *in vivo* PK studies, rats were subjected to jugular vein cannulation on the day before drug administration. Rats under anaesthesia were subjected to jugular vein cannulation with a 15 cm-long fragment of medical-grade silicone tubing (inner diameter: 0.6 mm; R602-155) (Degania Silicone Ltd, Degania, Israel). 3.4 cm of the cannula were introduced into the jugular vein in the direction of the heart and the free end was subcutaneously conducted to the dorsal base of the neck, where it emerged. The cannula, previously filled with heparinized saline solution (20 IU/L), was closed on its exteriorised end with a polyethylene plug. Animals were fasted 4 hours prior to drug administration in order to prevent food-drug pharmacokinetic interaction, but were allowed free access to water.

## 2.5 Assay protocols

### 2.5.1 *In situ* intestinal perfusion assays

Drug administration and sampling were done with the aid of the syringes and stopcock valves through the surgically implanted intestinal cannulas. At the start of the assay, drug solutions (5 mL at 37°C) were introduced through the intestinal cannulas into each of the isolated intestinal segments. Samples of 200 µL were collected every 5 minutes up to a period of 30 minutes. At the end of the experiments, the remaining volume of intestinal perfusion solution was measured in order to calculate water absorption rate.

### 2.5.2 *In vivo* pharmacokinetic assays

Drug administrations were performed through the IV and the oral route. For IV administration, the required volume of the previously described solutions was loaded into a syringe. The syringe was then connected to the cannula emerging from the back of the rat and the dose was administered. In order to ensure complete administration, a sufficient amount of heparinized saline solution was flushed through the cannula. On the other side, for oral administration the required volume of the previously described dispersion systems (solution or suspension) was loaded into a syringe connected to a gavage cannula. The gavage cannula was introduced through the mouth, descending down the oesophagus, into the stomach where the syringe was unloaded.

Blood samples were obtained through the surgically implanted cannula. Blood samples (0.1 mL) were collected during an 8-hour

period in the case of rats receiving the IV erlotinib dose and over 27 hours in rats receiving the oral erlotinib dose. Blood samples were collected over a 30-hour period for rats receiving gefitinib (both, intravenously and orally administered). The number of samples processed in a 24-hour period was never higher than 10, in order to prevent an acute decrease of haematocrit. In all cases, the sampled volume was replaced with the same volume of saline solution. Blood samples were centrifuged at 8000 rpm for 10 minutes and the plasma was transferred to polypropylene tubes and stored at -20ºC until drug quantitation.

## 2.6 Analytical methods

### 2.6.1 mRNA quantitation

In order to perform protein enzyme expression measurements, liver and intestinal tissue samples were homogenized in TRIzol reagent (Invitrogen), and total RNA was isolated by the chloroform: phenol method (Sigma-Aldrich, St. Louis, MO). For mRNA detection, the isolated RNA was reverse-transcribed into cDNA using the Revert Aid kit (Thermo Fisher Scientific, Waltham MA, Fermentas). mRNA were quantified by qRT-PCR on a thermal cycler (Biorad I-Cycler + IQ Multicolor Real Time OCR Detection System) by using SYBR Green PCR Master Mix (Takara). The threshold cycle (Ct) was determined, and relative gene expression levels were subsequently calculated as $2^{-\Delta\Delta Ct}$. Results were normalized using β-actin as the housekeeping

gene. The qRT-PCR assays were performed in triplicate. Primers used for qRT-PCR experiments are shown in Table 2.3.

*Table 2.3. Primers used for qRT-PCR experiments in hepatic and intestinal tissues.*

| Gene | Hepatic tissue<br>Sequence (5'→3') | Intestinal tissue<br>Sequence (5'→3') |
|---|---|---|
| Cyp1A1 | F. TGAGTTTGGGGAGGTTACTGGTT<br>R. TGAAGGCATCCAGGGAAGAGT | F. TGAGTTTGGGGAGGTTACTGGTT<br>R. TGAAGGCATCCAGGGAAGAGT |
| Cyp 1A2 | F. TGCTCAACCTCGTGAAGAGC<br>R. GTGATGTCCTGGATACTGTTCTTG | |
| UDP | F. CTTCTTGGTCATCCAAAAACTAAGG<br>R. CCTTCAGTGCGTTGAGCAAA | |
| OATP | F. TTGGACCAATCCTTGGCTTT<br>R. ACAATGAAGCTGAGCCACCA | |
| MRP2 | F. TTGCCCATTATCCGTGCCTT<br>R. CAAGCCACCTGTTGGAGGTA | F. TTGCCCATTATCCGTGCCTT<br>R. CAAGCCACCTGTTGGAGGTA |
| P-gp | F. AACACCCTGGTTGGTGAGAG<br>R. GCACTGTAGACAAGCGGTGA | F. CATTGCTGGTTTTGATGGTG<br>R. CTGGATCCCGAATCTTTTGA |
| Actin | F. GGAGATTACTGCCCTGGCTCCTA<br>R. ACTCATCGTACTCCTGCTTGCTG | F. GGAGATTACTGCCCTGGCTCCTA<br>R. ACTCATCGTACTCCTGCTTGCTG |

*F: forward; R: reverse; UDP: Uridine 5'-diphospho-glucuronosyltransferase; OATP: organic anion-transporting polypeptide; MRP2: multidrug resistance protein 2; P-gp: P-glycoprotein.*

## 2.6.2 Whole blood and serum analysis

Whole blood aliquots were used for the analysis of red blood cell count, white blood cell count, platelet count, haemoglobin concentration, haematocrit and mean corpuscular volume. Serum samples were used for the analysis of alanine aminotransferase (ALAT/GPT), aspartate aminotransferase (ASAT/GOT), total protein concentration, acid-alpha glycoprotein concentration, and serum

protein electrophoresis bands (albumin, alpha-1 alpha-2, beta, gamma). Reagent kits were purchased from Spinreact (Girona, Spain).

### 2.6.3 Drug quantitation

Drug concentrations were quantified in different matrices. For this reason, different analytical techniques were employed for intestinal perfusion solution samples and for plasma samples. In this section, quantitation methods will be described separately for erlotinib and gefitinib with regard to sample preparation procedures and chromatographic conditions.

All quantitation methods were validated with regard to linearity, precision, accuracy and lower limit of quantification (LLOQ). Linearity was evaluated through least squares regression. Precision and accuracy were determined by analysing three quality control (QC) samples at different concentration levels. Estimated concentrations were used to estimate accuracy, as the relative error (RE), and precision, as the coefficient of variation (CV). The LLOQ was defined as least ten times the signal of a blank sample.

**Erlotinib**

Plasma and intestinal perfusion solution samples were assayed for erlotinib concentration by high-performance liquid chromatography (HPLC). Sample preparation differed for intestinal perfusion samples and plasma:

- Intestinal perfusion solution samples: Intestinal samples were centrifuged at 10000 rpm for 10 minutes at room temperature in order to separate solid components (mucus and intestinal

contents). The supernatant was separated and injected into the HPLC-system.

- Plasma samples: 50 µL of plasma samples were mixed with 50 µL of acetonitrile at -20ºC in order to precipitate proteins. Tubes were vortexed at maximum speed for 3 minutes and then centrifuged at 8000 rpm for 10 minutes at room temperature. The supernatant was separated and injected into the HPLC-system.

The chromatographic system consisted of a Flexar PerkinElmer liquid chromatography system equipped with a Flexar UV/VIS detector. Separation of the analyte was achieved at room temperature using an ultrabase C18 reversed-phase analytical column (250 mm x 4.6 mm, 5 µm particles) (Analisis Vinicos S.L, Ciudad Real, Spain) protected by a guard column. The mobile phase consisted of acetonitrile: sodium citrate buffer (50:50, v/v) (pH 4.8). The flow rate was set to 1.6 mL/min and injection volume was 50 µL. The detector was set at a wavelength of 345 nm (91). Data were collected and analysed using the TotalChrom software (version 6.3.2).

Calibration curves were built for the quantitation of erlotinib in intestinal perfusion solution and plasma samples covering a concentration range between 0.2 and 20 µg/mL.

**Gefitinib**

- Intestinal perfusion solution samples: Samples were centrifuged at 10000 rpm for 10 minutes at room temperature in order to separate solid components (mucus and intestinal contents). The supernatant was then separated and injected into the HPLC

system. Gefitinib concentrations were determined chromatographically using an Agilent 1100 HPLC equipped with a UV detector (330 nm) using a Nova-Pak® C18 column, 3.9 × 150 mm, 4 µm (Waters, Barcelona, Spain). Mobile phase consisted of acetonitrile/water acidified with trifluoroacetic acid (0.1%, pH = 2.5) (55:45). Flow rate was set to 1.0 mL/min and injection volume was 50 µL. Integration was carried out by Agilent ChemStation software (version B.04).

Two calibration curves were built for the quantitation of gefitinib in intestinal perfusion solution samples covering concentration ranges between 0.4 and 12 µg/mL and between 12 and 40 µg/mL, respectively.

- Plasma samples: Sample preparation procedure consisted in mixing 50 µL of plasma sample with 100 µL of acetonitrile at -20ºC in order to precipitate proteins. Tubes were vortexed at maximum speed for 3 minutes and then centrifuged at 13000 rpm for 10 minutes at room temperature. The supernatant was separated and injected into the liquid chromatography-tandem mass spectrometry (LC-MS/MS) system. The mass spectrometer system (Water ACQUITY® TQD) was equipped with a Z-spray electrospray ionization source. The column used in the analyses was a Nova-Pak® C18 column, 3.9 × 150 mm, 4 µm (Waters, Barcelona, Spain). Mobile phase consisted in acetonitrile/water (90:10, V/V). Flow rate was set to 1.0 mL/min and injection volume was 50 µL. Integration was carried out by MassLynx software (version 4.1).

A calibration curve was built for the quantitation of gefitinib in plasma samples covering a concentration range between 0.5 and 1000 ng/mL.

## 2.7 Pharmacokinetic analysis

Pharmacokinetic analysis was performed for the *in vivo* pharmacokinetic studies and for the *in situ* intestinal perfusion studies for gefitinib and erlotinib.

*In situ* intestinal perfusion studies evaluated drug absorption process. In these studies the experimental data used for pharmacokinetic analysis were perfusion solution drug concentrations-time pairs of values. *In vivo* pharmacokinetic studies evaluated LADME processes (liberation, absorption, distribution, metabolism and excretion). In these studies the experimental data used were total plasma drug concentrations-time pairs of values. An initial graphical exploration of these data was performed in order to guide the subsequent model development of each sub-experiment.

Thereafter, pharmacokinetic models were developed through non-linear mixed effects modelling using the NONMEM software, version 7.3 (92) in conjunction with a GFORTRAN compiler and the PsN-Toolkit (93). The first order conditional estimation (FOCE) method was implemented. Different subroutines were used; namely ADVAN 3, 6 and 9.

Developed models included structural, statistical and covariates models. In the following sections these models are described.

### 2.7.1 Structural model

A stepwise population pharmacokinetic approach was carried out. Models were developed sequentially so that, whenever modifications had to be made to the model, a backwards procedure was performed. The following sections describe general structural model building procedures used for drug absorption modelling (*in situ* data) and LADME modelling (*in vivo* data).

**Absorption process modelling**

The absorption process was evaluated through the development of models describing intestinal perfusion data. During the development of models for intestinal perfusion assays, concentration-time profiles in proximal and distal intestine were analysed independently. In order to consider the influence of volume reduction on drug concentration during the study period, the predicted remaining volume ($V_t$) was calculated as follows:

$$V_t = 5 + \left(\frac{V_{30}-5}{30}\right) \cdot t \qquad \textit{Equation 2.2}$$

where $V_t$ is the predicted remaining perfusion solution volume at time t, $V_{30}$ is the observed remaining perfusion solution volume at the end of the experiment (30 minutes) and $t$ is the sampling time in minutes. Water absorption was assumed to be characterized as an apparent zero order process (94).

Additionally, due to initial membrane adsorption of the solute, sample dilution and or presence of rapid metabolism, the calculated concentration at time 0 is usually lower than the initial perfused concentration. In order to overcome this effect, the inclusion of a

correction fraction (*fr*) was tested in the model to account for the fraction of initial concentration available for absorption from the intestinal lumen to the enterocyte (95).

In order to describe drug concentration-time profiles in small intestine of rats, compartments were considered for the development of a mechanistic population pharmacokinetic model. If compartmental analysis was not capable of describing data accurately, an empirical population pharmacokinetic model (i.e. Weibull model) was fitted to the experimental data in order to get an appropriate description of drug concentration profiles. Both approaches are outlined below.

Mechanistic population pharmacokinetic models consisted on two compartments representing intestinal lumen and enterocyte (Figure 2.5). Different combinations of passive, active or combined (passive and active) kinetics for the absorption and secretion processes of the investigated drug were considered during the model building procedure (Table 2.4). It has been previously described that a dynamic equilibrium between intestinal lumen and enterocyte is achieved in the first five minutes since the start of the perfusion. Consequently, concentration inside the enterocyte (E) and concentration in the intestinal lumen (L) are proportional, and the use of L as representative of the E is justified.

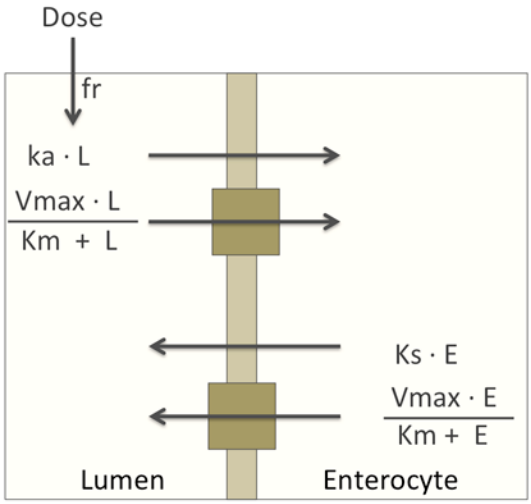


*Figure 2.5. Schematic representation of tested absorption and secretion mechanisms. Vertical line represents enterocyte apical membrane; brown squares represent absorption and secretion transporter systems. L and E: drug concentration in lumen and enterocyte, respectively; fr: correction factor; ka: first order absorption rate constant; ks: apparent first order secretion rate constant; Vmax: maximum transport rate; Km: Michaelis Menten constant.*

*Table 2.4. Mechanistic models describing drug absorption and secretion processes.*

| Mechanisms | | Differential equation |
|---|---|---|
| Absorption | Secretion | |
| First order | None | $\frac{dL}{dt} = -L \cdot ka$ |
| First order | First order | $\frac{dL}{dt} = -L \cdot ka + L \cdot ks$ |
| Michaelis-Menten | First order | $\frac{dL}{dt} = -\frac{Vmax_a \cdot L}{Km_a + L} + L \cdot ks$ |
| First order | Michaelis-Menten | $\frac{dL}{dt} = -L \cdot ka + \frac{Vmax_s \cdot L}{Km_s + L}$ |
| Michaelis-Menten | Michaelis-Menten | $\frac{dL}{dt} = -\frac{Vmax_a \cdot L}{Km_a + L} + \frac{Vmax_s \cdot L}{Km_s + L}$ |

*dL/dt: drug disappearance rate from intestinal lumen; L: drug concentration in intestinal lumen; ka: first order absorption rate constant; ks: first order secretion rate constant; $Vmax_a$: maximum absorption rate; $Km_a$: Michaelis Menten absorption rate constant; $Vmax_s$: maximum secretion rate; $Km_s$: Michaelis Menten secretion rate constant.*

If a mechanistic description of experimental data was not acceptable, data were fitted to a Weibull model, as described by the following equation:

$$\frac{dL}{dt} = -\frac{\alpha \cdot L}{\beta} \cdot \left(\frac{t}{\alpha}\right)^{\beta - 1} \qquad \textit{Equation 2.3}$$

L represents drug concentration in intestinal lumen. The scaling factor α (hours$^{-1}$) is proportional to the slope of the disappearance kinetics, and the shape factor β (dimensionless) determines the curvature of the disappearance kinetics. This equation converges to a first order equation when β=1, and under this conditions α represents the first order absorption rate constant.

In those cases in which a Weibull model was used to describe intestinal drug absorption, datasets for both intestinal segments were merged together and modelled simultaneously.

**LADME modelling**

Models were developed in order to describe data obtained from *in vivo* pharmacokinetic assays. These models had different structures to those tested for *in situ* data. Data were analysed in a sequential manner:

1) A structural model was built to describe IV administration data. One- and two- compartment models were tested. Linear elimination was implemented. To our knowledge, non-linear clearance models have not been previously described for the studied drugs and thus were not considered during model selection process. Volume of distribution parameters and clearance parameters were scaled on body mass as described in the covariates model section.

2) Estimated model parameters in step 1 were fixed. Oral administration data were incorporated into the dataset. All the data were analysed simultaneously to build a structural model for drug absorption linked to the model developed in step 1. If necessary, the use of intestinal transit compartments was explored by adding compartments until model fit did not improve significantly.

3) Finally, all parameters in the final model were estimated simultaneously.

## 2.7.2 Statistical model

Between-subject variability (BSV) was studied in all model parameters. Individual values of all pharmacokinetic parameters were

assumed to follow a log-normal distribution which was implemented as follows:

$$\theta_i = \theta \cdot exp^{\eta_i} \qquad \textit{Equation 2.4}$$

where $\theta_i$ is an individual pharmacokinetic parameter for the *i*th individual, $\theta$ is the typical value of the pharmacokinetic parameter and $\eta_i$ is a normally distributed random variable with zero-mean and variance $\omega^2$, that distinguishes the pharmacokinetic parameter of the *i*th individual from the population typical value $\theta$.

Residual variability (RV) was analysed. Differences between observed and individually predicted plasma concentrations were regarded as random and were modelled in terms of epsilon (ε) variables. Additive, proportional and exponential error models (described in Equations 2.5-2.7, respectively) were tested. These models were implemented as:

$$Y = IPRED + \varepsilon \qquad \textit{Equation 2.5}$$

$$Y = IPRED \cdot (1 + \varepsilon) \qquad \textit{Equation 2.6}$$

$$Y = IPRED \cdot e^{\varepsilon} \qquad \textit{Equation 2.7}$$

where Y is the observed concentration value, IPRED is the model-predicted concentration and ε is the random variable with a mean of zero and an estimated variance $\sigma^2$.

### 2.7.3 Covariate model

Continuous and dichotomous covariates were implemented into models as shown in Equations 2.8-2.9, respectively:

$$\theta_j = \theta * \left(1 + \theta_{CovCon} \cdot (cov_{con} - cov_m)\right) \qquad \textit{Equation 2.8}$$

$$\theta_j = \theta * (1 + \theta_{CovDi} \cdot cov_{Di}) \qquad \textit{Equation 2.9}$$

where $\theta_j$ is the model predicted pharmacokinetic parameter for an individual with continuous covariate equal $cov_{con}$ or dichotomous covariate equal $cov_{Di}$, $\theta$ is the population estimate for that parameter for individuals with $cov_{con}$ equal the median covariate value ($cov_m$) or $cov_{Di}$ equal 0 (reference group), $\theta_{CovCon}$ is the coefficient describing the covariate effect on the parameter per unit of this covariate, and $\theta_{CovDi}$ is the coefficient describing the effect on the parameter when $cov_{Di}$ equals 1. Under certain situations, as detailed in the following section, dichotomous covariates were implemented into models using a different parameter for each subgroup as:

$$\theta_j = \begin{cases} \theta_1 & if\ group = 1 \\ \theta_2 & if\ group = 2 \end{cases} \qquad \text{Equation 2.10}$$

where $\theta_j$ is the model predicted pharmacokinetic parameter taking a value of $\theta_1$ for individuals in group 1 and a value of $\theta_2$ for individuals in group 2.

For absorption mechanistic models, undernourishment, the presence of levofloxacin and the concentration of the infused solutions were investigated as potential covariates. Undernourishment was evaluated as a dichotomous covariate on absorption rate constant (ka) and maximum transport rate (Vmax) parameters in order to investigate possible differences in diffusion kinetics and in capacity of transporters. The presence of potential inhibitors (levofloxacin and sodium azide) was evaluated as a dichotomous covariate on Vmax and on the Michaelis-Menten constant (Km) parameters given their potential inhibitory activity. Concentration of infused solutions was evaluated as a dichotomous covariate on *fr* parameter. On the other side, for Weibull absorption models, dichotomous covariates (presence

or absence of inhibitor, nutritional status, perfused drug concentration and intestinal segment) were implemented into the model in order to test differences for model parameters $\alpha$, β, and $fr$.

For LADME models, covariates were tested on distribution, elimination and absorption parameters. First, central compartment clearance (CL), inter-compartmental clearance (Q), central compartment distribution volume (Vc) and peripheral compartment distribution volume (Vp) parameters were scaled on body weight and normalized to 70 kg by an allometric power model as shown in equation 2.11:

$$\theta_j = \theta * \left(\frac{WGT}{70}\right)^b \qquad \textit{Equation 2.11}$$

where $\theta_j$ is the model predicted pharmacokinetic parameter for individuals with body weight $WGT$ in kg , $\theta$ is the population estimate for that parameter in 70 kg individuals, and $b$ is the is the power scaling parameter. The typical values for b when scaling clearance parameters (CL and Q) and distribution volume parameters (Vc and Vp) are 0.75 and 1, respectively (96, 97). Thereafter, plasma albumin concentration (continuous) and nutritional status (dichotomous) were tested as covariates on distribution parameters as described by Equations. 2.8-2.9.

Regarding absorption parameters, nutritional status of rats was tested as a dichotomous covariate on ka, and as a different parameter for WN and UN rats on oral bioavailability (f) (constraining f estimates between 0 and 1). The type of dispersion system used for drug administration (solution or suspension) was tested as a covariate on f

and ka so that a different f and/or ka parameters were estimated for each subgroup.

*Table 2.5. Summary of tested covariates.*

| Covariate | Continuous/ Dichotomous | Parameters on which covariates were tested |
|---|---|---|
| **Absorption models** | | |
| Mechanistic models | | |
| Undernourishment | Dichotomous | ka, Vmax |
| Presence of potential inhibitors | Dichotomous | Vmax, Km |
| Concentration of infused solution | Dichotomous | fr |
| Weibull models | | |
| Undernourishment | Dichotomous | $\alpha$, β, fr |
| Presence of potential inhibitors | Dichotomous | $\alpha$, β, fr |
| Concentration of infused solution | Dichotomous | $\alpha$, β, fr |
| **LADME models** | | |
| Weight | Continuous (allometric scaling) | Vc, Vp, CL, Q |
| Plasma albumin | Continuous | Vc, Vp, CL, Q |
| Nutritional status | Dichotomous | Vc, Vp, CL, Q, ka, f |
| Type of dispersion system | Dichotomous | ka, f |

*ka: first order absorption rate constant; Vmax: maximum transport rate; Km: Michaelis-Menten constant; fr: correction fraction; α: scaling factor for the Weibull model; β: shape factor for the Weibull model; Vc: volume of distribution of central compartment; Vp: volume of distribution of peripheral compartment; CL: drug clearance from central compartment; Q: drug intercompartmental clearance; f: bioavailability.*

## 2.8 Data analysis and statistical methods

Statistical and graphical analyses of results were performed using R version 3.2.1 and NONMEM 7.3.

### 2.8.1 Descriptive statistics

For descriptive statistics, suitable measures of central tendencies and dispersion were applied. Measures of central tendency characterize the typical value of a distribution and include, for instance, arithmetic mean and median. In contrast, measures of dispersion include, for instance, standard deviation (sd), coefficient of variation (CV) and percentiles that characterize variability.

### 2.8.2 Mean-comparison tests

Mean-comparison tests were performed to compare results in WN and UN groups. Parametric mean-comparison tests assume that dependent variables of compared samples are well modelled by a normal distribution. Additionally, parametric mean-comparison tests assume that no differences exist across variances of two compared samples (homoscedasticity). On the other side, non-parametric tests do not make these assumptions. For these reasons, normality tests (Kolmogorov-Smirnov test) and variance homogeneity tests (Levene's test) were performed in order to decide whether parametric or non-parametric mean-comparison tests were going to be used.

If normality of distributions and homoscedasticity were proven, Student's t-test was applied to establish whether compared means were significantly different or not. In those cases in which homoscedasticity

and/or normality of samples was not proven, Wilcoxon signed-rank test was used. All tests were performed setting significance level at 0.05.

### 2.8.3 Linear regression analysis

Drug quantitation was carried out by performing linear regression analyses of drug concentrations as a function of chromatographic peak areas. Data were adjusted to a linear model by minimizing the sum of squares of the residuals of the adjusted line. To examine whether the intercept was significantly different from zero, the intercept was subjected to a t-test. The coefficient of correlation r was used to evaluate the degree of association between chromatographic peak areas and drug concentrations.

### 2.8.4 Model selection criteria

**Statistical criteria**

Minimum objective function value (MOFV) is the main metric for goodness-of-fit characterization when developing non-linear mixed effects models. This parameter is routinely reported as part of the NONMEM output. The objective function value (OFV) is calculated as -2log(likelihood), so the minimization of the OFV corresponds to the maximization of the likelihood. Given that for hierarchical models the difference between MOFV values is distributed as $\chi^2$, this parameter allows the best model to be selected taking into consideration the difference in degrees of freedom (df) between the compared models (ie. df = 1 and ΔMOFV = -3.84 corresponds to p = 0.05). When evaluating structural models, a p level of 0.05 (ie. df = 1 → ΔMOFV = -3.84; df = 2 → ΔMOFV = -5.99) was chosen as the criterion for accepting a more

complex model over a simpler model. Regarding covariates model, inclusion of covariates was carried out using a stepwise covariate inclusion procedure in which significance levels were set to 0.05 (df = 1 → ΔMOFV = -3.84) for the forward inclusion and 0.01 (df = 1 → ΔMOFV = -6.64) for the backward deletion.

**Graphical criteria**

Basic goodness-of-fit plots contrast the observed values with the associated model-predicted values. These plots were assessed both for population predictions (PRED) and individual predictions (IPRED). In the assessment of these plots, close scattering around the line of identity is regarded as an indication of adequate model performance.

Plots involving the weighted residuals (WRES), i.e. the differences between model predictions and the observed data normalised by the standard deviation of data, are also commonly used model diagnostics. The conditional weighted residuals (CWRES) are an advanced version of WRES that suit better if FOCE estimation method is used. Plots of CWRES against time should exhibit random scattering around the zero reference line and can be used to further assess model adequacy.

**Other criteria**

Another criteria taken into account for model selection was the precision of parameter estimation, quantified as the relative standard error (RSE %). Finally, BSV and RV were also taken into account when comparing models.

### 2.8.5 Model validation

Model evaluation was performed by means of visual predictive check plots and the bootstrap resampling technique.

As visual predictive check, 200 replicates of each study design were simulated from the developed final models. Simulated concentration-time profiles were represented together with the observed data for visual comparison (98).

The bootstrap resampling technique was used as an internal method to validate the final model. From the original dataset, random sampling with replacement generated 1,000 dataset replicates, and the final population pharmacokinetic model was fitted repeatedly to each replicate using the bootstrap option of PsN-Toolkit (93). Bootstrap runs with unsuccessful minimization were excluded from further analysis. The median parameter estimates and their 95% confidence intervals (CI) were obtained from the bootstrap replicates and compared with the population pharmacokinetic parameters obtained from the original dataset.

## 2.9 Model-based simulations

In pharmacometrics, simulations comprise the application of models to explore scenarios that have not o cannot be investigated. Simulations can be classified as deterministic (based on fixed-effects) and as stochastic or Monte Carlo simulations (based on fixed and random effects). In the present research project stochastic simulations were used to explore new scenarios.

Mechanistic models developed from *in situ* intestinal perfusion assays were used to simulate effective absorption rate constants in different conditions. Simulations were performed taking into account the variance-covariance matrix in order to explore the influence of covariates on effective absorption rate constant. Effective absorption rate constant was calculated as absorption rate divided by concentration in intestinal lumen. The importance of each covariate effect was visualized by plotting simulated effective absorption rate constants for different populations against lumen concentration.

On the other side, once population pharmacokinetic models built from *in vivo* studies had been validated, models were used to simulate two populations of well-nourished (n=1000) and under-nourished (n=1000) patients receiving a daily dose of one of the drugs (150 mg of erlotinib or 250 mg dose of gefitinib). Distribution of body weights and other required covariates for simulated WN and UN individuals were obtained from the study published by Piskorz et al. (99), where non-small cell lung cancer patients were classified into “relatively well-nourished patients” (72.93 ± 13.9 kg) and “patients with malnutrition of a slight degree” (69.39 ± 12.45 kg). BSV and RV were taken into account to perform the simulations. Simulations were computed using the R packages “MASS” and “deSolve”.

# 3 Results

# 3 | Results

## 3.1 Study population

At the end of the adaptation period, all rats were classified into different nutritional status levels (normal nutritional status, mild under-nutrition, moderate under-nutrition and severe under-nutrition). Body weight, serum albumin and nutritional status of rats included in all five assays of this research project are described in Tables 3.1-3.5. Undernourishment status was reached in all rats assigned to UN group. Most of UN rats developed mild and moderate undernourishment degrees. One rat developed severe undernourishment.

*Table 3.1. Body weight, serum albumin and degree of undernourishment for rats included in the assay for the evaluation of analytical and molecular alterations associated with undernourishment. Values displayed correspond to those at the end of the adaptation period.*

| Parameters | | Group | |
|---|---|---|---|
| | | Well-nourished (n=7) | Under-nourished (n=7) |
| Body weight (g) | | 290.3 ± 14.8 | 193.8 ± 13.6 |
| Serum albumin (g/dL) | | 3.20 ± 0.91 | 2.02 ± 0.16 |
| Degree of undernutrition | Normal | 7 | 0 |
| | Mild | 0 | 5 |
| | Moderate | 0 | 2 |
| | Severe | 0 | 0 |

*Mean ± standard deviation; n: number of rats per randomization group.*

*Table 3.2. Body weight, serum albumin and degree of undernourishment for rats included in the in situ intestinal perfusion study for **erlotinib**. Values displayed correspond to those at the end of the adaptation period.*

| Parameters | | Group | |
|---|---|---|---|
| | | Well-nourished (n=20) | Under-nourished (n=20) |
| Body weight (g) | | 306.3 ± 11.6 | 207.6 ± 11.0 |
| Serum albumin (g/dL) | | 3.36 ± 0.29 | 2.36 ± 0.30 |
| Degree of undernutrition | Normal | 20 | 0 |
| | Mild | 0 | 19 |
| | Moderate | 0 | 1 |
| | Severe | 0 | 0 |

*Mean ± standard deviation; n: number of rats per randomization group.*

*Table 3.3. Body weight, serum albumin and degree of undernourishment for rats included in the in situ intestinal perfusion study for **gefitinib**. Values displayed correspond to those at the end of the adaptation period.*

| Parameters | | Group | |
|---|---|---|---|
| | | Well-nourished (n=24) | Under-nourished (n=24) |
| Body weight (g) | | 294.1 ± 21.3 | 196.8 ± 7.7 |
| Serum albumin (g/dL) | | 2.76 ± 0.23 | 2.38 ± 0.41 |
| Degree of undernutrition | Normal | 24 | 0 |
| | Mild | 0 | 14 |
| | Moderate | 0 | 9 |
| | Severe | 0 | 1 |

*Mean ± standard deviation; n: number of rats per randomization group.*

*Table 3.4. Body weight, serum albumin and degree of undernourishment for rats included in the in vivo pharmacokinetic study for **erlotinib**. Values displayed correspond to those at the end of the adaptation period.*

| Parameters | | Group | |
|---|---|---|---|
| | | Well-nourished (n=19) | Under-nourished (n=23) |
| Body weight (g) | | 287.2 ±14.0 | 204.2 ± 10.7 |
| Serum albumin (g/dL) | | 3.70 ± 0.35 | 2,66 ± 0.33 |
| Degree of undernutrition | Normal | 19 | 0 |
| | Mild | 0 | 20 |
| | Moderate | 0 | 3 |
| | Severe | 0 | 0 |

*Mean ± standard deviation; n: number of rats per randomization group.*

*Table 3.5. Body weight, serum albumin and degree of undernourishment for rats included in the in vivo pharmacokinetic study for **gefitinib**. Values displayed correspond to those at the end of the adaptation period.*

| Parameters | | Group | |
|---|---|---|---|
| | | Well-nourished (n=11) | Under-nourished (n=10) |
| Body weight (g) | | 297.5 ± 20.3 | 196.8 ± 10.7 |
| Serum albumin (g/dL) | | 3.16 ± 0.19 | 2.96 ± 0.45 |
| Degree of undernutrition | Normal | 11 | 0 |
| | Mild | 0 | 9 |
| | Moderate | 0 | 1 |
| | Severe | 0 | 0 |

*Mean ± standard deviation; n: number of rats per randomization group.*

## 3.2 Analytical methods

### 3.2.1 Erlotinib

Erlotinib concentration in intestinal perfusion solutions and plasma samples was determined chromatographically using HPLC. Examples of the obtained chromatograms are shown in Figures 3.1-3.2.

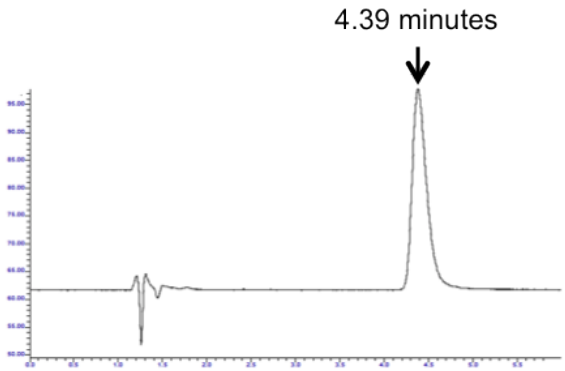


*Figure 3.1. Chromatogram from HPLC analysis of intestinal perfusion solution sample for **erlotinib** quantitation.*

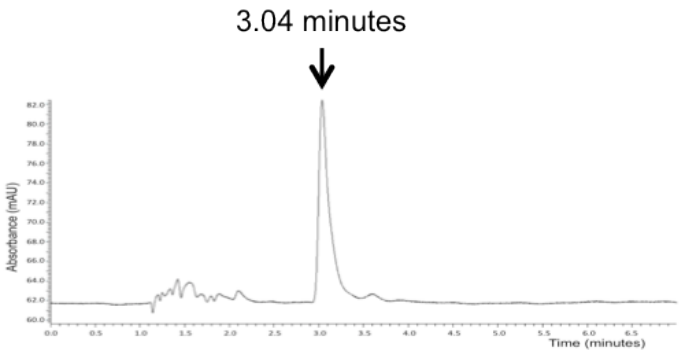


*Figure 3.2. Chromatogram from HPLC analysis of rat plasma sample after intravenous administration of **erlotinib**.*

**Linearity**: Statistical analysis using least squares regression indicated excellent linearity for erlotinib in the evaluated concentration range. Intercepts were significantly different from zero. Regression results for the calibration curves are presented in Table 3.6.

*Table 3.6. Calibration curves for erlotinib quantitation method in intestinal perfusion solution samples and for **erlotinib** quantitation method in plasma samples.*

| Parameter | Method for intestinal perfusion solution samples | Method for plasma samples |
|---|---|---|
| Intercept ± SE | -127.40 ± 42.61 | -214.47 ± 78.45 |
| Slope ± SE | 47607.88 ± 1387.43 | 37461.22 ± 78.49 |
| r | 0.999 | 0.999 |

*SE: Standard error, r: correlation coefficient.*

**Precision and accuracy**: Precision and accuracy results are shown in Table 3.7.

*Table 3.7. Accuracy (coefficient of variation) and precision (relative error) results for erlotinib quantitation method in intestinal perfusion solution and for **erlotinib** quantitation method in plasma samples.*

| Concentrations (µg/mL) | Method for intestinal perfusion solution samples | | Method for plasma samples | |
|---|---|---|---|---|
| | CV (%) | RE (%) | CV (%) | RE (%) |
| 0.2 | 5.91 | 3.26 | 8.44 | 1.75 |
| 10 | 5.44 | -8.35 | 1.7 | -0.96 |
| 15 | - | - | 4.51 | 0.55 |
| 20 | 0.40 | -0.56 | - | - |

*CV: Coefficient of variation; RE: Relative error.*

**LLOQ**: The back-calculated concentrations for the mean blank signal were 0.004 and 0.006 μg/mL in the methods for intestinal perfusion solutions and for plasma samples, respectively. The LLOQ was established at 0.06 μg/mL (over 10 times the mean blank signal) for both methods.

### 3.2.2 Gefitinib

**Intestinal perfusion solution samples**

**Linearity**: Statistical analysis using least squares regression indicated excellent linearity for gefitinib in the mentioned concentration ranges. Intercepts were not significantly different from zero. Therefore, calibration curves did not include intercept term. Regression results for both calibration curves are presented in Table 3.8.

*Table 3.8. Regression results for calibration curves of **gefitinib** quantitation method in intestinal perfusion samples.*

| Parameters | Calibration curve concentration range | |
|---|---|---|
| | 0.4 - 12 μg/mL | 12 - 40 μg/mL |
| Slope ± SE | 89.12 ± 0.19 | 90.52 ± 0.57 |
| r | 0.999 | 0.999 |

*SE: Standard error; r: correlation coefficient.*

**Precision and accuracy**: Precision and accuracy results are shown in Table 3.9.

*Table 3.9. Accuracy (coefficient of variation) and precision (relative error) results for HPLC **gefitinib** quantitation method in intestinal perfusion samples.*

| Calibration curve range μg/mL | Concentration μg/mL | CV (%) | RE (%) |
|---|---|---|---|
| 0.4 – 12 | 0.41 | 1.21 | 1.72 |
| | 2.86 | 0.49 | 0.69 |
| | 12.2 | 0.02 | 0.03 |
| 12 – 40 | 12.2 | 0.86 | 1.21 |
| | 28.5 | 0.06 | 0.09 |
| | 40.8 | 0.5 | 0.71 |

*CV: Coefficient of variation; RE: Relative error.*

**LLOQ**: The back-calculated concentration for the mean blank signal was 0.01 μg/mL. The LLOQ was established at 0.10 μg/mL (over 10 times the mean blank signal).

**Plasma samples**

Gefitinib concentration in plasma samples was determined using LC-MS/MS. An example of the obtained chromatograms is shown in Figure 3.3.

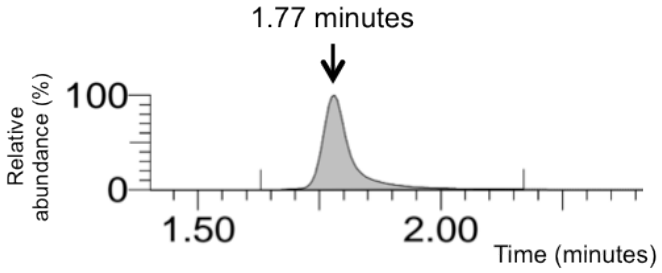


*Figure 3.3. Chromatogram from LC-MS/MS analysis of rat plasma sample after intravenous administration of **gefitinib***

**Linearity**: Statistical analysis using least squares regression indicated excellent linearity for gefitinib in the evaluated concentration range. Intercepts were significantly different from zero. Regression results for the calibration curve are presented in Table 3.10.

*Table 3.10. Regression results for calibration curve of **gefitinib** quantitation method in plasma samples.*

| Parameters | Parameter values |
|---|---|
| Intercept ± SE | -137.12 ± 43.45 |
| Slope ± SE | 1615.89 ± 14.47 |
| r | 0.999 |

*SE: Standard error; r: correlation coefficient.*

**Precision and accuracy**: Precision and accuracy results are shown in Table 3.11.

*Table 3.11. Accuracy (coefficient of variation) and precision (relative error) results for LC-MS/MS **gefitinib** quantitation method in plasma samples.*

| Concentration ng/mL | CV (%) | RE (%) |
|---|---|---|
| 1 | 5.98 | -1.81 |
| 5 | 4.64 | -0.80 |

*CV: Coefficient of variation; RE: Relative error.*

**LLOQ**: The back-calculated concentration for the mean blank signal was 0.09 ng/mL. The LLOQ was established at 1 ng/mL (over 10 times the mean blank signal).

## 3.3 Evaluation of molecular and analytical alterations associated with undernourishment

Fourteen rats were included in this assay (7 WN rats and 7 UN rats). Results of qRT-PCR analyses for hepatic and intestinal tissues are shown in Figures 3.4 and 3.5 respectively. Analytical parameters along with total body and liver relative weight values are shown in Table 3.12.

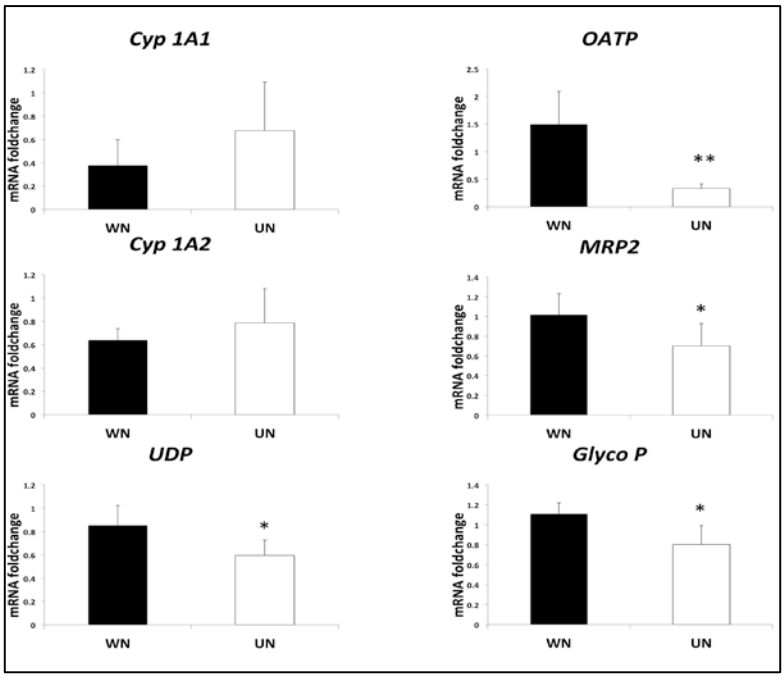


*Figure 3.4. qRT-PCR results for hepatic enzymes and transporters expression in well-nourished (WN) and undernourished (UN) rats. Statistical significance: * = p<0.05; ** = p<0.01.*

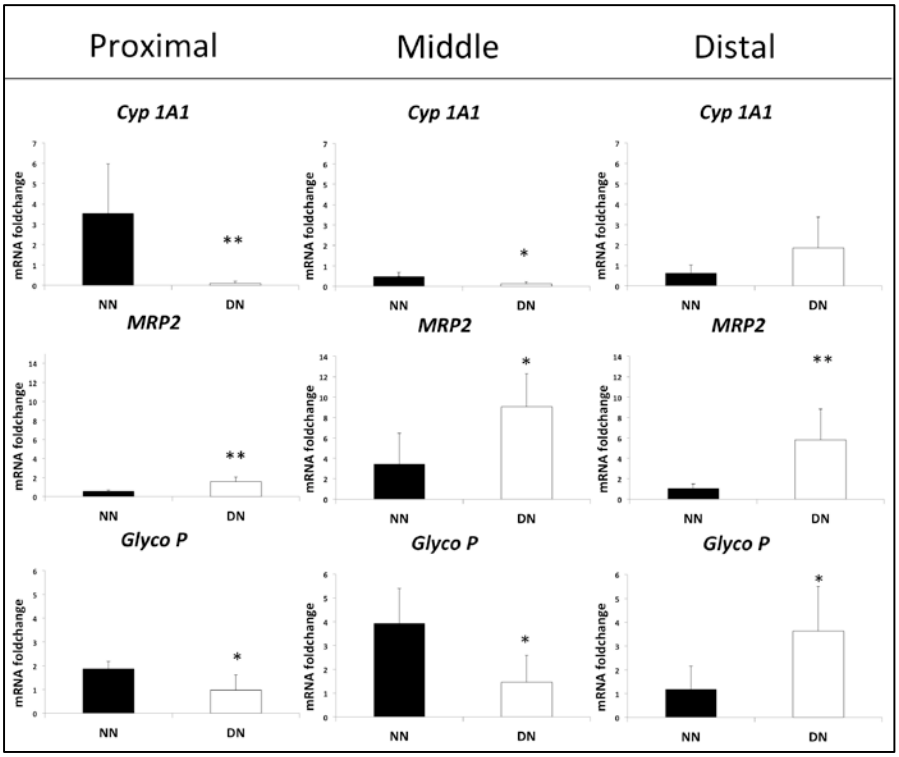


*Figure 3.5. qRT-PCR results for intestinal enzymes and transporters expression in well-nourished (WN) and undernourished (UN) rats. Intestinal segments: Proximal (left), middle (centre), distal (right); Statistical Significance: * = p<0.05; ** = p<0.01.*

*Table 3.12. Haemogram parameters, biochemical parameters, total body weight, liver weight and liver relative weight at the end of the follow-up period for well-nourished and undernourished rats.*

| Parameter | WN rats[(a)] (n = 7) | UN rats[(a)] (n = 7) | p value |
|---|---|---|---|
| Haemogram | | | |
| Red blood cell count ($10^6$/µL) | 7.4 (1.8) | 4.7 (0.8) | 0.003 |
| White blood cell count ($10^3$/µL) | 3.09 (1.1) | 1.79 (0.6) | 0.012 |
| Platelet count ($10^3$/µL) | 507.8 (445.1) | 69.3 (40.5) | 0.032 |
| Haemoglobin concentration (g/dL) | 13.3 (2.7) | 8.6 (1.4) | <0.001 |
| Haematocrit (%) | 41.6 (7.8) | 29.1 (6.1) | 0.004 |
| Mean corpuscular volume (fL) | 57.6 (6.0) | 60.6 (4.8) | 0.297 |
| Biochemical analysis | | | |
| ALAT/GPT (U/L) | 42.0 (18.1) | 69.4 (11.8) | 0.006 |
| ASAT/GOT (U/L) | 143.0 (77.9) | 282.7 (77.9) | <0.001 |
| Total protein concentration (g/L) | 61.1 (11.0) | 46.3 (3.9) | 0.006 |
| Acid-alpha glycoprotein concentration (mg/dL) | 14.6 (2.7) | 17.9 (2.1) | 0.025 |
| Serum protein electrophoresis bands | | | |
| Albumin (%) | 51.6 (7.09) | 43.9 (1.3 | 0.015 |
| Alpha-1 (%) | 8.1 (0.5) | 9.8 (0.8) | <0.001 |
| Alpha-2 (%) | 14.6 (1.2) | 16.2 (0.54) | <0.001 |
| Beta (%) | 21.6 (0.5) | 24.9 (1.4) | 0.15 |
| Gamma (%) | 4.0 (0.5) | 5.2 (0.5) | 0.001 |
| Body weight (g) | 290.2 (14.8) | 193.8 (13.6) | <0.001 |
| Liver weight (g) | 10.2 (0.93) | 6.2 (0.4) | <0.001 |
| Liver weight/Body weight coefficient | 0.036 (0.001) | 0.032 (0.001) | <0.001 |

*[(a)] Mean (standard deviation). WN: well-nourished; UN: under-nourished; n: number of rats; ALAT/GPT: alanine aminotransferase; ASAT/GOT: aspartate aminotransferase; fL: fentolitre*

## 3.4 Intestinal absorption model selection for erlotinib.

*In situ* intestinal perfusion assays were carried out in proximal and distal intestines simultaneously in 40 rats (20 WN and 20 UN). Twelve intestinal perfusion solution samples were obtained from each rat (6 from proximal intestine and 6 from distal intestine). Concentration-time profiles obtained from *in situ* intestinal perfusion studies (Figure 3.6) were evaluated considering linear kinetics. Distribution of ka values for linear kinetics models are shown in Figure 3.7

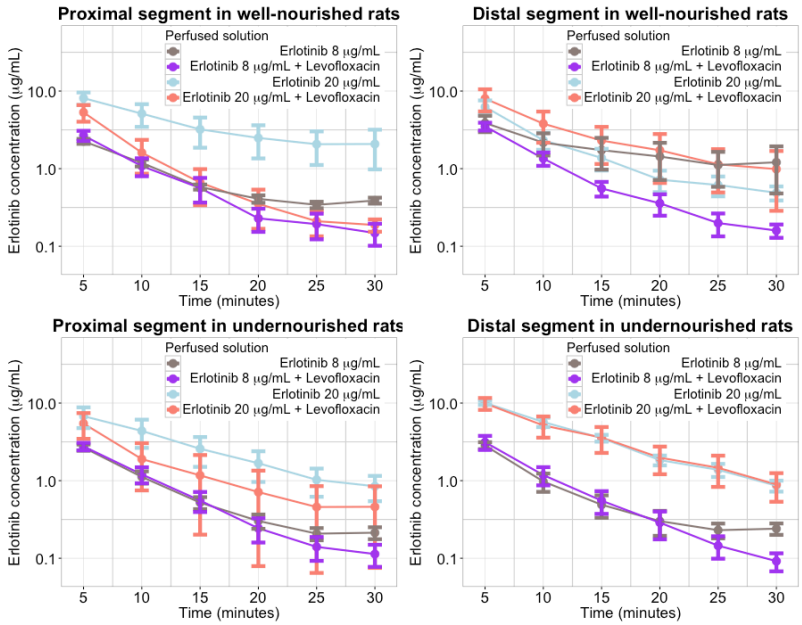


*Figure 3.6.* ***Erlotinib*** *intestinal lumen concentration – time profiles for proximal (left panels) and distal (right panels) intestinal segments in well-nourished (left panels) and undernourished (right panels) rats. Data are stratified by perfusion solution type (erlotinib 8 µg/mL: grey; erlotinib 8 µg/mL + levofloxacin: purple; erlotinib 20 µg/mL: blue; erlotinib 20 µg/mL + levofloxacin: red). Points represent mean concentration, error bars represent standard errors and solid lines represent central tendency.*

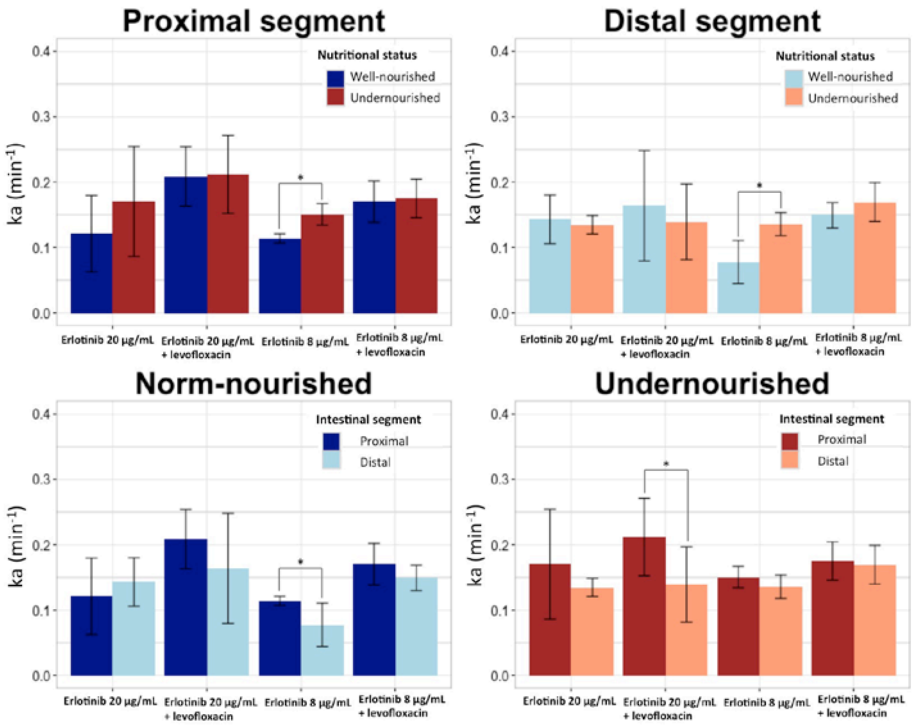


*Figure 3.7. ka values for* ***erlotinib****. Top panels represent ka values for proximal (left) and distal (right) intestinal segments for each perfused solution in well-nourished (blue) and undernourished (salmon) animals. Bottom panels represent ka values for norm-nourished (left) and undernourished (right) rats for each perfused solution and intestinal segment (proximal: blue; distal: salmon).*

Two independent mechanistic models were developed to describe erlotinib disappearance rate in proximal and distal intestine. Tested structural models are described in section 2.7.1 (Table 2.4). MOFV for main models are shown in Table 3.13-3.14.

*Table 3.13. Selection of the main structural absorption and secretion models evaluated for **erlotinib** absorption process in **proximal** intestine.*

| Model | Description | | | FE (n) | RE (n) | MOFV |
|---|---|---|---|---|---|---|
| | Absorption | Secretion | *fr* | | | |
| 9001 | First order | None | No | 1 | 2 | -12.40 |
| 9002 | First order | First order | No | 2 | 2 | -12.84 |
| 9003 | First order | Michaelis-Menten | No | 3 | 2 | -176.60 |
| 9004 | Michaelis-Menten | Michaelis-Menten | No | 4 | 2 | -176.61 |
| **9007** | **First order** | **Michaelis-Menten** | **Yes** | **4** | **2** | **-304.19** |

*FE (n): Number of estimated fixed effect parameters; RE (n): Number of estimated random effects parameters; MOFV: Minimum objective function value; fr: correction factor; bold: selected model.*

*Table 3.14. Selection of the main structural absorption and secretion models evaluated for **erlotinib** absorption process in **distal** intestine.*

| Model | Description | | | FE (n) | RE (n) | MOFV |
|---|---|---|---|---|---|---|
| | Absorption | Secretion | *fr* | | | |
| 9901 | First order | None | No | 1 | 2 | 2.65 |
| 9902 | First order | First order | No | 2 | 2 | 2.65 |
| 9903 | First order | Michaelis-Menten | No | 3 | 2 | -130.02 |
| 9904 | Michaelis-Menten | Michaelis-Menten | No | 4 | 2 | -130.02 |
| **9907** | **First order** | **Michaelis-Menten** | **Yes** | **4** | **2** | **-177.88** |

*FE (n): Number of estimated fixed effects parameters; RE (n): Number of estimated random effects parameters; MOFV: Minimum objective function value; fr: correction factor; bold: selected model.*

The selected structural absorption and secretion models for erlotinib in proximal and distal intestine had the same structure (Figure 3.8). A combination of first order absorption and a Michaelis-Menten secretion processes, together with a correction factor parameter (*fr*),

best-described erlotinib absorption from lumen to enterocyte as shown in Tables 3.13 and 3.14.

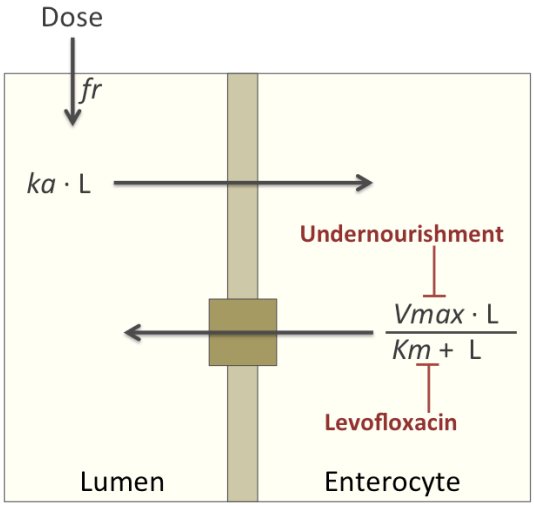


*Figure 3.8. Schematic representation of* ***erlotinib*** *absorption model selected.Vertical line represents apical membrane; brown square represents efflux transporter. fr: correction fraction; ka: absorption rate constant; L: erlotinib concentration in lumen (L was used as representative of erlotinib concentration in the enterocyte); $Vmax_s$: maximal secretion rate; $Km_s$: Michaelis Menten constant.*

Main covariate models evaluated during the covariate selection process are described in Tables 3.15-3.16.

*Table 3.15. Main absorption and secretion covariate models for* ***erlotinib*** *in proximal intestine.*

| *Model* | *Covariates on pharmacokinetic parameters* | | *Reference model* | *ΔMOFV* |
|---|---|---|---|---|
| | *Absorption ($k_a$)* | *Secretion ($Vmax_s$, $Km_s$)* | | |
| *9007* | - | - | - | - |
| *9009* | $k_a = \theta_1 \cdot(1+\theta_2 \cdot UN)$ | - | *9007* | *-1.11* |
| *9010* | - | $Vmax_s = \theta_1 \cdot(1+\theta_2 \cdot UN)$ | *9007* | *-10.37* |
| *9012* | - | $Vmax_s = \theta_1 \cdot(1+\theta_2 \cdot UN)$<br>$Km_s = \begin{cases} \theta_{NL} \ if \ levofloxacin = 0 \\ \theta_L \ if \ levofloxacin = 1 \end{cases}$ | *9010* | *-21.12* |
| ***9013*** | - | $\boldsymbol{Vmax_s = \theta_1 \cdot(1+\theta_2 \cdot UN)}$<br>$\boldsymbol{Km_s = \begin{cases} 0 \ if \ levofloxacin = 0 \\ \theta_L \ if \ levofloxacin = 1 \end{cases}}$ | ***9010*** | ***-20.86*** |

*$Vmax_s$: maximum secretion rate; $Km_s$: Michaelis-Menten secretion constant; UN: undernourished rats; $\theta_1$: estimated pharmacokinetic parameter for well-nourished rats; $\theta_2$: estimated relative change of pharmacokinetic parameter in undernourished rats in comparison with well-nourished rats; $\theta_{NL}$: pharmacokinetic parameter in absence of levofloxacin; $\theta_L$: pharmacokinetic parameter in presence of levofloxacin; ΔMOFV: minimum objective function value change with regard to reference model; bold: selected model.*

*Table 3.16. Main absorption and secretion covariate models for* ***erlotinib*** *in distal intestine*

| *Model* | *Covariates on pharmacokinetic parameters* | | *Reference model* | *ΔMOFV* |
|---|---|---|---|---|
| | *Absorption* ($k_a$) | *Secretion* ($Km_s$, $Vmax_s$) | | |
| *9907* | - | - | - | - |
| *9909* | $k_a = \theta_1 \cdot (1+\theta_2 \cdot UN)$ | - | *9907* | *-1.84* |
| *9910* | - | $Vmax_s = \theta_1 \cdot (1+\theta_2 \cdot UN)$ | *9907* | *-35.97* |
| *9912* | - | $Vmax_s = \theta_1 \cdot (1+\theta_2 \cdot UN)$<br>$Km_s = \begin{cases} \theta_{NL} \ if \ levofloxacin = 0 \\ \theta_L \ if \ levofloxacin = 1 \end{cases}$ | *9910* | *-33.35* |
| ***9913*** | - | $\boldsymbol{Vmax_s = \theta_1 \cdot (1+\theta_2 \cdot UN)}$<br>$\boldsymbol{Km_s = \begin{cases} 0 \ \ if \ levofloxacin = 0 \\ \theta_L \ if \ levofloxacin = 1 \end{cases}}$ | ***9910*** | ***-33.29*** |

*$Vmax_s$: maximum secretion rate; $Km_s$: Michaelis-Menten secretion constant; UN: undernourished rats; $\theta_1$: estimated pharmacokinetic parameter for well-nourished rats; $\theta_2$: estimated relative change of pharmacokinetic parameter in undernourished rats in comparison with well-nourished rats; $\theta_{NL}$: pharmacokinetic parameter in absence of levofloxacin; $\theta_L$: pharmacokinetic parameter in presence of levofloxacin; ΔMOFV: minimum objective function value change with regard to reference model; bold: selected model.*

In the absence of levofloxacin, Michaelis Menten constant for the secretion process ($Km_s$) was near to zero (models 9012 and 9912) and imprecise parameter estimates were obtained. In this context, erlotinib intestinal secretion process in the absence of levofloxacin was well described by zero order kinetics so $Km_s$ was fixed to 0 (models 9013 and 9913):

$$\frac{dL}{dt} = -ka \cdot L + \frac{Vmax_S \cdot L}{0+L} = -ka \cdot L + Vmax_s \quad \textit{Equation 3.1}$$

On the other hand, in the presence of levofloxacin all pharmacokinetic parameters ($Km_s$, $Vmax_s$ and ka) were estimated. In conclusion, in the absence of levofloxacin $Km_s$ was fixed to 0 and not estimated whereas in the presence of levofloxacin $Km_s$ was not fixed and this parameter was estimated (as shown in models 9013 and 9913 in Tables 3.15-6).

Regarding the effect of nutritional status, under-nutrition proved to significantly decrease the maximum capacity of the secretion process (as represented by $Vmax_s$). This pharmacokinetic behaviour was evidenced both in proximal and distal intestine: $Vmax_s$ was 63 % lower in proximal intestine and 72 % lower in distal intestine in UN rats when compared with WN rats.

Regarding the statistical model, BSV was incorporated to ka and $Vmax_s$. Additive, proportional and exponential RV models were tested. Finally, an exponential RV model was selected.

Diagnostic plots for both selected models (proximal and distal intestine) showed random, uniform scatter distribution around the identity line indicating absence of bias in these models (Figure 3.9).

Model parameter estimates and bootstrap results of proximal and distal intestine absorption models are shown in Tables 3.17-3.18, respectively. The population estimates for both final models were similar to the median and contained within the 95% CI of the bootstrap results. Additionally, bootstrap analyses evidenced an acceptable precision in parameter estimates. Visual predictive check results are shown in Figure 3.10.

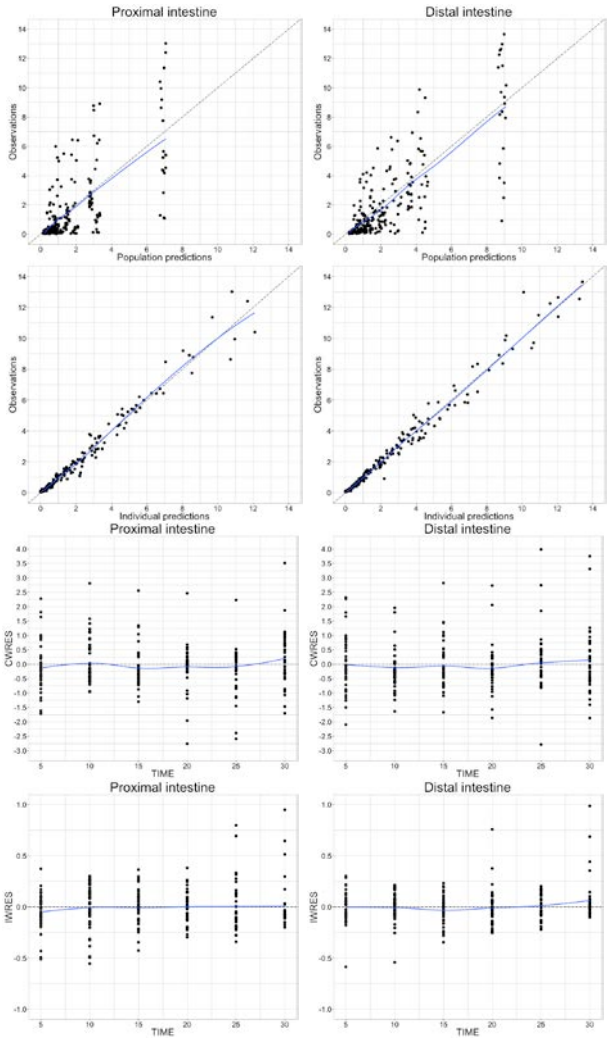


*Figure 3.9. Goodness-of-fit plots for proximal (left) and distal (right) intestine **erlotinib** absorption models. Observations versus population and individual predictions (top) and conditional weighted residuals (CWRES) and individual weighted residuals (IWRES) versus time (bottom). Blue line represents central tendency.*

*Table 3.17. Proximal intestine **erlotinib** absorption-model parameter estimates and bootstrap results.*

| Model Parameter | Estimate | RSE (%) | Bootstrap results | |
|---|---|---|---|---|
| | | | Median | 95% CI |
| Fixed effect parameters | | | | |
| ka ($min^{-1}$) | 0.159 | 12 | 0.162 | 0.131-0.269 |
| $Vmax_s$ (μg/min) | 0.209 | 24 | 0.221 | 0.142-0.379 |
| $Km_s$ (μg/mL) | 0 (FIX) | - | - | - |
| *fr* | 0.861 | 6 | 0.873 | 0.790-0.990 |
| Undernourishment on $Vmax_s$ | -0.634 | 16 | -0.644 | (-0.792)-(-0.269) |
| $Km_s$ Levofloxacin (μg/mL) | 6.49 | 45 | 5.89 | 0.17-104.25 |
| Between subject variability | | | | |
| $\omega^2$ ka | 0.256 | 17 | 0.233 | 0.104-0.436 |
| $\omega^2$ $Vmax_s$ | 0.213 | 32 | 0.262 | 0.148-0.673 |
| Residual error | | | | |
| $\varepsilon_{exp}$ | 0.0197 | 12 | 0.0209 | 0.0123-0.0572 |

*RSE: Relative standard error; CI: confidence interval; ka: absorption rate constant; $Vmax_s$: maximal secretion rate; $Km_s$: concentration of erlotinib at which the secretion rate is half maximal in the absence of levofloxacin; fr: correction fraction; $Km_s$ Levofloxacin: concentration of erlotinib at which the secretion rate is half maximal in presence of levofloxacin; $\omega^2$: between subject variance; $\varepsilon_{exp}$: exponential residual variability.*

*Table 3.18. Distal intestine **erlotinib** absorption-model parameter estimates and bootstrap results.*

| Parameter | Estimate | RSE (%) | Bootstrap results | |
|---|---|---|---|---|
| | | | Median | 95% CI |
| Fixed effect parameters | | | | |
| ka ($min^{-1}$) | 0.138 | 12 | 0.140 | 0.112-0.180 |
| $Vmax_s$ (μg/min) | 0.423 | 29 | 0.443 | 0.250-0.711 |
| $Km_s$ (μg/mL) | 0 (FIX) | - | - | - |
| *fr* | 0.978 | 1 | 0.971 | 0.929-0.997 |
| Undernourishment on $Vmax_s$ | -0.715 | 13 | -0.731 | (-0.835)-(-0.492) |
| $Km_s$ Levofloxacin (μg/mL) | 4.70 | 56 | 4.75 | 1.31-18.00 |
| Between subject variability | | | | |
| $\omega^2$ ka | 0.284 | 19 | 0.259 | 0.134-0.537 |
| $\omega^2$ $Vmax_s$ | 0.116 | 24 | 0.107 | 0.014-0.238 |
| Residual error | | | | |
| ε (exponential error) | 0.0146 | 20 | 0.0156 | 0.0069-0.0319 |

*RSE: relative standard error; CI: Confidence interval; ka: absorption rate constant; $Vmax_s$: maximal secretion rate; $Km_s$: concentration of erlotinib at which the secretion rate is half maximal in the absence of levofloxacin; fr: correction fraction; $Km_s$ Levofloxacin: concentration of erlotinib at which the secretion rate is half maximal in presence of levofloxacin; $\omega^2$: between subject variance; $\varepsilon_{exp}$: exponential residual variability.*

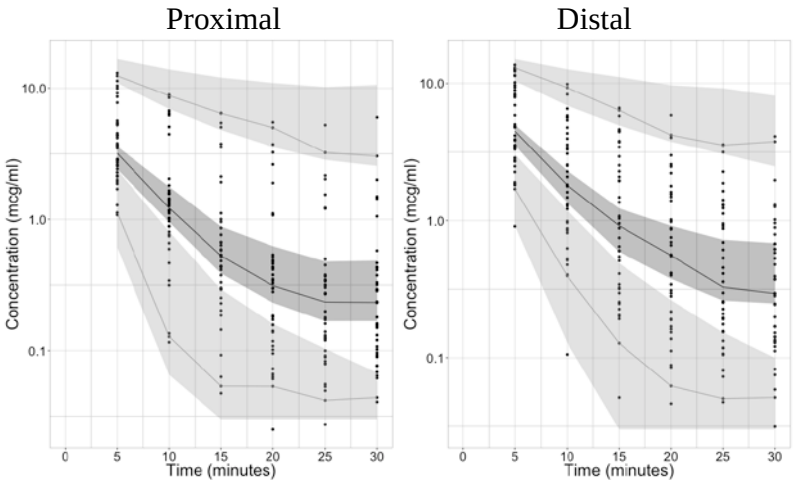


*Figure 3.10. Visual predictive check plots for* ***erlotinib*** *absorption and secretion models. Left: proximal intestinal segment; right: distal intestinal segment. Points represent observed concentrations; solid lines represent the 2.5$^{th}$, 50$^{th}$ and 97.5$^{th}$ percentiles of the observations; shaded areas indicate the 95% confidence intervals of the 2.5$^{th}$ and 97.5$^{th}$ (light grey) and 50$^{th}$ (dark grey) percentiles of the simulated values.*

Once the final model had been developed and validated, the influence of erlotinib concentration, undernourishment and levofloxacin co-administration on effective absorption rate constant (includes both, entrance and secretion process) was evaluated through simulations. Results are shown in Figure 3.11.

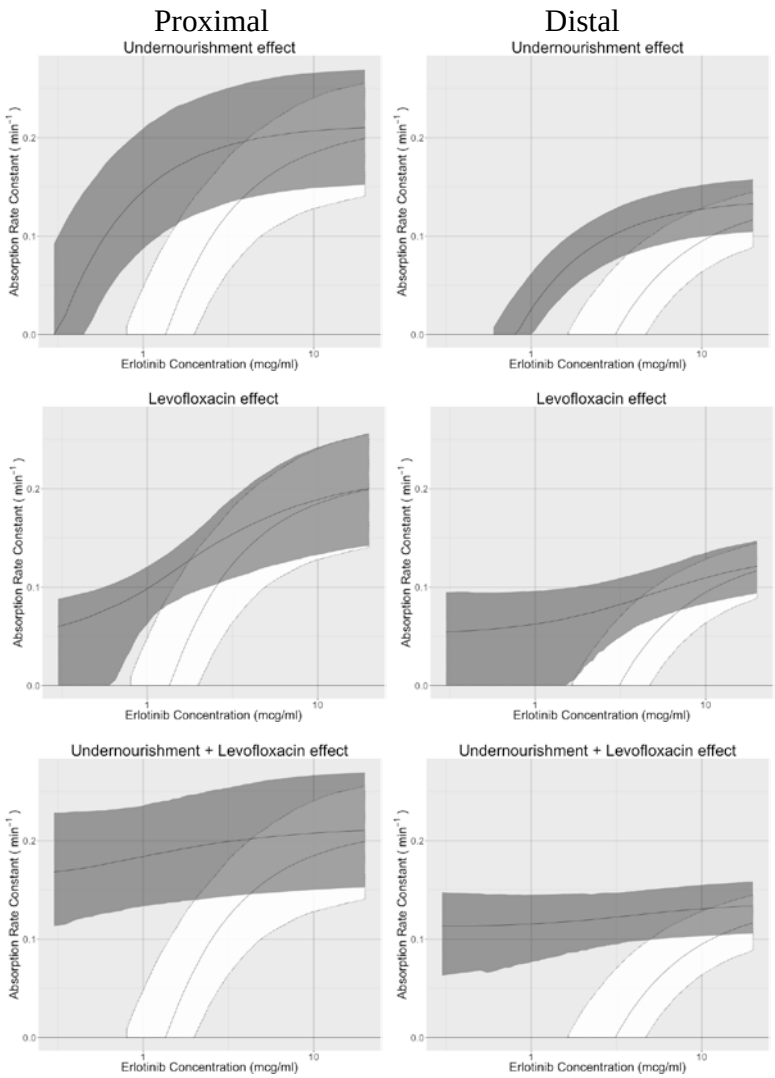


*Figure 3.11. Sensitivity analysis for covariates influence on proximal (left) and distal (right) intestine* ***erlotinib*** *absorption models. Effective absorption rate constants are represented against erlotinib concentration in intestinal lumen. White: well-nourished without levofloxacin (top, middle, bottom); Grey: undernourished without levofloxacin (top), well-nourished with levofloxacin (middle), undernourished with levofloxacin (bottom).*

## 3.5 Intestinal absorption model selection for gefitinib

Concentration-time profiles obtained from *in situ* intestinal perfusion studies (Figure 3.12) were evaluated considering linear kinetics. Distribution of ka values for linear kinetics models are shown in Figure 3.13

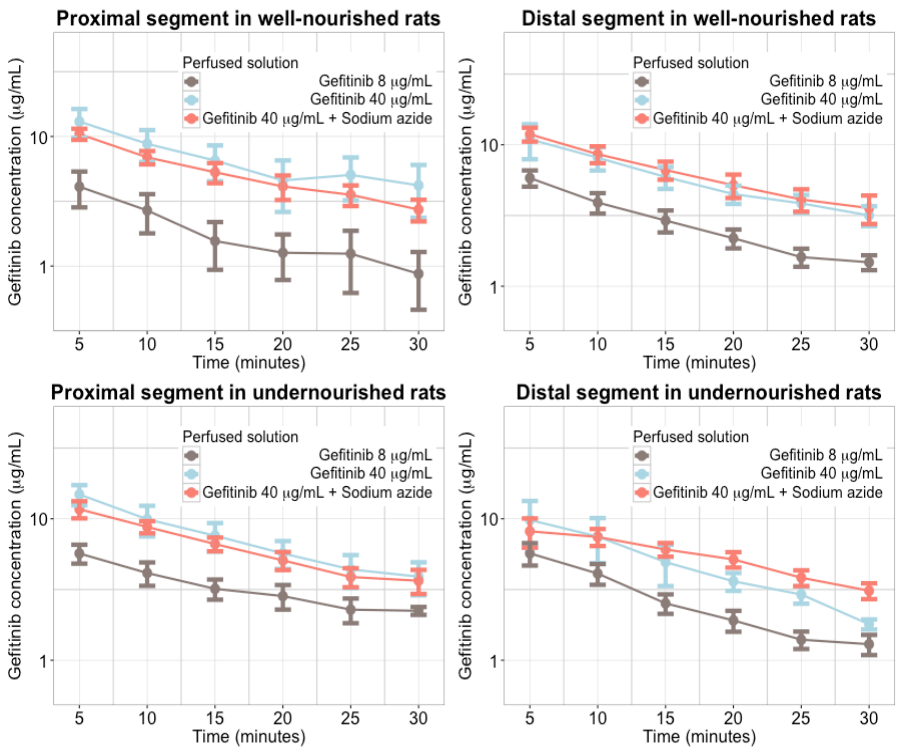


*Figure 3.12.* ***Gefitinib*** *intestinal lumen concentration – time profiles for proximal (upper panels) and distal (bottom panels) intestinal segments in well-nourished (left panels) and undernourished (right panels) rats. Data are stratified by perfusion solution type (Gefitinib 8 μg/mL: brown; Gefitinib 40 μg/mL: blue; Gefitinib 40 μg/mL + sodium azide: red). Points represent mean concentration, error bars represent standard errors and solid line represents central tendency.*

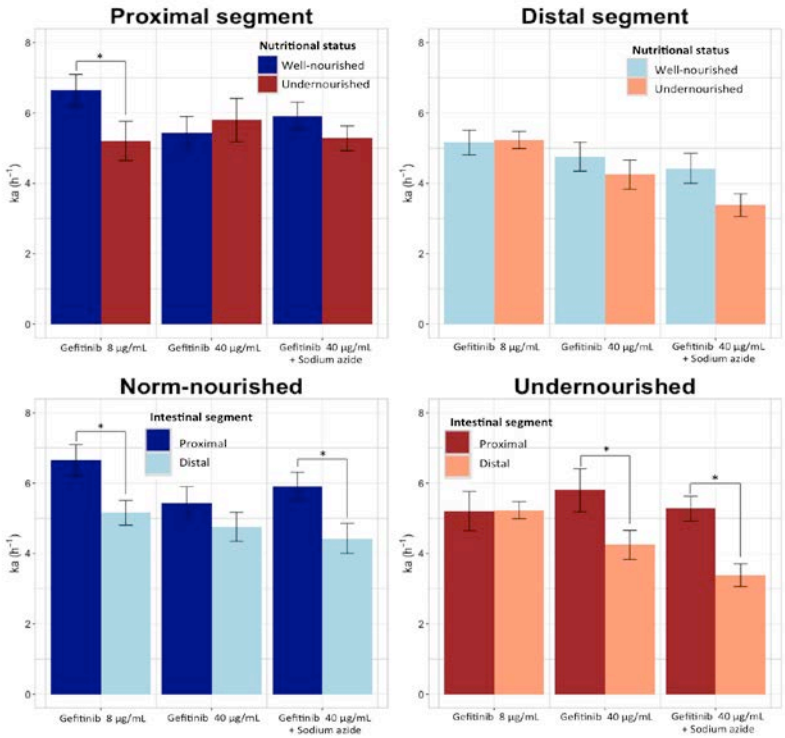


*Figure 3.13. ka values for **gefitinib**. Top panels represent ka values for proximal (left) and distal (right) intestinal segments for each perfused solution in well-nourished (blue) and undernourished (salmon) animals. Bottom panels represent ka values for norm-nourished (left) and undernourished (right) rats for each perfused solution and intestinal segment (proximal: blue; distal: salmon).*

Additionally, data were evaluated using mechanistic models considering linear and non-linear kinetics. Main tested mechanistic models for proximal and distal intestinal segments are shown in Tables 3.19-20.

*Table 3.19. Selection of the main structural absorption and secretion models for **gefitinib** in **proximal** intestine.*

| Model | Description | | FE (n) | RE (n) | MOFV | Performance |
|---|---|---|---|---|---|---|
| | Absorption | Secretion | | | | |
| 701 | First order | None | 1 | 2 | 174.23 | Biased goodness-of-fit plots |
| 702 | First order | First order | 2 | 2 | 174.23 | Unstable estimates |
| 703 | First order | Michaelis-Menten | 3 | 2 | 168.89 | Unstable estimates for $Km_s$ and $Vmax_s$. Biased goodness-of-fit plots |
| 704 | Michaelis-Menten | Michaelis-Menten | 4 | 2 | - | Did not minimize successfully |

*FE (n): Number of estimated fixed effects parameters; RE (n): Number of estimated random effects parameters; MOFV: Minimum objective function value; $Km_s$: Michaelis menten constant for secretion process; $Vmax_s$: Maximum secretion rate.*

*Table 3.20. Selection of the main structural absorption and secretion models for **gefitinib** in **distal** intestine.*

| Model | Description | | FE (n) | RE (n) | MOFV | Performance |
|---|---|---|---|---|---|---|
| | Absorption | Secretion | | | | |
| 801 | First order | None | 1 | 2 | 182.24 | Biased goodness-of-fit plots |
| 802 | First order | First order | 2 | 2 | 182.02 | Unstable estimates |
| 803 | First order | Michaelis-Menten | 3 | 2 | 154.23 | Unstable estimates for $Km_s$ and $Vmax_s$. Biased goodness-of-fit plots |
| 804 | Michaelis-Menten | Michaelis-Menten | 4 | 2 | - | Did not minimize successfully |

*FE (n): Number of estimated fixed effects parameters; RE (n): Number of estimated random effects parameters; MOFV: Minimum objective function value; $Km_s$: Michaelis menten constant for secretion process; $Vmax_s$: Maximum secretion rate.*

The developed compartmental models were not capable of correctly describing observed data. Furthermore, model parameter estimates were unstable, highly dependent on initial parameter estimates and covariance step in NONMEM failed in most of the models. Figure 3.14 exemplifies bias of one of the evaluated compartmental models (model 803). Even though some of the models had significantly lower MOFV as compared to the simplest model, these were not selected due to instability and bias of the model.

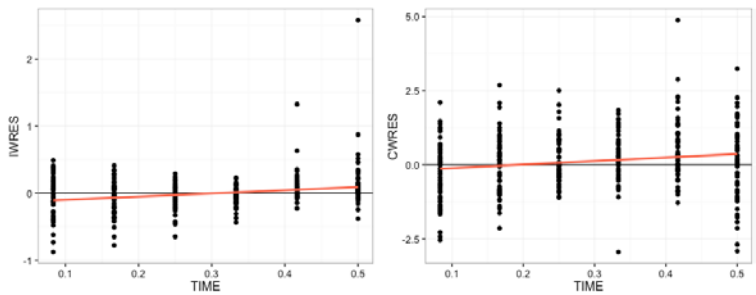


*Figure 3.14. Residual variability-based goodness-of-fit plots for a mechanistic model consisting on linear absorption and non-linear secretion of **gefitinib** across intestinal barrier (model 803). Red line represents central tendency. IWRES: individual weighted residuals; CWRES: conditional weighted residuals; TIME: time in hours since solution perfusion.*

Given that models obtained through a mechanistic approach were not completely satisfactory, the Weibull equation was evaluated. Tested Weibull models as well as final model parameter estimates are shown in Tables 3.21-22, respectively.

*Table 3.21. Main Weibull models tested for **gefitinib** intestinal absorption*

| Model | Parameters | | | MOFV |
|---|---|---|---|---|
| | $\alpha$ | $\beta$ | fr | |
| 901 | $\alpha = \theta$ | $\beta = \theta$ | $fr_{40} = fr_8 = 1$ | 344.99 |
| 902 | $\alpha = \begin{cases} \theta_1 if\ proximal \\ \theta_2\ if\ distal \end{cases}$ | $\beta = \theta$ | $fr_{40} = fr_8 = 1$ | 342.56 |
| 903 | $\alpha = \theta$ | $\beta = \begin{cases} \theta_1 if\ proximal \\ \theta_2\ if\ distal \end{cases}$ | $fr_{40} = fr_8 = 1$ | 343.67 |
| 904 | $\alpha = \theta$ | $\beta = \theta$ | $fr_{40} = \theta\ ; fr_8 = 1$ | 329.42 |
| **905** | $\boldsymbol{\alpha = \theta}$ | $\boldsymbol{\beta = \theta}$ | $\boldsymbol{fr_{40} = \begin{cases} \theta_1 if\ proximal \\ \theta_2\ if\ distal \end{cases}}$ $\boldsymbol{fr_8 = 1}$ | **313.23** |
| 908 | $\alpha = \theta$ | $\beta = \theta$ | $fr_{40} = 1; fr_8 = \theta$ | 343.06 |

*α: scaling factor; β: shape parameter; $fr_{40}$ and $fr_8$: correction factor for 40 µg/mL and 8 µg/mL solutions respectively; MOFV: minimum objective function value; θ: estimated parameter; proximal: intestinal proximal segment data; distal: intestinal distal segment data; bold: selected model*

*Table 3.22. Final model parameter estimates and bootstrap results for **gefitinib** intestinal perfusion study.*

| Parameter | Estimate | RSE (%) | Bootstrap results | |
|---|---|---|---|---|
| | | | Median | 95% CI |
| Fixed effect parameters | | | | |
| α ($h^{-1}$) | 2.40 | 5.6 | 3.27 | 2.34 – 4.52 |
| β | 0.78 | 2.1 | 0.86 | 0.75 – 0.95 |
| $fr_{40}$ – proximal | 0.61 | 7.7 | 0.54 | 0.46 – 0.66 |
| $fr_{40}$ – distal | 0.51 | 8.7 | 0.48 | 0.38 – 0.59 |
| Between subject variability | | | | |
| $\omega^2\ \beta_{proximal}$ | 0.0069 | 13.2 | 0.0057 | 0.0031 – 0.0090 |
| $\omega^2\ \beta_{distal}$ | 0.0049 | 13.7 | 0.0040 | 0.0017 – 0.0071 |
| Residual error | | | | |
| $\varepsilon_{exp}$ | 0.051 | 15.1 | 0.047 | 0.032 – 0.072 |

*RSE: relative standard error; CI: confidence interval; α: scaling factor; β: shape factor; $fr_{40}$ – proximal: correction factor for proximal intestine; $fr_{40}$ – distal: correction factor for distal intestine; $\omega^2$: between subject variance; $\varepsilon_{exp}$: exponential residual variability.*

Final model only took into account the incorporation of *fr* parameter for 40 µg/mL gefitinib solution ($fr_{40} < 1$) but not for 8 µg/mL gefitinib solution ($fr_8 = 1$). Statistically significant differences were not

found for model parameters $\alpha$ and $\beta$ between intestinal segments as shown in Table 3.21. On the other hand, parameter $fr_{40}$ proved to be 19% higher for the proximal intestine ($fr_{40}$ = 0.606) than for the distal segment ($fr_{40}$ = 0.510). Regarding sodium azide administration and undernutrition status, statistically significant differences between groups were not evidenced in model parameters.

Goodness of fit plots evidenced an adequate performance of the final model (Figure 3.15). Finally, internal validation of the model was successfully performed. Bootstrap and visual predictive check results are shown in Table 3.22 and Figure 3.16, respectively.

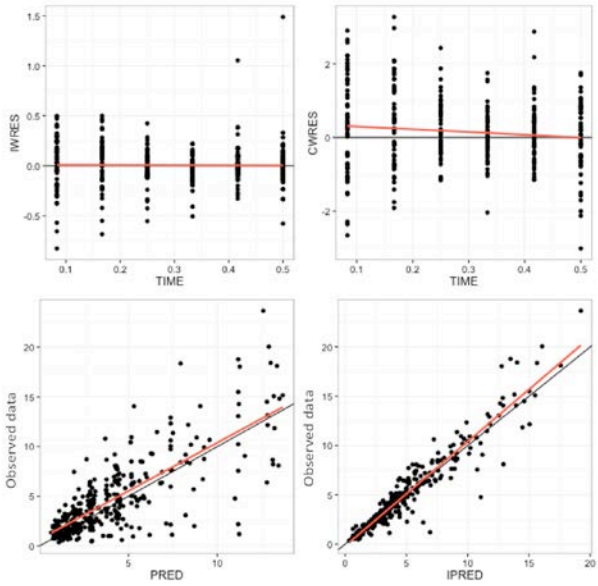


*Figure 3.15. Goodness of fit plots of final model for **gefitinib** intestinal perfusion study. IWRES: Individual weighted residuals; CWRES: Conditional weighed residuals; PRED: Population predictions; IPRED: Individual predictions. Red line represents central tendency.*

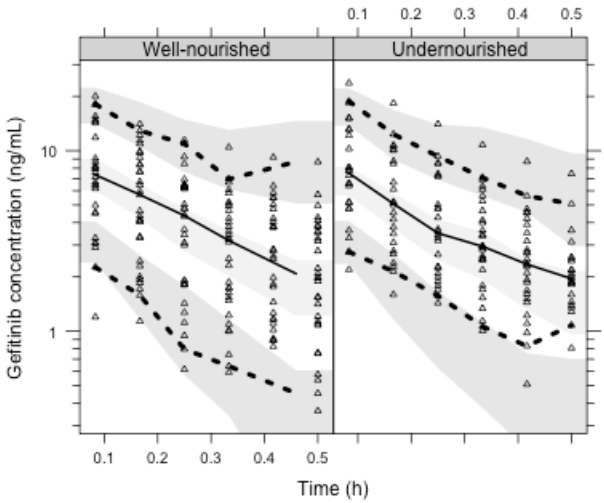


*Figure 3.16 Visual predictive check plots of final model for **gefitinib** intestinal perfusion study. Triangles represent observed concentrations; solid line represents the median value of the observations; dashed lines represent the 2.5th and 97.5th percentiles of the observations; light grey shaded area indicates the 95% confidence interval (CI) of the median simulated values; dark grey shaded areas indicate the CIs of the 2.5th and 97.5th percentiles of the simulated values.*

## 3.6 Pharmacokinetic model selection for erlotinib

One- and two-compartment models were tested for IV administration data (using data obtained from both WN and UN rats simultaneously). As shown in Table 3.23 a two-compartment model best described disposition of erlotinib in well- and undernourished rats.

*Table 3.23. Structural models for **erlotinib** disposition after intravenous administration in well- and undernourished rats.*

| Model | Description | FE (n) | RE (n) | MOFV |
|---|---|---|---|---|
| 031 | One-compartment model | 2 | 3 | 404.72 |
| **032** | **Two-compartment model** | **4** | **3** | **238.073** |

*FE (n): Number of estimated fixed effects parameters; RE (n): Number of estimated random effects parameters; MOFV: Minimum objective function value; bold: selected model.*

Once the disposition structural model had been selected, covariates were tested on structural parameters. Main evaluated models are shown in Table 3.24. Among them, the model in which nutritional status influenced drug clearance (CL) was selected (Model 035).

*Table 3.24. Main tested covariate models for **erlotinib** disposition after intravenous administration in well- and undernourished rats.*

| *Model* | *Covariates on pharmacokinetic parameters* | | | *Reference model* | *ΔMOFV* |
|---|---|---|---|---|---|
| | *Vc* | *Vp* | *CL* | | |
| *032* | - | - | - | - | - |
| ***035*** | **-** | **-** | $CL=\theta_1\cdot(1+\theta_2\cdot UN)$ | ***032*** | ***-12.33*** |
| *036* | $Vc=\theta_1\cdot(1+\theta_2 UN)$ | - | - | *032* | *-1.55* |
| *038* | - | $Vp=\theta_1\cdot(1+\theta_2\cdot UN)$ | - | *032* | *-0.74* |
| *039* | $Vc=\theta_1\cdot(1+\theta_2\cdot(Albumin-3.7))$ | - | - | *032* | *-0.13* |

*Vc: central compartment volume of distribution; Vp: peripheral compartment volume of distribution; CL: drug clearance from central compartment; θ: estimated parameters; ΔMOFV: minimum objective function value change with regard to reference model; bold: selected model.*

Thereafter, oral administration data was incorporated into the modelling dataset and the structural absorption model was constructed. Regarding the statistical model, BSV was incorporated to CL, peripheral volume of distribution (Vp) and ka. Additive, proportional and exponential RV models were tested and the exponential RV model was selected.

The inclusion of a parameter to account for oral bioavailability (f) was tested and then nutritional status (WN or UN) as well as dispersion system used for the administration (solution or suspension) were tested as dichotomous covariates on ka and f parameters. Description of the main models developed during this stage of the modelling process is shown in Table 3.25

*Table 3.25. Selection of tested models evaluating undernourishment and type of dispersion systems as covariates on bioavailability and absorption rate constant of* ***erlotinib****.*

| *Model* | *Covariates on pharmacokinetic parameter* | | *Reference model* | *ΔMOFV* |
|---|---|---|---|---|
| | *Ka* | *f* | | |
| *045* | - | *f=1* | - | - |
| *046* | $ka = \begin{cases} \theta_1 \; if \; WN \\ \theta_2 \; if \; UN \end{cases}$ | *f=1* | *045* | *-9.49* |
| *047* | $ka = \begin{cases} \theta_1 \; if \; Solution \\ \theta_2 \; if \; Suspension \end{cases}$ | *f=1* | *045* | *-34.93* |
| *048* | $ka = \begin{cases} \theta_1 \; if \; WN + Solution \\ \theta_2 \; if \; WN + Suspension \\ \theta_3 \; if \; UN + Solution \\ \theta_4 \; if \; UN + Suspension \end{cases}$ | *f=1* | *047* | *-16.96* |
| *050* | $ka = \begin{cases} \theta_1 \; if \; WN + Solution \\ \theta_2 \; if \; WN + Suspension \\ \theta_3 \; if \; UN + Solution \\ \theta_4 \; if \; UN + Suspension \end{cases}$ | $f = \begin{cases} 1 \\ \theta \; if \; UN + Solution \end{cases}$ | *048* | *-0.00* |
| *051* | $ka = \begin{cases} \theta_1 \; if \; WN + Solution \\ \theta_2 \; if \; WN + Suspension \\ \theta_3 \; if \; UN + Solution \\ \theta_4 \; if \; UN + Suspension \end{cases}$ | $f = \begin{cases} 1 \\ \theta \; if \; UN + Supension \end{cases}$ | *048* | *-0.12* |
| *052* | $ka = \begin{cases} \theta_1 \; if \; WN + Solution \\ \theta_2 \; if \; WN + Suspension \\ \theta_3 \; if \; UN + Solution \\ \theta_4 \; if \; UN + Suspension \end{cases}$ | $f = \begin{cases} 1 \\ \theta \; if \; WN + Solution \end{cases}$ | *048* | *-1.41* |
| *053* | $ka = \begin{cases} \theta_1 \; if \; WN + Solution \\ \theta_2 \; if \; WN + Suspension \\ \theta_3 \; if \; UN + Solution \\ \theta_4 \; if \; UN + Suspension \end{cases}$ | $f = \begin{cases} 1 \\ \theta \; if \; WN + Suspension \end{cases}$ | *048* | *-13.36* |
| ***054*** | $\boldsymbol{ka = \begin{cases} \theta_1 \; if \; WN + Solution \\ \theta_2 \; if \; UN + Solution \\ \theta_3 \; if \; UN + Suspension \end{cases}}$ | $\boldsymbol{f = \begin{cases} 1 \\ \theta \; if \; WN + Suspension \end{cases}}$ | ***053*** | ***+0.14*** |

*ka: first order absorption rate constant; f: oral bioavailability; ΔMOFV: minimum objective function value change with regard to reference model; WN: well-nourished rats; UN: undernourished rats.; θ: estimated parameter; bold: selected model.*

Once the final model had been selected (model 054), all parameters were estimated simultaneously. Parameter estimates for the final model are shown in Table 3.26.

*Table 3.26. Pharmacokinetic parameters estimates and bootstrap results of final model for **erlotinib** in vivo pharmacokinetic study.*

| Pharmacokinetic parameter | | Final Model | | Bootstrap Replicates | |
|---|---|---|---|---|---|
| | | Estimate | RSE(%) | Median | 95% CI |
| Fixed effect parameters | | | | | |
| CL (L/h) | | 9.9 | 8.1 | 9.8 | 8.62-11.5 |
| $FCL_{UN}$ | | -0.051 | 12.6 | -0.050 | -0.068-(-0.010) |
| Vc (L) | | 21.6 | 49.1 | 20.8 | 8.1-62.6 |
| Vp (L) | | 108.0 | 12.1 | 105.3 | 74.6-132.4 |
| Q (L/h) | | 36.4 | 17.9 | 33.4 | 20.5-47.3 |
| $k_a$ ($h^{-1}$) | $WN_{sol}$ | 0.417 | 18.1 | 0.408 | 0.238-0.555 |
| | $UN_{sol}$ | 0.200 | 24.5 | 0.187 | 0.082-0.310 |
| | $WN_{susp}$ and $UN_{susp}$ | 0.147 | 18.7 | 0.310 | 0.098-0.209 |
| f | $WN_{sol}$, and $UN_{sol}$ and $UN_{susp}$ | 1 (FIX) | - | - | - |
| | $WN_{susp}$ | 0.872 | 12.0 | 0.860 | 0.685-0.988 |
| Between-subject variability | | | | | |
| $\omega^2$ CL (%) | | 38.6 | 12.5 | 37.4 | 28.6-49.0 |
| $\omega^2$ Vp (%) | | 110.0 | 29.8 | 106.0 | 1.1-191.0 |
| $\omega^2$ ka (%) | | 50.4 | 40.6 | 50.5 | 0.504-86.6 |
| Residual variability | | | | | |
| $\varepsilon_{exp}$ (%) | | 38.1 | 15.8 | 37.4 | 31.4-43.8 |

*RSE: Relative estimation error; CI: Confidence Interval; CL: Clearance; $FCL_{UN}$: Factor that quantifies the clearance change in undernourished rats (expressed as a fraction) with regard to clearance in well-nourished rats; Vc: Volume of distribution of the central compartment; Vp: Volume of distribution of the peripheral compartment; Q: Inter-compartmental clearance; ka: Absorption rate constant; f: Bioavailability; $\omega^2$: Between-subject variance; $\varepsilon_{exp}$: Exponential residual variability.*

In the final model, undernourishment (as a dichotomous covariate) caused approximately a 5% decrease of CL parameter. Furthermore, the selected model revealed that groups receiving erlotinib through the oral route had different absorption rates depending on their nutritional status and on the dispersion system employed:

- WN and UN rats receiving erlotinib as a solution had ka values of 0.417 and 0.200 $h^{-1}$, respectively
- Rats receiving erlotinib as a suspension had a ka value of 0.147 $h^{-1}$ irrespectively of nutritional status.

Regarding oral bioavailability (f) estimates, f = 1 for rats receiving erlotinib as a solution. On the other hand, when erlotinib was administered as a suspension, oral bioavailability depended on nutritional status: for WN rats f = 0.872 and for UN rats f = 1 (as for those receiving erlotinib as a solution).

Goodness of fit plots evidenced an adequate performance of the final model (Figure 3.17). Regarding model validation, median values of the bootstrap procedure with successful minimisation were similar to the population parameter estimates of the original dataset (Table 3.26). Furthermore, fixed and random parameter estimates of the original data fell within the 95% CI obtained for the bootstrap replicates (100). The results of the visual predictive check (Figure 3.18) endorsed the selected model.

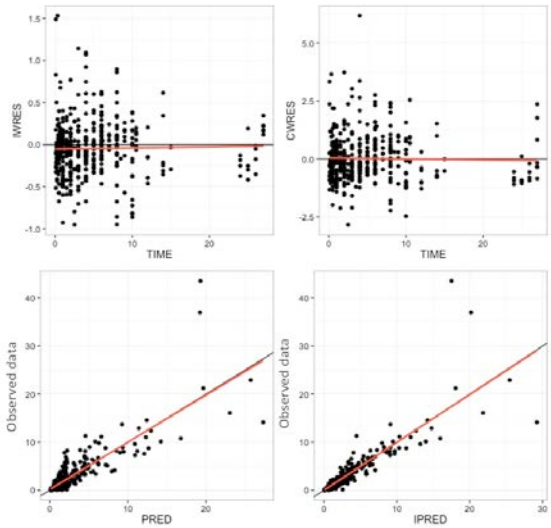


*Figure 3.17. Goodness of fit plots of final pharmacokinetic model for* ***erlotinib*** *in vivo study. IWRES: Individual weighted residuals; CWRES: Conditional weighted residuals; PRED: Population predictions; IPRED: Individual predictions. Red line represents central tendency.*

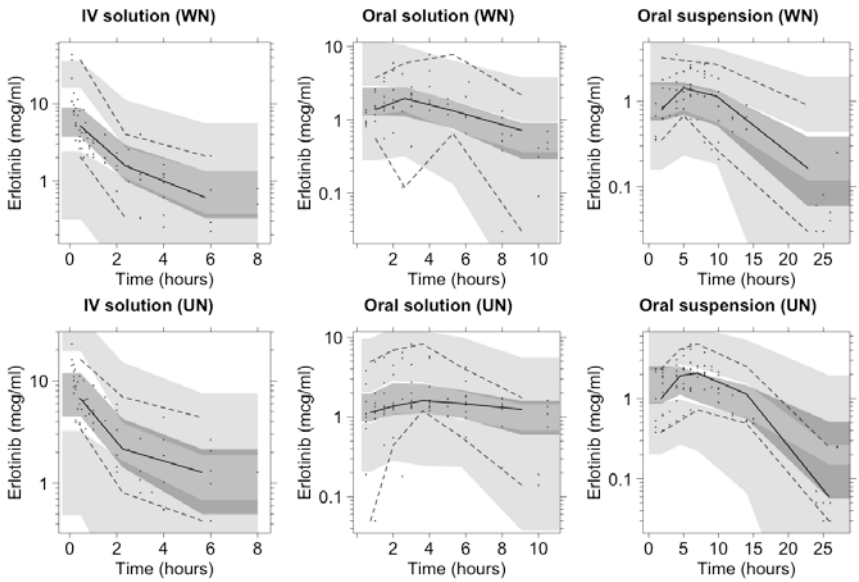


*Figure 3.18. Visual predictive check plots for **erlotinib** in vivo pharmacokinetic study. Points represent observed concentrations; solid lines represents the 50$^{th}$ percentile of the observations; dashed lines represent the 2.5$^{th}$ and 97.5$^{th}$ percentiles of the observations; shaded areas indicate the 95% confidence intervals for the 50$^{th}$ (dark grey), and for the 2.5$^{th}$ and 97.5$^{th}$ (light grey) percentiles of the simulated values. IV. Intravenous administration; WN: well-nourished rats; UN: under-nourished rats.*

The extrapolation of results obtained in rats up to human patients was performed through simulations. A graphical representation of simulated concentration-time profiles for WN and UN humans receiving erlotinib 150 mg dose is shown in Figure 3.19. Median steady-state minimum concentrations (before dose administration) for WN and UN individuals were 299.7 (95%CI 36.5 – 1118.8) ng/mL and 370.2 (95%CI 46.5 – 1330.2) ng/mL, respectively. Median AUC for simulated WN and UN individuals were 12919.3 (95%CI 4629.4 – 36986.1) ng/mL·h and 15375.7 (95%CI 5513.9 – 44471.6) ng/mL·h, respectively.

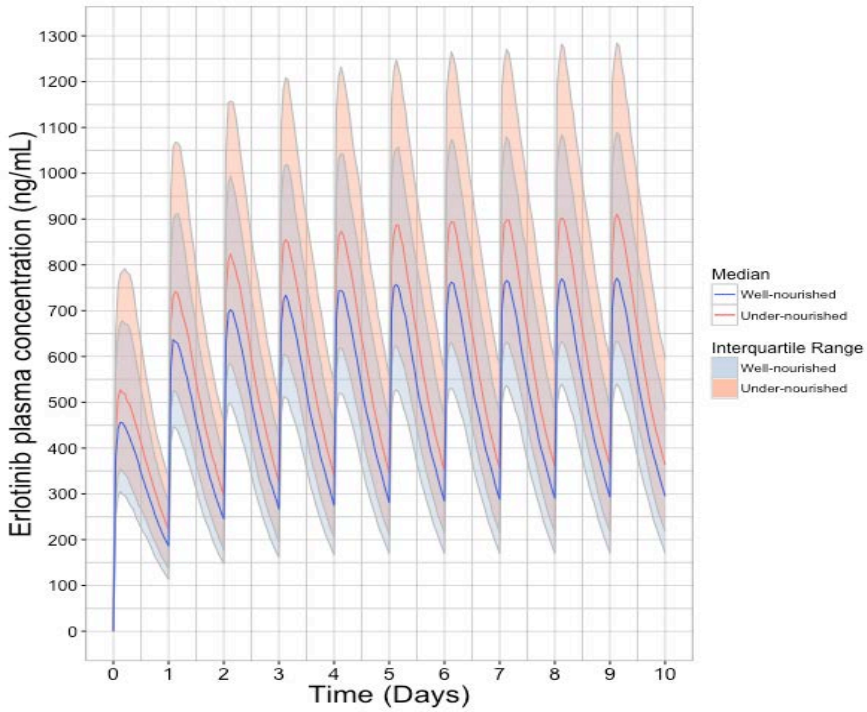


*Figure 3.19. Allometric scale-up simulations of **erlotinib** pharmacokinetic profiles in well-nourished and under-nourished individuals receiving erlotinib 150 mg / 24 hours.*

## 3.7 Pharmacokinetic model selection for gefitinib

One- and two-compartment models were tested for IV administration data. As shown in Table 3.27, a two-compartment model best described IV administration data.

*Table 3.27. Structural models for **gefitinib** disposition after intravenous administration in well- and undernourished rats.*

| Model | Description | FE (n) | RE (n) | MOFV |
|---|---|---|---|---|
| 000 | One-compartment model | 2 | 3 | 1276.50 |
| **001** | **Two-compartment model** | **4** | **3** | **1022.12** |

*FE (n): Number of estimated fixed effects parameters; RE (n): Number of estimated random effects parameters; MOFV: Minimum objective function value; bold: selected model.*

Once the disposition structural model had been selected, covariates were tested on structural parameters. Main evaluated models are shown in Table 3.28. Among them, the model in which nutritional status influenced central compartment distribution volume was selected.

*Table 3.28. Main covariate models tested for **gefitinib** disposition after intravenous administration in well- and undernourished rats.*

| *Model* | *Covariates on pharmacokinetic parameters* | | | *Reference model* | *ΔMOFV* |
|---|---|---|---|---|---|
| | *Vc* | *Vp* | *CL* | | |
| *001* | - | - | - | - | - |
| *004* | - | - | $CL = \theta_1 \cdot (1+\theta_2 \cdot UN)$ | *001* | *-0.38* |
| ***005*** | $\boldsymbol{Vc = \theta_1 \cdot (1+\theta_2 \cdot UN)}$ | - | - | ***001*** | ***-7.41*** |
| *006* | - | $Vp = \theta_1 \cdot (1+\theta_2 \cdot UN)$ | - | *001* | *-1.03* |
| *007* | $Vc=\theta_1 \cdot (1+\theta_2 \cdot (Albumin-3.7))$ | - | - | *001* | *-2.24* |

*Vc: central compartment volume of distribution; Vp: peripheral compartment volume of distribution; CL: drug clearance from central compartment; ΔMOFV: minimum objective function value change with regard to reference model; θ: estimated parameter; bold: selected model.*

Thereafter, oral administration data were incorporated into the modelling dataset and the structural absorption model was built. An oral administration compartment was incorporated and transit compartments in-between the oral administration compartment and the central compartment, as well as f parameter incorporation, were tested. The best-fitting structural absorption model consisted of an administration compartment (where $f < 1$) and one transit compartment as described in Figure 3.20. Description of main structural models tested at this stage of the modelling process is shown in Table 3.29

*Table 3.29. Absorption structural models for **gefitinib** after oral administration in well- and undernourished rats.*

| Model | Description | FE (n) | RE (n) | MOFV |
|---|---|---|---|---|
| 504 | No transit compartment | 1 | 2 | 1878.43 |
| 507 | One transit compartment | 1 | 2 | 1845.92 |
| 508 | Two transit compartments | 1 | 2 | 1924.41 |
| **510** | **One transit compartment + f** | **2** | **2** | **1839.32** |

*FE (n): Number of estimated fixed effects parameters; RE (n): Number of estimated random effects parameters; MOFV: Minimum objective function value; bold: selected model.*

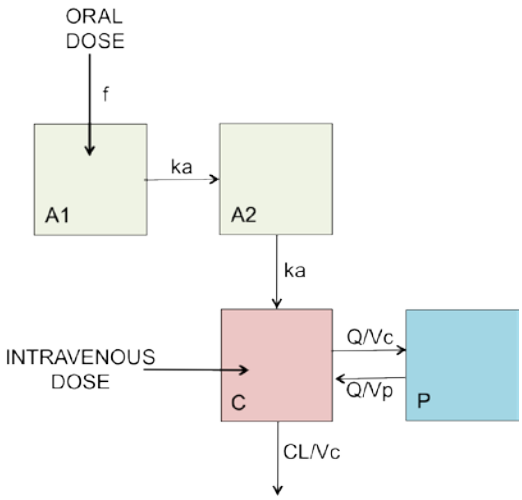


*Figure 3.20. Schematic representation of final pharmacokinetic model for gefitinib. A1: oral administration compartment; A2: absorption transit compartment; C: central compartment; P: peripheral compartment; ka: absorption rate constant; Q: inter-compartmental clearance; CL: clearance from central compartment; f: oral bioavailability.*

Finally, undernourishment was tested as a covariate on oral bioavailability (f) and ka. Here, f proved to be higher in UN rats as

compared with WN rats. MOFV for these models are shown in Table 3.30

*Table 3.30. Models evaluating undernourishment effect on bioavailability and absorption rate constant for **gefitinib** after oral administration in well- and undernourished rats.*

| *Model* | *Covariates on pharmacokinetic parameters* | | *Reference model* | *ΔMOFV* |
|---|---|---|---|---|
| | *ka* | *f* | | |
| *510* | - | - | - | - |
| *512* | $ka = \theta_1 \cdot (1+\theta_2 \cdot UN)$ | - | *510* | *-0.01* |
| ***513*** | - | $\boldsymbol{f = \begin{cases} \theta_1 \; if \; WN \\ \theta_2 \; if \; UN \end{cases}}$ | ***510*** | ***-7.28*** |
| *515* | $ka = \theta_1 \cdot (1+\theta_2 \cdot UN)$ | $f = \begin{cases} \theta_1 \; if \; WN \\ \theta_2 \; if \; UN \end{cases}$ | *513* | *-0.00* |

*ka: first order absorption rate constant; f: oral bioavailability; ΔMOFV: minimum objective function value change with regard to reference model; WN: well-nourished rats; UN: undernourished rats; θ: estimated parameter; bold: selected model.*

Regarding the statistical model, BSV was incorporated to CL and ka. Additive, proportional and exponential RV models were tested. Finally, an exponential RV model was selected. Once the final model had been selected, all parameters were estimated simultaneously. Final model parameters are shown in Table 3.31.

Goodness of fit plots evidenced an adequate performance of the final model (Figure 3.21). Internal validation of the model was successfully performed: bootstrap and visual predictive check (IV and oral administration) results are shown in Table 3.31 and Figures 3.22-3.23, respectively.

*Table 3.31. Pharmacokinetic parameter estimates and bootstrap results of the final model for **gefitnib** in vivo pharmacokinetic study.*

| Parameter | Estimate | RSE (%) | Bootstrap results | |
|---|---|---|---|---|
| | | | Median | 95% CI |
| Fixed effect parameters | | | | |
| Vc (L) | 22.8 | 50.9 | 26.7 | 12.5 – 77.6 |
| Vp (L) | 366 | 28.7 | 397 | 258 – 601 |
| CL (L $h^{-1}$) | 14.1 | 21.0 | 14.0 | 9.08 – 19.7 |
| Q (L $h^{-1}$) | 19.5 | 38.3 | 21.6 | 12.1 – 40.8 |
| Undernutrition on Vc | 0.321 | 39.1 | 0.326 | 0.047 – 0.975 |
| ka ($h^{-1}$) | 0.198 | 30.5 | 0.207 | 0.115 – 0.410 |
| Norm-nourished f | 0.446 | 33.6 | 0.472 | 0.160 – 0.759 |
| Under-nourished f | 0.681 | 23.2 | 0.683 | 0.373 – 0.961 |
| Between subject variability | | | | |
| $\omega^2$ CL | 0.168 | 59.1 | 0.160 | 0.0227 – 0.469 |
| $\omega^2$ ka | 0.442 | 59.0 | 0.443 | 0.0401 – 0.966 |
| Residual error | | | | |
| $\varepsilon_{exp}$ | 0.163 | 18.1 | 0.153 | 0.108 – 0.217 |

*RSE: Relative standard error, CI: confidence interval; ka: absorption rate constant; Vc: Distribution volume of central compartment; Vp: Distribution volume of peripheral compartment; CL: central compartment gefitinib clearance; Q: intercompartmental clearance; Undernutrition on Vc: effect of undernutrition on distribution volume of central compartment.*

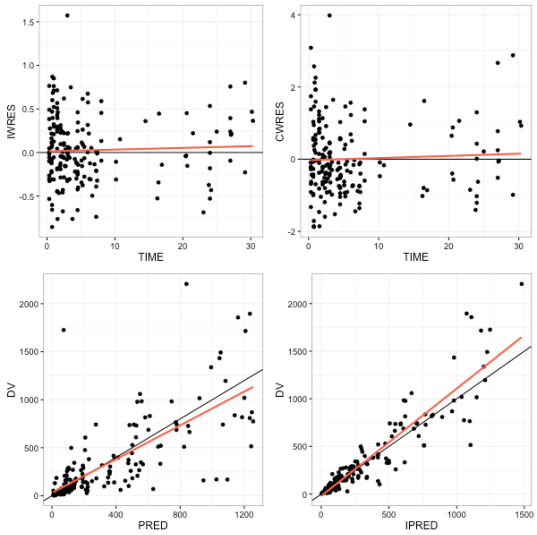


*Figure 3.21. Goodness of fit plots of final pharmacokinetic model for **gefitinib** in vivo study. IWRES: Individual weighed residuals; DV: Observed data; CWRES: Conditional weighed residuals; PRED: Population predictions; IPRED: Individual predictions. Red line represents central tendency.*

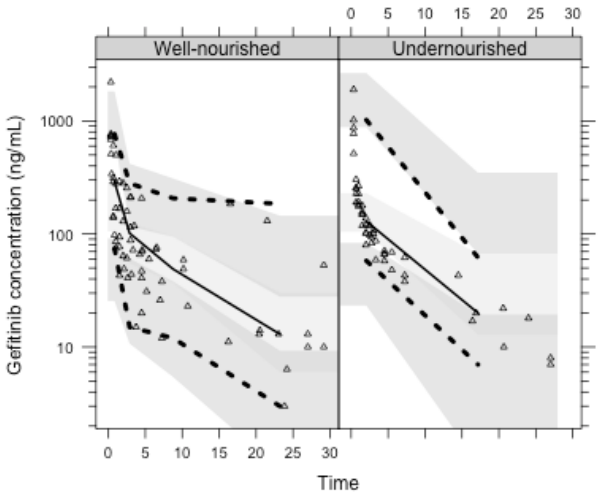


*Figure 3.22. Visual predictive check plot for **gefitinib** after intravenous administration. Triangles represent observed concentrations; solid line represents the median value of the observations; dashed lines represent the 2.5th and 97.5th percentiles of the observations; light grey area indicates the 95% confidence interval (CI) of the median simulated values; dark grey shaded areas indicate the CIs of the 2.5th and 97.5th percentiles of the simulated values.*

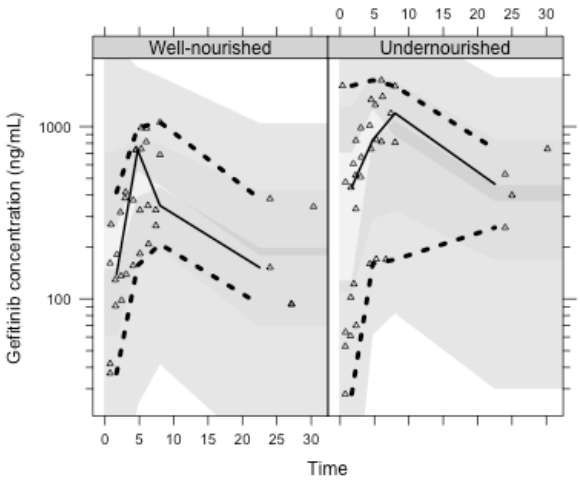


*Figure 3.23. Visual predictive check plot for **gefitinib** after oral administration. Triangles represent observed concentrations; solid line represents the median value of the observations; dashed lines represent the 2.5th and 97.5th percentiles of the observations; light grey area indicates the 95% confidence interval (CI) of the median simulated values; dark grey shaded areas indicate the CIs of the 2.5th and 97.5th percentiles of the simulated values.*

The extrapolation of results obtained in rats up to human patients was performed through simulations. Graphical representation of simulated concentration-time profiles for WN and UN humans receiving gefitinib 250 mg dose is shown in Figure 3.24. Median steady-state minimum concentrations (before dose administration) for WN and UN individuals were 215.8 (95%CI 54.8 – 811.8) ng/mL and 333.7 (95%CI 81.4 – 1268.7) ng/mL, respectively. Median AUC for simulated WN and UN individuals were 7509.8 (2436.3 – 24155.5) ng/mL·h and 11357.5 (3825.2 – 37336.4) ng/mL·h, respectively.

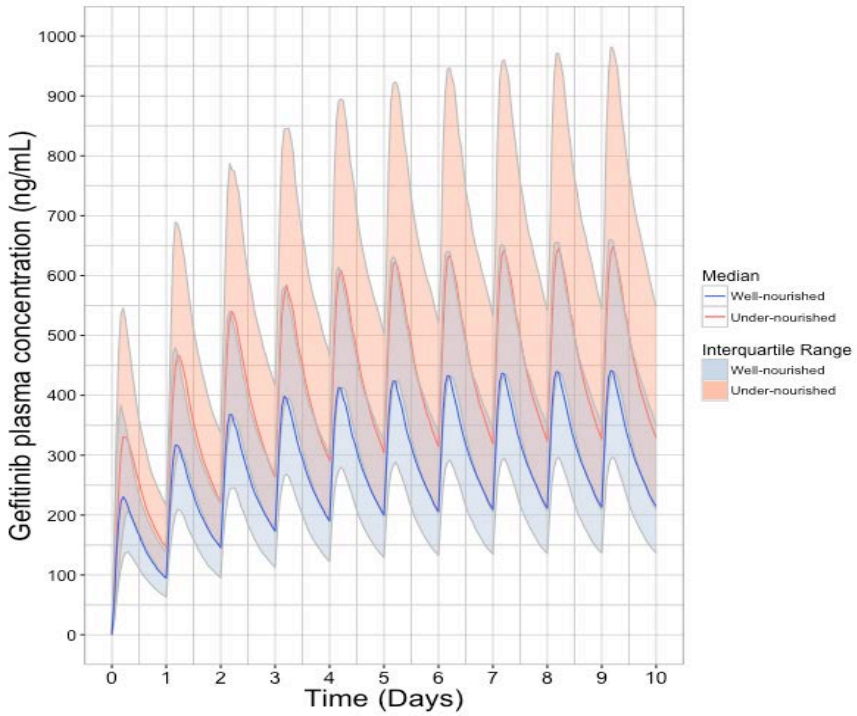


*Figure 3.24. Allometric scale-up simulations of **gefitinib** pharmacokinetic profiles in well-nourished and under-nourished individuals receiving gefitinib 250 mg / 24 hours.*

# 4 Discussion

There are many reports in the literature describing the pharmacokinetic parameters of drugs that are altered in states of protein-energy malnutrition but, surprisingly, very few focus on anticancer drugs (25, 26). Taking into account that cancer victims suffer severe undernourishment (in lung cancer, patients lose 30% of their pre-illness stable weight, 85% of their total body fat, and a 75% of their skeletal muscle protein mass) (101) and that antineoplastic drugs have, in most of the cases, a narrow therapeutic index, it is important to consider how this physio-pathological state can influence pharmacokinetic behaviour of antineoplastic drugs.

A wide variety of treatment modalities can be found among the therapeutic possibilities in cancer treatment. Treatments can be administered through different routes (ie. IV, oral, subcutaneous), can last different time periods (ie. weeks, months, until disease progression) and can be administered with different frequencies (ie. daily, weekly, monthly). This implies very diverse pharmacokinetic profiles in which pharmacokinetic alterations can have different implications. Given that the absorption process represents an additional potential source of pharmacokinetic variability when compared with the IV route, those treatments which are administered through routes different to the IV one are potentially more susceptible of being affected by systemic alterations caused by undernourishment. Furthermore, those drugs administered for long periods of time (ie. until disease progression) and which are given with a high frequency in comparison to their elimination half life, have a high susceptibility of accumulating in patients and are potentially susceptible of being impacted by clearance alterations related to UN.

In this context, two orally administered anti-cancer drugs were chosen for the evaluation of undernourishment on their PK: erlotinib and gefitinib. Even though these two drugs have similar chemical properties, they present pharmacokinetic differential characteristics (ie. absorption and elimination pathways). This fact enabled the evaluation of how UN status influences pharmacokinetic profiles of drugs with different pharmacokinetic determinants.

In this Thesis, the effect of under-nutrition on the pharmacokinetics of erlotinib and gefitinib has been evaluated through *in vivo* population pharmacokinetic analyses. Additionally, *in situ* intestinal perfusion studies have also been analysed through population analysis to provide more specific insight on how undernourishment influences drug absorption. In order to complement results obtained through *in vivo* and *in situ* experiments, an evaluation of how undernourishment influences analytical and molecular parameters was also carried out. In the following sections, the main findings will be discussed, and an overview of how the results of *in situ* and *in vivo* studies complement each other will be provided.

## 4.1 Study population

The animal species chosen for this research project was the Wistar rat. This animal species has important physiological similarities with humans which makes it a suitable species for pre-clinical testing (102).

The scoring system developed by Merino-Sanjuán et al. was used for the classification of rats into different nutritional status levels. This scoring system is based on the CONUT human nutritional status screening-tool (80). The CONUT screening tool is considered a good option for its adaptation to a preclinical environment given that it has proved to have a high sensitivity and specificity in the clinical setting. The employed scoring system used weight and serum albumin concentration as biomarkers. Given the long biological half-life of albumin (7 days), rats underwent an adaptation period of 23-26 days in order to ensure that under-nutrition was reflected in albumin levels.

A total of 165 male Wistar rats (81 WN and 84 UN) were included in this research project. Undernourishment status was reached in all rats assigned to UN group at the end of the adaptation period. Most of the rats in this group developed mild (n = 67; 79.8%) and moderate (n = 16; 19.0%) undernourishment degrees and only one rat developed severe under-nutrition, thus limiting the impact of undernourishment on physiopathological status of rats.

## 4.2 Drug quantitation methods

Reliability of information obtained from analytical determinations of drug concentrations was a critical aspect for the success of all the mathematical analyses performed on the obtained data.

All quantitation methods were validated with regard to linearity, precision, accuracy and lower limit of quantification (LLOQ). Least squares regression analyses evidenced excellent linearity for all

analytical methods. Precision and accuracy results were also considered adequate. The LLOQ, defined as ten times the signal of a blank sample, were sufficiently low to ensure that all quantitated concentrations in *in situ* and *in vivo* experiments were above this limits. Given that all sample concentrations were above the LLOQ, all experimental data points obtained in *in situ* and *in vivo* pharmacokinetics studies were used for pharmacokinetic analyses.

## 4.3 Evaluation of analytical and molecular alterations associated with undernourishment

Inadequate energy and protein intake leads to various physiological adaptations. Physiopathological changes resulting from under-nutrition cause functional alterations in every organ-system of the body and thus alterations of analytical and molecular biomarkers are expected. The assay evaluating the analytical and molecular alterations associated to undernourishment was intended to provide a general picture of how these biomarkers are altered in undernourishment. With this purpose, gene expression levels (in terms of mRNA) of proteins involved in PK, blood cell counts and other haemogram derived markers, and bioanalytical markers obtained from a biochemical analyses, were measured in WN and UN rats. Liver and total body weight were also recorded and compared between groups.

**Gene expression analyses**

mRNA expression was measured through qRT-PCR analyses. Intestinal and hepatic enzymes and transporters commonly implicated in drug PK were selected for this analysis.

When evaluating results of this analysis, the possibility of compensatory mechanisms causing an increase in mRNA expression must be kept in mind. These compensatory mechanisms take place when there is a decreased availability of amino acids for protein synthesis (e.g. undernourishment status). In these circumstances, the organism can sometimes avoid the potential decrease in protein synthesis by increasing gen transcription rate, resulting in increased mRNA levels but not necessarily in normal protein levels. Van Zutphen et al. (103) carried out a study in UN and WN rats in which they evidenced that a compensatory transcriptional up-regulation of major pathways takes place when rats are fed with a low protein diet. Thus, decrease in mRNA levels can represent a decrease in protein synthesis, but an increase in mRNA levels does not necessarily imply an increase in protein expression since it can be caused by the before mentioned compensatory mechanism.

Firstly, the influence of under-nutrition on hepatic molecular markers (shown in Figure 3.4) was evaluated. The obtained results proved that OATP, MRP2, P-gp and UDP mRNA levels were significantly lower in UN as compared with WN rats. These results emphasize the potential risk of PK alterations in undernourishment status when these enzymes are involved in the processes of secretion or metabolic biotransformation of drugs. On the other hand, statistically

significant differences were not evidenced for metabolic enzymes CYP 1A1 and CYP 1A2 in liver samples between well- and undernourished rats. These results are controversial when compared to other published studies. Studies in rodents illustrating a protein-calorie-malnutrition-related inhibition of P450s have been previously reported, including CYP1A1 and CYP1A2 (104). The results obtained in our assay might not reflect the underlying decreased CYP1A1 and CYP1A2 synthesis described by other authors as a consequence of the before mentioned compensatory mechanisms. Nevertheless, this hypothesis could not be confirmed since protein expression levels were not available.

The analysis of molecular biomarkers was also carried out in tissue samples of the proximal, medial and distal segments of the intestine. Results for these analyses are shown in Figure 3.5. These results evidenced that the influence of undernourishment on P-gp mRNA levels was irregular across the investigated intestinal segments, whereas MRP2 mRNA levels increased in undernourishment status in all the investigated segments (maybe due to a compensatory mechanism). Consequently, final balance of secretion transporters expression could explain the observed drug bioavailability differences between well- and undernourished rats when drugs are administered through the oral route (Table 3.26 and Table 3.31). Regarding the influence of undernourishment on the expression of the intestinal biomarker CYP1A1, this proved to have an irregular pattern (statistically significant decrease was evidenced in proximal and medial intestinal segments whereas a slight increase was observed in the distal segments without reaching statistical significance). Ultimately, drug

absorption will be altered in undernourishment status to a greater o lesser extent depending on the molecular determinants involved in the absorption process of the evaluated drug.

**Haemogram analyses**

Whole blood aliquots were used for the analysis of red blood cell count, white blood cell count, platelet count, haemoglobin concentration, haematocrit and mean corpuscular volume determination. All evaluated parameters except for mean corpuscular volume proved to have statistically significant lower values in UN rats. Diet restriction is known to cause severe alterations in hematopoietic bone marrow, such as hypocellularity, necrosis and extracellular matrix modifications (105). The results of this experiment evidence the haematological disturbances that take place in this situation. UN rats developed anaemia, as evidenced by red blood cell counts and haemoglobin concentrations, and experienced a decrease of white blood cells and platelets.

Most of the analytical alterations associated to undernourishment evidenced in haemogram analyses in rats are in accordance with analytical alterations observed in undernourished lung cancer patients as compared to well-nourished lung cancer patients (99). Parameters such as haemoglobin concentration, haematocrit, and red blood cell count proved to be decreased in undernourishment status both in undernourished rats and patients. The only evidenced difference between results in our study and results in cancer patients was white blood cell count. In undernourished cancer patients this parameter was increased whereas in undernourished rats white blood cell count was

decreased. This difference could be, among other reasons, due to the controlled conditions in which rats were housed, as compared to cancer patients who have a higher risk of infections.

The results obtained in this assay support the chosen under-nutrition protocol, evidencing its capability to reproduce in a preclinical setting under-nutritional status in rats. Furthermore, the evidenced alterations can have an influence on drug distribution (due to alterations of intracellular deposits in blood cells) and, likewise, can also have a clinically relevant implication in the risk of suffering hematologic adverse events secondary to anti-cancer treatments.

**Biochemical analyses and liver weight comparison**

Blood samples where used for the analysis of ALAT, ASAT, total protein concentration, acid-alpha glycoprotein concentration, and serum protein electrophoresis bands. Additionally liver weight was compared between WN and UN rats.

Biochemical analyses evidenced alterations in acute phase proteins: decreased albumin, increased alpha acid glycoprotein and increased alpha-2 band in the electrophoretic analyses.

Regarding ALAT and ASAT, both significantly increased ($p<0.01$ and $p<0.001$, respectively) in UN rats as compared to WN rats. The increase of these two biomarkers can happen in those situations in which hepatic injury exists, such as liver tissue degeneration or necrosis. Liver damage in undernourishment status has been previously described in the clinical setting. Pierre–Emmanuel et al. (106) reported that patients suffering anorexia experienced an increase in ALAT and ASAT concentrations, and autophagy was speculated as the mechanism

by which hepatic damage was taking place. When comparing liver weight, and liver-body weight coefficients for WN and UN rats, a decreased growth of hepatic tissue was evidenced ($p < 0.001$) in UN rats. These facts, together with the decreased albumin band ($p < 0.05$) in the protein electrophoresis analysis, indicate that hepatic injury could be happening in UN rats. Once again, the results of this assay, in addition to providing information about the functional deterioration secondary to undernourishment, support the chosen under-nutrition protocol, evidencing its capability to reproduce in a preclinical setting under-nutritional status in rats.

Overall, the results obtained demonstrate that the response of the organism to compensate the deficiencies generated by the inadequate energy and protein intake is very complex. Consequently, it is expected that general changes in pharmacokinetics in undernourishment status are very variable, difficult to predict and highly dependent on the evaluated drug.

## 4.4 Intestinal absorption

The main objective of intestinal perfusion studies was to analyse the influence of under-nutrition on drug disappearance rate from intestinal lumen. Secondarily, these studies were designed to analyse the potential interaction of inhibitors on the absorption of erlotinib and gefitinib and the role of nutritional status on this interactions by means of population pharmacokinetic modelling using data obtained from WN and UN rats.

Studies in the literature have previously described alterations in drug absorption for multiple drugs. It has been reported that oral absorption of drugs such as carbamazepine, chloroquine, sulphadiazine, and chloramphenicol is significantly decreased in children with PEM when compared with healthy normal children (107). On the other hand, the literature review by Oshikoya et al. found that the extent of absorption of 8 drugs was significantly increased in undernourishment status. For this reason, this project had a deeper look into the absorption process of erlotinib and gefitinib through *in situ* intestinal assays (108).

Drug intestinal permeability has been widely investigated by *in situ* and *in vivo* experimental approaches using animal models, and results have been translated into humans (109). In this study, a rat model based on a closed loop technique was employed to analyse the absorption processes of erlotinib and gefitinib as well as the role of intestinal drug transporters, the interaction of drug transporter inhibitors, and the role of nutritional status on this processes. The adequacy of the study design relies on the fact that human perfusion studies have an excellent correlation with results obtained in rats for many compounds (110).

The selection of transport inhibitors was based on the knowledge of pharmacokinetic molecular determinants for erlotinib and gefitinib. The selected potential inhibitor for erlotinib assays was levofloxacin, a broad-spectrum fluoroquinolone-class antibiotic, commonly used for multiple infections treatment (mainly respiratory and urinary tract infections). An increased risk of infections during erlotinib treatment versus standard chemotherapy has been previously reported in clinical

trials (111, 112). The utilization of levofloxacin in patients treated with erlotinib might have an underestimated clinical relevance since recent publications have described the interaction of levofloxacin with tyrosine kinase inhibitors (imatinib, dasatinib and sunitinib) due to P-gp inhibition by levofloxacin (113, 114). This hypothesis is also supported by the fact that both erlotinib and levofloxacin are substrates of the P-gp active transporter (115, 116). Thus, levofloxacin was chosen as a potential inhibitor for erlotinib in *in situ* assays due to its mechanistic plausibility and to its potential clinical relevance. On the other hand, information in the literature regarding molecular pharmacokinetic determinants of gefitinib is limited. As shown in Table 1.5, gefitinib is not a substrate of P-gp, and none or conflicting information is available regarding the influence of multidrug resistance proteins and breast cancer resistance protein on the pharmacokinetics of gefitinib. For this reason, in order to evaluate the potential loss of linearity in gefitinib intestinal absorption, the 40 μg/mL solution was perfused in the presence and absence of sodium azide, an unspecific metabolic inhibitor capable of inhibiting ATPase-mediated transporters (117).

With regard to the chosen mathematical analysis approach, nonlinear mixed effect modelling using the NONMEM software has been widely employed to investigate absorption processes using data from *in situ* studies in rats (95, 117, 118). Thus, the population approach was considered adequate for these analyses.

Modelling of *in situ* data was intended to permit the development of mechanistic models describing the underlying mechanisms governing the absorption processes of erlotinib and gefitinib. Given the variability in drug-transporter-expression and permeability

characteristics along gut segments, drug absorption was modelled independently for the studied gut segments in order to identify potential differences regarding structural models between segments. In the same manner, model validation was performed independently.

Nevertheless, given the complexity of underlying mechanism and the possibility of encountering technical difficulties to build an unbiased mechanistic model, an empirical modelling approach using the Weibull equation was considered in those situations in which mechanistic models where not robust enough to describe the observed data. Weibull model was chosen due to its flexibility to adapt to heterogeneous scenarios. In these situations, the same structural model was used to describe drug disappearance rate from intestinal lumen, but the developed model was not used for extrapolation (since mechanistic interpretation was not possible). For these reasons, it was decided that under these circumstances datasets for both intestinal segments were going to be merged together and modelled simultaneously in order to test differences between intestinal segments for model parameters $\alpha$ and $\beta$.

### 4.4.1 Erlotinib *in situ* data modelling

Two independent mechanistic models were developed to describe data from proximal and distal intestinal segments. The model building procedures led to identical structural models (Figure 3.8) for both segments. A combination of first order absorption and a Michaelis-Menten secretion processes, together with a correction factor parameter (*fr*), best-described erlotinib absorption from lumen to enterocyte as

shown in Tables 3.13-3.14. As shown in these tables, the selection of the structural model was statistically justified ($p<0.01$).

Given that the range of erlotinib concentrations assayed in this study was limited due to poor solubility of the drug and to analytical limitations, $Km_s$ estimation issues in the absence of levofloxacin (below the lowest observed erlotinib concentration) were encountered. Nevertheless, in the presence of levofloxacin $Km_s$ was estimated with enough precision. In order to overcome this problem and enable the implementation of a Michaelis-Menten secretion system in the model, $Km_s$ value was fixed to 0 in the absence of levofloxacin and estimated in its presence. A similar approach was previously implemented by Muñoz et al. (95).

Regarding covariates inclusion procedure (Tables 3.15-3.16), both the influence of levofloxacin on $Km_s$ and the influence of undernourishment on $Vmax_s$ caused a significant drop in MOFV and thus their inclusion in the final model was statistically supported.

Diagnostic plots for both selected models (proximal and distal intestine) showed random, uniform scatter distribution around the identity line indicating absence of bias (Figure 3.9). Furthermore, bootstrap results of proximal and distal intestine absorption models (Tables 3.17-3.18) evidence that population estimates were similar to the bootstrap median results and contained within the 95% CI of the bootstrap results. Additionally, bootstrap analyses evidenced an acceptable precision in parameter estimates. Regarding model predictive performance, visual predictive check results (Figure 3.10) proved that observed data exhibited similar profiles to those of simulated data and thus, supported the selected models.

The fact that both final models had the same structure indicates that mechanisms implicated in erlotinib absorption along the gut are qualitatively similar. The selected models indicate that an active secretion system is involved in erlotinib absorption. Other authors have previously described an efficient transport of erlotinib by P-gp (116). In this study, $Vmax_s$ in the distal segment model (0.423, CI95% 0.250-0.711) was higher than the estimated $Vmax_s$ in the proximal segment model (0.209, CI95% 0.142-0.379). Makhey et al. reported in a previous study that the efflux activity of P-gp is highest in the ileum of rat and human, whereas moderately expressed in duodenum, jejunum, and colon (119). Similarly, Valenzuela et al. reported that the expression of the mRNA encoding the P-gp in the small intestine follows a gradient, increasing from the proximal to distal portion (120). Furthermore, the advanced dissolution, absorption and metabolism (ADAM) model (121), one of the most sophisticated models currently available, takes into account an increase in P-gp expression from duodenum to ileum. Results obtained from the literature are supported by the results obtained in most of the qRT-PCR analyses: P-gp in proximal, middle and distal segments showed an increasing tendency of P-gp mRNA levels across segments in all the subgroup results, except for the norm-nourished distal segment results. This exception could have been due to the limited sample size and to the observed high mRNA variability. Therefore, taking into account qRT-PCR results and previous literature, we can conclude that the observed $Vmax_s$ values in the distal segment could be higher, as compared to the proximal

segment, most probably due to the increasing gradient of P-gp expression from the proximal to distal intestinal segments.

Regarding the impact of under-nutrition on intestinal capacity to transport erlotinib back to lumen, the estimated values for maximum secretion capacity ($Vmax_s$) were significantly lower in undernourished rats: 63 and 72% decrease in proximal and distal absorption models, respectively. Results are in accordance with the hypothesis of a decreased expression of P-gp in undernourishment, which was confirmed in qRT-PCR analyses for proximal and middle intestine segments. Nevertheless, again our results for the distal segment are contradictory with this hypothesis, but based on available literature, this outcome in the distal segment could be a consequence of the limited sample size and of the observed high variability in mRNA levels.

The developed absorption models in proximal and distal intestine indicate that levofloxacin exerts an inhibition on efflux transporters of the gut epithelium and thus, the hypothesis of a pharmacokinetic interaction between levofloxacin and erlotinib is re-enforced (113). Taking into account the previously mentioned evidence, this phenomenon is most probably taking place on the P-gp transporters, since erlotinib might be competing with levofloxacin to bind P-gp transporters. Regarding the clinical implications of this interaction, both the absorption rate and the bioavailability of erlotinib are susceptible of being increased when levofloxacin is co-administered, resulting in an increased exposure, especially in undernourished patients.

Finally, the influence of erlotinib concentration, nutritional status and levofloxacin co-administration was investigated through

simulations considering parameter uncertainty by employing the variance-covariance matrix of final models. Simulation results (shown in Figure 3.11) indicate that in well-nourished rats and in absence of levofloxacin, erlotinib effective absorption in proximal intestinal segment only takes place when drug concentrations are above 1 μg/mL, whereas in distal intestinal segment 5-fold higher erlotinib concentrations are required for erlotinib absorption to be effective. This outcome can be explained taking into account that when erlotinib concentrations are above the before mentioned thresholds, saturation of efflux transporters takes place and passive drug diffusion from intestinal lumen to blood prevails over the secretion process. On the other hand, in undernourished rats, in which the maximum capacity of systems involved in drug secretion is diminished, erlotinib effective absorption in the presence of levofloxacin takes places even when erlotinib concentrations are below the before-mentioned concentrations. These results indicate that the proximal intestine could the preferential absorption segment for erlotinib, explaining, at least partly, the incomplete bioavailability of the drug when administered as oral tablets.

### 4.4.2 Gefitinib *in situ* data modelling

Drug absorption for some drugs is a very complex process, and the assumption of a first order process or a simple mechanistic approach is sometimes an over-simplified approach. The flexibility of the Weibull model allowed the identification of an equation that correctly fitted the data, and thus permitted the evaluation of covariates influence on parameter estimates.

The results of the covariate analysis indicated that disappearance-rate of gefitinib from intestinal lumen is not influenced by undernourishment nor by the presence of azide (metabolic inhibitor) at the used concentration. These results are in accordance with some of the previous studies, which indicate that gefitinib absorption is not dependent on active transporters (Table 1.4) and thus the absorption process for gefitinib is most probably governed by a passive diffusion process. The better fit of the Weibull model over the first order mechanistic absorption model could be due to, among other reasons, absorption and desorption processes of gefitinib on the intestinal mucosa, causing non-linear appearance of the observed concentration time-curves. Regarding the influence of under-nutrition, it has been previously postulated that the impact of undernourishment on drug intestinal absorption can be partly dependent on the participation of active transporters in drug intestinal absorption, but more studies are required to confirm this hypothesis.

On the other side, *fr* parameter was evidenced to be different between dosing levels and intestinal segments ($p<0.01$; Table 3.21). This parameter accounts for membrane adsorption, sample dilution and or presence of rapid metabolism. The evidenced differences could be caused by the sparse solubility of gefitinib and the different pH conditions in proximal and distal intestine, which might cause membrane drug-adsorption in a dose and pH dependent manner.

The non-mechanistic approach to describe these data limited its applicability to perform simulations under different conditions. Thus, simulations under varying gefitinib concentrations were not performed.

## 4.5 Pharmacokinetic studies

The main objective of *in vivo* studies was to describe through population pharmacokinetic modelling how undernourishment influences pharmacokinetic behaviour for erlotinib and gefitinib in rats. Additionally, these analyses intended to predict the impact of nutritional status on drug-exposure in humans, exploiting the capability of pharmacokinetic models to scale-up results using allometric principles. In the following sections, modelling for erlotinib and gefitinib *in vivo* experiments will be discussed. Then, scale-up simulation results will be overviewed and compared to clinical PK studies.

### 4.5.1 Erlotinib *in vivo* data modelling

Although erlotinib is approved for oral administration, in this study of basic research the drug was administered by IV and oral route in order to evaluate the impact of nutritional status on disposition and absorption, since it would not be possible to distinguish whether the changes occur due to alterations of disposition or absorption if only data from oral administration were used. Likewise, by oral route the drug was administered using two dispersion systems: a solution for direct comparison with the IV administration and a suspension because it is the disaggregation product of commercial tablets that best reproduces the usage conditions of this drug.

Among the tested models to obtain the pharmacokinetic disposition parameters from IV data, a two-compartment model with first order elimination was chosen. Qiong et al. had previously

described erlotinib PK in mice with a two-compartment model (122), supporting the selection of the structural model in the present study.

Different CL for WN and UN rats was then evidenced and incorporated into the model (Tables 3.24 and 3.26). This model showed a 5% decrease in CL among UN rats. The observed decrease in CL among undernourished rats could have been a result of variations in drug metabolism caused by under-nutrition. Studies in rodents illustrating a protein-calorie-malnutrition-related inhibition of P450s have been previously reported. This inhibition includes the rodent counterparts of those reportedly associated with erlotinib metabolism in humans (CYP1A1, CYP1A2, CYP3A4 and CYP3A5) (104). These results are in accordance with the modelling results and thus, we can conclude that erlotinib CL reduction in UN rats could be occurring as a result of such a reduction in metabolism. Nevertheless, results arising from the molecular analysis of hepatic CYP1A1 and CYP1A2 carried out in this research project indicate that there are no statistical differences in mRNA expression levels for these hepatic enzymes between WN and UN rats. As discussed previously, these results do not necessarily imply that enzymatic synthesis is equivalent in WN and UN rats since decreased availability of amino acids for protein synthesis can result in a decreased enzymatic synthesis even if mRNA levels are not different or even higher in under-nutrition status.

Models with different ka values for solution and suspension administrations accurately described erlotinib PK behaviour (Table 3.25; $p < 0.01$). The estimated ka value was lower for those rats receiving erlotinib as a suspension (0.147 $h^{-1}$) than for those receiving erlotinib as a solution (0.417 $h^{-1}$ and 0.200 $h^{-1}$ in WN and UN rats,

respectively), probably due to a slow dissolution of the drug in suspension that would have limited the absorption process.

Regarding the influence of nutritional status on drug absorption, it was evidenced that it produced a significant impact on the rate and extent of absorption. Nevertheless, changes in parameter estimates were dependent on the type of dispersion system employed: 1) differences in absorption rate were obvious only when erlotinib oral solution was administered, and; 2) absorption extent differences were obvious only when the drug suspension was administered orally (f = 0.872 for WN and f = 1 for UN rats).

Absorption rate constant was approximately 52% lower in UN rats as compared with WN rats when erlotinib solution was administered. This decrease in undernourished rats may have been partly due to a decreased gastric solubility of the drug in UN rats. Lower gastric acid secretion levels in undernourishment leads to an increase in gastric pH (123, 124), a change that can modify drug ionization, thus having an effect on drug solubility in the gastrointestinal lumen. In fact, erlotinib has a pKa of 5.4 and a higher solubility at a pH under 5 due to protonation of the secondary amine in its structure (125). Indeed, an erlotinib pH-dependent solubility phenomenon has previously been described, with concomitant use of erlotinib and acid-reducing agents, reason for which the manufacturer recommends that this combination should be avoided (126). Although the precipitation of a solution can lead to the formation of solid drug particles in the gastrointestinal tract, which could affect both the rate and extent of a low solubility-drug intestinal absorption (127), a

modification in the absorption rate was observed, but not in its extent when the erlotinib solution was administered.

On the other hand, it is interesting to point out that the results obtained in the *in situ* assay for erlotinib did not evidence a decrease in absorption rate. The fact that a decreased absorption rate in undernourished rats was not observed in the *in situ* assays supports the hypothesis of a pH-dependent solubility phenomenon. *In situ* assays were carried out under different experimental conditions. Intestinal segments were cannulated and drug was perfused into isolated compartments. Under these conditions, the drug does no pass through the stomach and gastric acid secretion does not influence pH in the compartment in which the drug is being absorbed. Accordingly, the pH-dependent solubility phenomenon is not expected to influence drug absorption rate in *in situ* assays.

The developed model evidenced that there were no statistically significant differences in ka (ka = 0.147 $h^{-1}$) when administering erlotinib suspension in WN and UN rats (as shown in Table 3.26). This fact indicates that when erlotinib is administered as a suspension, the liberation process from the suspension system (including drug dissolution in fluids at the absorption site) is the limiting factor conditioning drug absorption, most probably as a consequence of the low solubility of this drug.

The developed model also evidenced that both, the type of dispersion system employed for oral administration and the nutritional status of rats, have a significant influence on oral bioavailability of erlotinib. Actually, complete bioavailability was observed after oral administration of erlotinib solution in all subgroups whereas for oral

administration of erlotinib suspension complete bioavailability was only observed in UN rats but incomplete bioavailability (f = 87%) occurred in WN rats.

Complete bioavailability after erlotinib solution administration could happen as a result of the saturation of transport systems involved in drug secretion due to the high concentration of erlotinib in the administered dispersion system (prepared with co-solvents). On the other hand, the administration of erlotinib suspension (without co-solvents) could expose intestinal epithelium to lower erlotinib concentrations since erlotinib solubility is about 1 μg/mL (128). Therefore, erlotinib suspension administration might not reach high enough concentration for secretion system saturation and this can result in incomplete bioavailability in WN rats. On the other hand, the decreased capacity of drug efflux systems in UN rats, together with mucosal damage associated to undernourishment (129), could have been the factors favouring complete absorption of erlotinib in UN rats receiving erlotinib suspension.

Undernourishment is associated to physiopathological alterations of the intestinal absorbent membrane. These physiopathological alterations consist in changes in the length of the intestine and in the thickness of muscular, submucosa and mucosa layers of the intestine, along with flattened, shortened and a decreased count of villi, displaying also hypoplasia of crypts (129). In addition, undernourishment status is also associated to changes in intestinal motility, which is reduced in undernourished rats (130), resulting in a

higher residence time of the drug in the intestine, thus contributing to the absorption of a higher fraction of the administered dose.

Regarding model performance, the final model was successfully validated. VPC plots proved a good performance of the model when predicting the observed data and bootstrap results confirmed the adequacy of the model.

### 4.5.2 Gefitinib *in vivo* data modelling

Similarly to how erlotinib was administered in *in vivo* studies, IV and oral routes were used for gefitinib administration. In this experiment, only gefitinib suspension was administered by oral route. Gefitinib solution was not assayed through the oral route since low solubility of the drug limited the dose levels, and the consequent low gefitinib oral doses could yield plasma concentrations near the LLOQ of the analytical method. Gefitinib suspension was used for oral administration, as done in erlotinib *in vivo* study, because it represents the disaggregation product of commercial tablets that reproduces the usage conditions of this drug.

Among the tested models to obtain the pharmacokinetic disposition parameters from IV data, a two-compartment model was chosen. Wang et al. had previously described gefitinib PK in mice with a two-compartment model (131), thus supporting the selected structural model in the present study.

During the procedure of covariate inclusion into the distribution model, under-nutrition proved to be related to an increased volume of distribution in the central compartment but no relation was evidenced with drug clearance. The underlying mechanism behind this finding is

most probably related to gefitinib binding to plasmatic proteins (approximately 90%). Studies with purified human serum albumin and purified α-1 acid glycoprotein have shown that gefitinib binds to both proteins (85) but, to our knowledge, the proportion at which it binds to each of them remains unknown. For this reason, a decrease in plasma proteins in under-nutrition situations can result in an increased volume of distribution for the central compartment. Results from the evaluation of analytical alterations conducted in this Thesis confirm a lower albumin concentration in UN status (24% decrease, p=0.015) along with a decreased total protein concentration (p=0.006). On the other side α-1 acid glycoprotein proved to be increased in undernourishment status (22% increase, p=0.025). Nevertheless, the increase of α-1 acid glycoprotein does not seem to counter balance the effect of albumin depletion on drug distribution and the overall result is a 30% increase in volume of distribution. Regarding drug clearance, given that gefitinib is known to have a high extraction ratio, a decrease in plasma proteins in undernourishment status and the resulting change of free drug concentration is not expected to have an impact on drug clearance, reinforcing the results of the present study.

Gefitinib intestinal absorption was characterized with a one-transit compartment model. This model accounts for absorption delay, which is usually due to processes such as disintegration of delivery systems, drug dissolution/release, transit through intestine up to absorption site, and/or migration through absorption site tissues. Transit compartments can accurately describe the concentration-time profiles but do not assign a physiological meaning to each compartment (132).

In this study, the inclusion of one transit compartment significantly improved the performance of the model and caused more than 50% decrease of the BSV on the absorption rate constant. Further inclusion of transit compartments did not improve the model.

In the last step of the modelling process, nutritional status was evidenced to cause an increase in gefitinib bioavailability from 0.45 in WN rats to 0.68 in UN rats. This represents more than a 50% exposure increase in undernourishment status in relative terms. According to the public assessment report for gefitinib, bioavailability in rat studies ranged between 39 and 88 % while the geometric mean in cancer patients was 59 % (85). These results are in accordance with those obtained in the present study and support the estimated values. The mechanism behind the increased bioavailability in undernourishment status is unknown, but could be multifactorial. Increased bioavailability in magnitude in undernourishment status could happen as a consequence of: 1) decreased intestinal motility (resulting in an increased residence time in the absorption site) (130), and; 2) reduced expression of CYP1A1 metabolic system in proximal and medial intestinal segments. These undernourishment-associated alterations result in a decrease of estimated bioavailability in magnitude in the *in vivo* assays. On the other, the implications of these alterations are not captured by the results of the *in situ* perfusion assays given that the experimental technique employed is not capable of detecting these kind of alterations.

The final model was successfully validated. VPC plots proved a good performance of the model when predicting the observed data and bootstrap results confirmed the adequacy of the model.

### 4.5.3 Scale-up simulations

Finally, simulations were performed in order to test the capability of the models to scale-up to human individuals and to predict results in a clinical study where patients, classified as UN or WN, would receive erlotinib or gefitinib. The results obtained in this simulations yield the first estimation of the expected impact of undernourishment on erlotinib and gefitinib exposure in humans.

In the present study, the estimated $t_{1/2\beta}$ for erlotinib in 70 kg individuals was approximately 11 hours as compared to 14 hours estimated in the study conducted by Jawhari et al. in a population of healthy volunteers (133); other clinical PK studies for erlotinib were conducted in cancer patients and estimated longer half-lifes. Consequently, absolute concentration values obtained from PK scale-up should be interpreted with caution (134). Regarding gefitinib, in the present study, the estimated $t_{1/2\beta}$ for gefitinib in 70 kg individuals was approximately 36 hours as compared to approximately 2 days in cancer patients and lower in healthy volunteers (135). The results obtained through allometric scaling in this study are in line with the results obtained in trials with healthy volunteers.

For erlotinib, simulation results indicate that approximately 24% higher erlotinib trough concentrations and 20% higher AUC values are expected in UN patients as compared with WN patients. Erlotinib trough concentrations and AUC values were in accordance with clinical PK studies in healthy volunteers but apparently lower as compared with results obtained in cancer patients (133, 134).

For gefitnib, simulation results also predict an increased exposure in UN patients. As shown in Figure 3.24, median steady state trough concentrations and AUC suffer more than 50% increase in undernourishment. When comparing results obtained in this simulation with those obtained in clinical trials, the performance of the scaling was considered adequate. Population data from the two Phase II studies conducted in patients with advanced non-small cell lung cancer showed that the mean predicted steady state trough concentration following a 250 mg oral dose was 261 ng/mL (95% CI: 88.0 to 774 ng/mL) (136). Given that these populations were expected to comprise WN and UN patients, these results are in accordance with those obtained in our simulations where WN and UN individuals had 215.18 and 333.7 ng/mL median steady state trough concentrations when following the same dosing regimen.

Results obtained from *in vivo* studies in rats provide information that can be of great importance in the clinical setting. Understanding the magnitude of undernourishment's impact on pharmacokinetics can be valuable for clinicians when deciding dose adjustments in undernourished patients. But in addition, the possibility of scaling-up results from rats to humans expands the applicability of preclinical results. These simulations, which were possible thanks to the availability of an under-nutrition animal model, provide the first prediction of nutritional status impact on the pharmacokinetics of erlotinib and gefitinib in humans and thus, represents valuable information for a rational design of clinical trials in terms of sampling-times selection and sample size calculation.

## 4.6 Research limitations

Although the research project has reached its objective, there were some unavoidable limitations.

Firstly, it should be emphasized that, due to ethical reasons, undernourishment degree of rats included in this study was limited to mild and moderate undernourishment. This fact limits the observed effects of undernourishment since only one severely undernourished rat was included. A bigger impact of undernourishment is expected in severe under-nutrition situations. An example of how this limitation might have constrained the observed impact of undernourishment is the slight undernourishment-related decrease of drug CL in the *in vivo* pharmacokinetic study for erlotinib. In this study 20 mildly undernourished and 3 moderately undernourished rats were included. A more pronounced alteration of pharmacokinetic parameters could be expected in severely undernourished rats. (137).

Secondly, this research was performed in an animal model and translation of results to humans must be carried out with caution. Nevertheless, given that there is no validated tool for nutritional status screening in cancer patients and that intensive blood sampling is required in order to perform a thorough investigation to detect which pharmacokinetic processes are altered in undernourishment status, preclinical studies represent a highly informative approach overcoming the problems encountered in the clinical setting. Furthermore, the use of a fit-for-purpose animal model permits the evaluation of the impact of under-nutrition on the pharmacokinetics of drugs in a controlled setting

where confounding factors are minimized and the investigated phenomenon is isolated for its analysis.

Interpretation of qRT-PCR results was limited due to the lack of protein expression levels as complementary results. When evaluating results of these analyses, the possibility of a compensatory mechanism causing an increase in mRNA expression was always considered. A decrease in mRNA levels could represent a decrease in protein synthesis, but increases in mRNA levels do not necessarily imply an increase in protein expression since they could be caused by this compensatory mechanism.

Regarding mathematical analysis limitations, it must be taken into account that non-linear mixed effect modelling requires certain assumptions to be made. Thus, general model assumptions were made (e.g. parameter distributions). On the other side, simulations performed with final models are valuable to quantify effects but are not useful for significance testing since significance value is completely dependent on simulation sample size. For this reason, significance was not tested between WN and UN simulated individuals. Additionally, erlotinib up-scaling results were not as satisfactory as those for gefitinib when comparing simulated drug concentrations in humans with those obtained in clinical trials. Nevertheless, erlotinib simulations provided valuable information in relative terms of the expected impact of undernourishment in patients.

# 5 | Conclusions

# 5 Conclusions

# 5 | Conclusions

This PhD dissertation, which had the objective of evaluating the impact of undernourishment on the pharmacokinetics of erlotinib and gefitinib, has yielded the following conclusions:

1. Undernourishment causes significant alterations on mRNA expression levels of intestinal and hepatic metabolic enzymes (Cyp1A1, Cyp1A2 and UDP) and transporter proteins (OATP, MRP2 and P-gp). In liver tissue, mRNA levels of all the quantified metabolic enzymes, except for cytochromes, were diminished in undernourishment status. On the other side, alterations of mRNA levels in intestinal tissue do not follow a particular trend and the final outcome is dependent on the assayed intestinal segment and on the evaluated enzyme.
2. The observed alterations in alanine-aminotransferase and aspartate-aminotransferase hepatic enzymes, along with the reduction of albumin plasmatic concentration, confirm the occurrence of hepatic damage as a result of undernourishment status. Likewise, the decreased count of blood cells corroborates bone-marrow dysfunction under protein-energy under-nutrition.
3. A passive diffusion uptake process and an active secretion process control erlotinib intestinal absorption through both of the assayed intestinal segments. This active secretion process is sensitive to nutritional status and to the presence of levofloxacin.
4. A passive diffusion uptake process governs gefitinib intestinal absorption, which proved not to be influenced by the addition of sodium azide to the perfusion solution. Furthermore, under this *in situ* assay conditions, alterations of gefitinib absorption

process did not take place as a consequence of the nutritional status of rats.

5. A two-compartment model proved to describe best the pharmacokinetic profiles both for erlotinib and gefitinib.
6. A 5% decrease in erlotinib clearance takes place in undernourishment status. Drug bioavailability in magnitude (f) and rate (ka) are dependent on nutritional status and on the type of dispersion system employed for oral administration:
    - Bioavailability in magnitude is incomplete only when erlotinib suspension is administered to norm-nourished rats.
    - Absorption rate constant is 52% lower when erlotinib solution is administered in undernourished rats as compared to the administration in norm-nourished rats.

    These results yield an expected 20% higher area under the concentration-time curve for erlotinib in undernourished patients as compared with norm-nourished ones.
7. Volume of distribution and bioavailability parameters for gefitinib are increased 30 and 50%, respectively, in protein-energy undernourishment status. This preclinical results yield simulation outcomes, which indicate that minimum trough concentration and area under the concentration-time curve in undernourished patients are expected to be 50% higher when compared to norm-nourished patients.
8. The response of the organism to compensate the deficiencies generated by an inadequate energy and protein intake is very

complex. Consequently, general pharmacokinetic changes in undernourishment status are very variable, difficult to predict and dependent on the evaluated drug, given that all LADME processes are sensitive to these alterations.

# 6 References

1. de Onis M, Monteiro C, Akre J, Glugston G. The worldwide magnitude of protein-energy malnutrition: an overview from the WHO Global Database on Child Growth. Bull World Health Organ. 1993;71(6):703-12.
2. Morley JE. Overview of Undernutrition. In: Corp. MSD, editor. Merck Manual: Merck Sharp & Dohme Corp.; 2014.
3. Ryan AM, Power DG, Daly L, Cushen SJ, Ni Bhuachalla E, Prado CM. Cancer-associated malnutrition, cachexia and sarcopenia: the skeleton in the hospital closet 40 years later. Proc Nutr Soc. 2016 May;75(2):199-211.
4. Paci A, Veal G, Bardin C, Leveque D, Widmer N, Beijnen J, et al. Review of therapeutic drug monitoring of anticancer drugs part 1--cytotoxics. Eur J Cancer. 2014 Aug;50(12):2010-9.
5. Arroyave G, Viteri F, Behar M, Scrimshaw NS. Impairment of intestinal absorption of vitamin A palmitate in severe protein malnutrition (kwashiorkor). Am J Clin Nutr. 1959 Mar-Apr;7(2):185-90.
6. Gomez F, Galvan RR, Cravioto J, Frenk S, Santaella JV, De La Pena C. Fat absorption in chronic severe malnutrition in children. Lancet. 1956 Jul 21;271(6934):121-2.
7. Brewster DR, Manary MJ, Menzies IS, O'Loughlin EV, Henry RL. Intestinal permeability in kwashiorkor. Arch Dis Child. 1997 Mar;76(3):236-41.
8. Bravo IG, Bravo ME, Plate G, Merlez J, Arancibia A. The pharmacokinetics of cotrimoxazole sulphonamide in malnourished (marasmic) infants. Pediatr Pharmacol (New York). 1984;4(3):167-76.
9. Ashworth A. Treatment of severe malnutrition. J Pediatr Gastroenterol Nutr. 2001 May;32(5):516-8.
10. Buchanan N, Eyberg C. Intramuscular tobramycin administration in kwashiorkor. S Afr Med J. 1978 Feb 25;53(8):273-4.
11. Gartner A, Berger J, Simondon KB, Maire B, Traissac P, Ly C, et al. Change in body water distribution index in infants who become stunted between 4 and 18 months of age. Eur J Clin Nutr. 2003 Sep;57(9):1097-106.
12. Krishnaswamy. Effects of malnutrition on drug metabolism and toxicity in humans. Nutritional Toxicology.
13. Krishnaswamy. Drug/Xenobiotic-Metabolism, Disposition and Toxicity in Malnutrition. Defence Science Journal. 1987;37(2):133-42.
14. Brewster DR. Critical appraisal of the management of severe malnutrition: 3. Complications. J Paediatr Child Health. 2006 Oct;42(10):583-93.

15. Muller O, Krawinkel M. Malnutrition and health in developing countries. CMAJ. 2005 Aug 2;173(3):279-86.
16. Buchanan N, Van der Walt LA. The binding of chloroquine to normal and Kwashiorkor serum. Am J Trop Med Hyg. 1977 Sep;26(5 Pt 1):1025-7.
17. Pussard E, Barennes H, Daouda H, Clavier F, Sani AM, Osse M, et al. Quinine disposition in globally malnourished children with cerebral malaria. Clin Pharmacol Ther. 1999 May;65(5):500-10.
18. Syed GB, Sharma DB, Raina RK. Pharmacokinetics of phenobarbitone in protein energy malnutrition. Dev Pharmacol Ther. 1986;9(5):317-22.
19. Krishnaswamy K. Drug metabolism and pharmacokinetics in malnourished children. Clin Pharmacokinet. 1989;17 Suppl 1:68-88.
20. Alleyne GA. The effect of severe protein calorie malnutrition on the renal function of Jamaican children. Pediatrics. 1967 Mar;39(3):400-11.
21. Jahoor F, Badaloo A, Reid M, Forrester T. Protein metabolism in severe childhood malnutrition. Ann Trop Paediatr. 2008 Jun;28(2):87-101.
22. Rajeswari R, Shetty PA, Gothoskar BP, Akolkar PN, Gokhale SV. Pharmacokinetics of methotrexate in adult Indian patients and its relationship to nutritional status. Cancer Treat Rep. 1984 May;68(5):727-32.
23. Murry DJ, Riva L, Poplack DG. Impact of nutrition on pharmacokinetics of anti-neoplastic agents. Int J Cancer Suppl. 1998;11:48-51.
24. Thorn CF, Marsh S, Carrillo MW, McLeod HL, Klein TE, Altman RB. PharmGKB summary: fluoropyrimidine pathways. Pharmacogenet Genomics. 2011 Apr;21(4):237-42.
25. Motawi TK, Abd-Elgawad HM, Shahin NN. Effect of protein malnutrition on the metabolism and toxicity of cisplatin, 5-fluorouracil and mitomycin C in rat stomach. Food Chem Toxicol. 2013 Jun;56:467-82.
26. Davis LE, Lenkinski RE, Shinkwin MA, Kressel HY, Daly JM. The effect of dietary protein depletion on hepatic 5-fluorouracil metabolism. Cancer. 1993 Dec 15;72(12):3715-22.
27. Mikkelsen TS, Thorn CF, Yang JJ, Ulrich CM, French D, Zaza G, et al. PharmGKB summary: methotrexate pathway. Pharmacogenet Genomics. 2011 Oct;21(10):679-86.
28. Charland SL, Bartlett D, Torosian MH. Effect of protein-calorie malnutrition on methotrexate pharmacokinetics. JPEN J Parenter Enteral Nutr. 1994 Jan-Feb;18(1):45-9.
29. Dunki Jacobs PB, Ruevekamp M, Varossiau FJ, Hart GA, de Graaf PW. Alterations in serum levels, anti-tumor activity and toxicity of methotrexate

in rats after a short period of nutritional depletion. Eur J Cancer Clin Oncol. 1989 Mar;25(3):415-22.

30. Grossie VB, Jr., Loo TL. Effect of nutritional status on the hepatobiliary excretion of methotrexate in the rat. Cancer Treat Rep. 1983 Mar;67(3):253-7.
31. Kumar RV, Gokhale SV, Ambaye RY, Shetty PA. Pharmacokinetics of methotrexate in Indian children and its relationship to nutritional status. Chemotherapy. 1987;33(4):234-9.
32. Mihranian MH, Wang YM, Daly JM. Effects of nutritional depletion and repletion on plasma methotrexate pharmacokinetics. Cancer. 1984 Nov 15;54(10):2268-71.
33. Thorn CF, Oshiro C, Marsh S, Hernandez-Boussard T, McLeod H, Klein TE, et al. Doxorubicin pathways: pharmacodynamics and adverse effects. Pharmacogenet Genomics. 2011 Jul;21(7):440-6.
34. Cusack BJ, Young SP, Loseke VL, Hurty MR, Beals L, Olson RD. Effect of a low-protein diet on doxorubicin pharmacokinetics in the rabbit. Cancer Chemother Pharmacol. 1992;30(2):145-8.
35. El-Demerdash E, Ali AA, El-Taher DE, Hamada FM. Effect of low-protein diet on anthracycline pharmacokinetics and cardiotoxicity. J Pharm Pharmacol. 2012 Mar;64(3):344-52.
36. Kapelanski DP, Daly JM, Copeland EM, 3rd, Dudrick SJ. Doxorubicin pharmacokinetics--the effects of protein deprivation. J Surg Res. 1981 Apr;30(4):331-7.
37. Kim YG, Cho MK, Kwon JW, Kim SG, Lee MG. Effects of cysteine on the pharmacokinetics of intravenous adriamycin in rats with protein-calorie malnutrition. Res Commun Mol Pathol Pharmacol. 2000 May-Jun;107(5-6):361-76.
38. Whirl-Carrillo M, McDonagh EM, Hebert JM, Gong L, Sangkuhl K, Thorn CF, et al. Pharmacogenomics knowledge for personalized medicine. Clin Pharmacol Ther. 2012 Oct;92(4):414-7.
39. Israels T, Damen CW, Cole M, van Geloven N, Boddy AV, Caron HN, et al. Malnourished Malawian patients presenting with large Wilms tumours have a decreased vincristine clearance rate. Eur J Cancer. 2010 Jul;46(10):1841-7.
40. Yang J, Bogni A, Schuetz EG, Ratain M, Dolan ME, McLeod H, et al. Etoposide pathway. Pharmacogenet Genomics. 2009 Jul;19(7):552-3.

41. Lagas JS, Fan L, Wagenaar E, Vlaming ML, van Tellingen O, Beijnen JH, et al. P-glycoprotein (P-gp/Abcb1), Abcc2, and Abcc3 determine the pharmacokinetics of etoposide. Clin Cancer Res. 2010 Jan 1;16(1):130-40.
42. Suh JH, Kang HE, Yoon IS, Yang SH, Kim SH, Lee HJ, et al. Cysteine effects on the pharmacokinetics of etoposide in protein-calorie malnutrition rats: increased gastrointestinal absorption by cysteine. Xenobiotica. 2011 Oct;41(10):885-94.
43. Torosian MH, Jalali S, Nguyen HQ. Protein intake and 5-fluorouracil toxicity in tumor-bearing animals. J Surg Res. 1990 Oct;49(4):298-301.
44. Borelli P, Barros FE, Nakajima K, Blatt SL, Beutler B, Pereira J, et al. Protein-energy malnutrition halts hemopoietic progenitor cells in the G0/G1 cell cycle stage, thereby altering cell production rates. Braz J Med Biol Res. 2009 Jun;42(6):523-30.
45. Fleming RA, Milano GA, Etienne MC, Renee N, Thyss A, Schneider M, et al. No effect of dose, hepatic function, or nutritional status on 5-FU clearance following continuous (5-day), 5-FU infusion. Br J Cancer. 1992 Oct;66(4):668-72.
46. Young AM, Kidston S, Banks MD, Mudge AM, Isenring EA. Malnutrition screening tools: comparison against two validated nutrition assessment methods in older medical inpatients. Nutrition. 2013 Jan;29(1):101-6.
47. Gusella M, Toso S, Ferrazzi E, Ferrari M, Padrini R. Relationships between body composition parameters and fluorouracil pharmacokinetics. Br J Clin Pharmacol. 2002 Aug;54(2):131-9.
48. Hasenberg T, Essenbreis M, Herold A, Post S, Shang E. Early supplementation of parenteral nutrition is capable of improving quality of life, chemotherapy-related toxicity and body composition in patients with advanced colorectal carcinoma undergoing palliative treatment: results from a prospective, randomized clinical trial. Colorectal Dis. 2010 Oct;12(10 Online):e190-9.
49. Torosian M. Effect of protein-intake on dihydrofolate-reductase activity of host and tumor-tissues. Int J Oncol. 1994 Nov;5(5):1119-23.
50. Grossie VB, Jr., Ho DH, Loo TL. Effect of malnutrition on methotrexate toxicity and tissue levels of dihydrofolate reductase in the rat. Cancer Treat Rep. 1982 Jan;66(1):85-9.
51. Torosian MH, Mullen JL, Miller EE, Zinnser KR, Buzby GP. Reduction of methotrexate toxicity with improved nutritional status in tumor-bearing animals. Cancer. 1988 May 1;61(9):1731-5.

52. Daly JM, Reynolds HM, Rowlands BJ, Dudrick SJ, Copeland EM, 3rd. Tumor growth in experimental animals: nutritional manipulation and chemotherapeutic response in the rat. Ann Surg. 1980 Mar;191(3):316-22.
53. Reynolds HM, Jr., Daly JM, Rowlands BJ, Dudrick SJ, Copeland EM, 3rd. Effects of nutritional repletion on host and tumor response to chemotherapy. Cancer. 1980 Jun 15;45(12):3069-74.
54. Lobato-Mendizabal E, Ruiz-Arguelles GJ, Marin-Lopez A. Leukaemia and nutrition. I: Malnutrition is an adverse prognostic factor in the outcome of treatment of patients with standard-risk acute lymphoblastic leukaemia. Leuk Res. 1989;13(10):899-906.
55. Israels T, van de Wetering MD, Hesseling P, van Geloven N, Caron HN, Molyneux EM. Malnutrition and neutropenia in children treated for Burkitt lymphoma in Malawi. Pediatr Blood Cancer. 2009 Jul;53(1):47-52.
56. Crescimanno M, Flandina C, Rausa L, Sanguedolce R, D'Alessandro N. Morphological changes and catalase activity in the hearts of CD 1 mice following acute starvation or single doses of doxorubicin, epirubicin or mitoxantrone. Chemioterapia. 1988 Feb;7(1):53-9.
57. Prado CM, Lima IS, Baracos VE, Bies RR, McCargar LJ, Reiman T, et al. An exploratory study of body composition as a determinant of epirubicin pharmacokinetics and toxicity. Cancer Chemother Pharmacol. 2011 Jan;67(1):93-101.
58. Gomber S, Dewan P, Chhonker D. Vincristine induced neurotoxicity in cancer patients. Indian J Pediatr. 2010 Jan;77(1):97-100.
59. Kumar N. Nutritional neuropathies. Neurol Clin. 2007 Feb;25(1):209-55.
60. Weber GA, Sloan P, Davies D. Nutritionally induced peripheral neuropathies. Clin Podiatr Med Surg. 1990 Jan;7(1):107-28.
61. Spronck JC, Nickerson JL, Kirkland JB. Niacin deficiency alters p53 expression and impairs etoposide-induced cell cycle arrest and apoptosis in rat bone marrow cells. Nutr Cancer. 2007;57(1):88-99.
62. Scheffler M, Di Gion P, Doroshyenko O, Wolf J, Fuhr U. Clinical pharmacokinetics of tyrosine kinase inhibitors: focus on 4-anilinoquinazolines. Clin Pharmacokinet. 2011 Jun;50(6):371-403.
63. Stuurman FE, Nuijen B, Beijnen JH, Schellens JH. Oral anticancer drugs: mechanisms of low bioavailability and strategies for improvement. Clin Pharmacokinet. 2013 Jun;52(6):399-414.
64. McMurray DN, Bartow RA, Mintzer CL. Protein malnutrition alters the distribution of Fc gamma R+ (T gamma) and Fc mu R+ (T mu) T

lymphocytes in experimental pulmonary tuberculosis. Infect Immun. 1990 Feb;58(2):563-5.

65. Kuo TT, Baker K, Yoshida M, Qiao SW, Aveson VG, Lencer WI, et al. Neonatal Fc receptor: from immunity to therapeutics. J Clin Immunol. 2010 Nov;30(6):777-89.
66. Park S, Han B, Cho JW, Woo SY, Kim S, Kim SJ, et al. Effect of nutritional status on survival outcome of diffuse large B-cell lymphoma patients treated with rituximab-CHOP. Nutr Cancer. 2014;66(2):225-33.
67. Seltzer MH, Bastidas JA, Cooper DM, Engler P, Slocum B, Fletcher HS. Instant nutritional assessment. JPEN J Parenter Enteral Nutr. 1979 May-Jun;3(3):157-9.
68. Potosnak L, Chudnow LP, Simko MD. A simple tool for identifying patients at nutritional risk. QRB Qual Rev Bull. 1983 Mar;9(3):81-3.
69. Neelemaat F, Meijers J, Kruizenga H, van Ballegooijen H, van Bokhorst-de van der Schueren M. Comparison of five malnutrition screening tools in one hospital inpatient sample. J Clin Nurs. 2011 Aug;20(15-16):2144-52.
70. Leuenberger M, Kurmann S, Stanga Z. Nutritional screening tools in daily clinical practice: the focus on cancer. Support Care Cancer. 2010 May;18 Suppl 2:S17-27.
71. Huhmann MB, August DA. Review of American Society for Parenteral and Enteral Nutrition (ASPEN) Clinical Guidelines for Nutrition Support in Cancer Patients: nutrition screening and assessment. Nutr Clin Pract. 2008 Apr-May;23(2):182-8.
72. Ottery FD. Rethinking nutritional support of the cancer patient: the new field of nutritional oncology. Semin Oncol. 1994 Dec;21(6):770-8.
73. Kondrup J, Allison SP, Elia M, Vellas B, Plauth M, Educational, et al. ESPEN guidelines for nutrition screening 2002. Clin Nutr. 2003 Aug;22(4):415-21.
74. Kyle UG, Kossovsky MP, Karsegard VL, Pichard C. Comparison of tools for nutritional assessment and screening at hospital admission: a population study. Clin Nutr. 2006 Jun;25(3):409-17.
75. Vellas B, Guigoz Y, Baumgartner M, Garry PJ, Lauque S, Albarede JL. Relationships between nutritional markers and the mini-nutritional assessment in 155 older persons. J Am Geriatr Soc. 2000 Oct;48(10):1300-9.
76. Read JA, Crockett N, Volker DH, MacLennan P, Choy ST, Beale P, et al. Nutritional assessment in cancer: comparing the Mini-Nutritional

Assessment (MNA) with the scored Patient-Generated Subjective Global Assessment (PGSGA). Nutr Cancer. 2005;53(1):51-6.

77. Ignacio de Ulibarri J, Gonzalez-Madrono A, de Villar NG, Gonzalez P, Gonzalez B, Mancha A, et al. CONUT: a tool for controlling nutritional status. First validation in a hospital population. Nutr Hosp. 2005 Jan-Feb;20(1):38-45.
78. Detsky AS, McLaughlin JR, Baker JP, Johnston N, Whittaker S, Mendelson RA, et al. What is subjective global assessment of nutritional status? JPEN J Parenter Enteral Nutr. 1987 Jan-Feb;11(1):8-13.
79. Ottery FD. Cancer cachexia: prevention, early diagnosis, and management. Cancer Pract. 1994 Mar-Apr;2(2):123-31.
80. Merino-Sanjuan M, Catalan-Latorre A, Nacher A, Miralles-Arnau S, Jimenez-Torres NV. Animal model of undernutrition for the evaluation of drug pharmacokinetics. Nutr Hosp. 2011 Nov-Dec;26(6):1296-304.
81. Arora A, Scholar EM. Role of tyrosine kinase inhibitors in cancer therapy. J Pharmacol Exp Ther. 2005 Dec;315(3):971-9.
82. Moyer JD, Barbacci EG, Iwata KK, Arnold L, Boman B, Cunningham A, et al. Induction of apoptosis and cell cycle arrest by CP-358,774, an inhibitor of epidermal growth factor receptor tyrosine kinase. Cancer Res. 1997 Nov 1;57(21):4838-48.
83. Perez-Soler R. Phase II clinical trial data with the epidermal growth factor receptor tyrosine kinase inhibitor erlotinib (OSI-774) in non-small-cell lung cancer. Clin Lung Cancer. 2004 Dec;6 Suppl 1:S20-3.
84. EMA. Scientific Discussion Tarceva. 2005.
85. EMA. Assessment report for Iressa 2008.
86. Scholler JL, D. Molecular pharmacokinetic determinants of anticancer kinase inhibitors in humans. Oncol Rev. 2011;5:77-92.
87. Yu H, Steeghs N, Nijenhuis CM, Schellens JH, Beijnen JH, Huitema AD. Practical guidelines for therapeutic drug monitoring of anticancer tyrosine kinase inhibitors: focus on the pharmacokinetic targets. Clin Pharmacokinet. 2014 Apr;53(4):305-25.
88. Pérez-Pitarch A, Guglieri-López, B; Merino, V; Nacher, A; Ferriols-Lisart, R; Merino-Sanjuán, M. Growing evidence supporting therapeutic drug monitoring of erlotinib in non-small-cell lung cancer patients: a time-to-progression model. 2015.
89. Nair AB, Jacob S. A simple practice guide for dose conversion between animals and human. J Basic Clin Pharm. 2016 Mar;7(2):27-31.

90. Doluisio JT, Billups NF, Dittert LW, Sugita ET, Swintosky JV. Drug absorption. I. An in situ rat gut technique yielding realistic absorption rates. J Pharm Sci. 1969 Oct;58(10):1196-200.
91. Fouad Chiadmi MD JS, Jean-Eudes Fontan. . Validation of a simple high-performance liquid chromatography analysis method for the determination of erlotinib in human plasma. The European Journal of Hospital Pharmacy Science. 2007;13(2):48-51.
92. Beal SL SL. NONMEM User's Guide, NONMEM. Project Group, University of California, San Francisco. 1989.
93. Lindbom L, Pihlgren P, Jonsson EN. PsN-Toolkit--a collection of computer intensive statistical methods for non-linear mixed effect modeling using NONMEM. Comput Methods Programs Biomed. 2005 Sep;79(3):241-57.
94. Martin-Villodre A, Pla-Delfina JM, Moreno J, Perez-Buendia D, Miralles J, Collado EF, et al. Studies on the reliability of a bihyperbolic functional absorption model. I. Ring-substituted anilines. J Pharmacokinet Biopharm. 1986 Dec;14(6):615-33.
95. Munoz MJ, Merino-Sanjuan M, Lledo-Garcia R, Casabo VG, Manez-Castillejo FJ, Nacher A. Use of nonlinear mixed effect modeling for the intestinal absorption data: application to ritonavir in the rat. Eur J Pharm Biopharm. 2005 Sep;61(1-2):20-6.
96. Holford NH. A size standard for pharmacokinetics. Clin Pharmacokinet. 1996 May;30(5):329-32.
97. Mager DE, Woo S, Jusko WJ. Scaling pharmacodynamics from in vitro and preclinical animal studies to humans. Drug Metab Pharmacokinet. 2009;24(1):16-24.
98. Karlsson M HN. A tutorial on visual predictive checks. 2008; Available from: http://www.page-meeting.org/?abstract=1434.
99. Piskorz L, Lesiak T, Brocki M, Klimek-Piskorz E, Smigielski J, Misiak P, et al. Biochemical and functional indices of malnutrition in patients with operable, non-microcelullar lung cancer. Nutr Hosp. 2011 Sep-Oct;26(5):1025-32.
100. Bonate PL. Pharmacokinetic-pharmacodynamic modeling and simulation. New York, NY: Springer; 2006.
101. Tisdale MJ. Cancer anorexia and cachexia. Nutrition. 2001 May;17(5):438-42.

102. Zakeri-Milani P, Valizadeh H, Tajerzadeh H, Azarmi Y, Islambolchilar Z, Barzegar S, et al. Predicting human intestinal permeability using single-pass intestinal perfusion in rat. J Pharm Pharm Sci. 2007;10(3):368-79.
103. van Zutphen T, Ciapaite J, Bloks VW, Ackereley C, Gerding A, Jurdzinski A, et al. Malnutrition-associated liver steatosis and ATP depletion is caused by peroxisomal and mitochondrial dysfunction. J Hepatol. 2016 Dec;65(6):1198-208.
104. Li J, Zhao M, He P, Hidalgo M, Baker SD. Differential metabolism of gefitinib and erlotinib by human cytochrome P450 enzymes. Clin Cancer Res. 2007 Jun 15;13(12):3731-7.
105. Corrêa LH, R; Rodrigues, L; Nata, K; de C. Luz, J. Histopathology of hematopoietic bone marrow in the temporomandibular joint of rats subjected to undernutrition and to mandibular condyle fracture. Scand J Lab Anim. 2010;37(3).
106. Rautou PE, Cazals-Hatem D, Moreau R, Francoz C, Feldmann G, Lebrec D, et al. Acute liver cell damage in patients with anorexia nervosa: a possible role of starvation-induced hepatocyte autophagy. Gastroenterology. 2008 Sep;135(3):840-8, 8 e1-3.
107. Oshikoya KA, Senbanjo IO. Pathophysiological changes that affect drug disposition in protein-energy malnourished children. Nutr Metab (Lond). 2009 Dec 01;6:50.
108. Oshikoya KA, Sammons HM, Choonara I. A systematic review of pharmacokinetics studies in children with protein-energy malnutrition. Eur J Clin Pharmacol. 2010 Oct;66(10):1025-35.
109. Chiou WL, Barve A. Linear correlation of the fraction of oral dose absorbed of 64 drugs between humans and rats. Pharm Res. 1998 Nov;15(11):1792-5.
110. Amidon GL, Lennernas H, Shah VP, Crison JR. A theoretical basis for a biopharmaceutic drug classification: the correlation of in vitro drug product dissolution and in vivo bioavailability. Pharm Res. 1995 Mar;12(3):413-20.
111. Cappuzzo F, Ciuleanu T, Stelmakh L, Cicenas S, Szczesna A, Juhasz E, et al. Erlotinib as maintenance treatment in advanced non-small-cell lung cancer: a multicentre, randomised, placebo-controlled phase 3 study. Lancet Oncol. 2010 Jun;11(6):521-9.
112. Zhou C, Wu YL, Chen G, Feng J, Liu XQ, Wang C, et al. Erlotinib versus chemotherapy as first-line treatment for patients with advanced EGFR mutation-positive non-small-cell lung cancer (OPTIMAL, CTONG-0802): a

multicentre, open-label, randomised, phase 3 study. Lancet Oncol. 2011 Aug;12(8):735-42.

113. Haouala A, Widmer N, Duchosal MA, Montemurro M, Buclin T, Decosterd LA. Drug interactions with the tyrosine kinase inhibitors imatinib, dasatinib, and nilotinib. Blood. 2011 Feb 24;117(8):e75-87.
114. Szalek E, Karbownik A, Grabowski T, Sobanska K, Wolc A, Grzeskowiak E. Pharmacokinetics of sunitinib in combination with fluoroquinolones in rabbit model. Pharmacol Rep. 2013;65(5):1383-90.
115. Yamaguchi H, Yano I, Hashimoto Y, Inui KI. Secretory mechanisms of grepafloxacin and levofloxacin in the human intestinal cell line caco-2. J Pharmacol Exp Ther. 2000 Oct;295(1):360-6.
116. Marchetti S, de Vries NA, Buckle T, Bolijn MJ, van Eijndhoven MA, Beijnen JH, et al. Effect of the ATP-binding cassette drug transporters ABCB1, ABCG2, and ABCC2 on erlotinib hydrochloride (Tarceva) disposition in in vitro and in vivo pharmacokinetic studies employing Bcrp1-/-/Mdr1a/1b-/- (triple-knockout) and wild-type mice. Mol Cancer Ther. 2008 Aug;7(8):2280-7.
117. Fernandez-Teruel C, Gonzalez-Alvarez I, Casabo VG, Ruiz-Garcia A, Bermejo M. Kinetic modelling of the intestinal transport of sarafloxacin. Studies in situ in rat and in vitro in Caco-2 cells. J Drug Target. 2005 Apr;13(3):199-212.
118. Leal N, Calvo R, Agrad FZ, Lukas JC, de la Fuente L, Suarez E. Altered dose-to-effect of propofol due to pharmacokinetics in rats with experimental diabetes mellitus. J Pharm Pharmacol. 2005 Mar;57(3):317-25.
119. Makhey VD, Guo A, Norris DA, Hu P, Yan J, Sinko PJ. Characterization of the regional intestinal kinetics of drug efflux in rat and human intestine and in Caco-2 cells. Pharm Res. 1998 Aug;15(8):1160-7.
120. Valenzuela B, Nacher A, Ruiz-Carretero P, Martin-Villodre A, Lopez-Carballo G, Barettino D. Profile of P-glycoprotein distribution in the rat and its possible influence on the salbutamol intestinal absorption process. J Pharm Sci. 2004 Jun;93(6):1641-8.
121. Harwood MD, Neuhoff S, Carlson GL, Warhurst G, Rostami-Hodjegan A. Absolute abundance and function of intestinal drug transporters: a prerequisite for fully mechanistic in vitro-in vivo extrapolation of oral drug absorption. Biopharm Drug Dispos. 2013 Jan;34(1):2-28.
122. Wu Q, Li MY, Li HQ, Deng CH, Li L, Zhou TY, et al. Pharmacokinetic-pharmacodynamic modeling of the anticancer effect of erlotinib in a human

non-small cell lung cancer xenograft mouse model. Acta Pharmacol Sin. 2013 Nov;34(11):1427-36.

123. Gilman RH, Partanen R, Brown KH, Spira WM, Khanam S, Greenberg B, et al. Decreased gastric acid secretion and bacterial colonization of the stomach in severely malnourished Bangladeshi children. Gastroenterology. 1988 Jun;94(6):1308-14.
124. Gracey M, Cullity GJ, Suharjono, Sunoto. The stomach in malnutrition. Arch Dis Child. 1977 Apr;52(4):325-7.
125. EMA. Tarceva: EPAR -Scientific discussion. Available from: http://www.ema.europa.eu/docs/en_GB/document_library/EPAR_-_Scientific_Discussion/human/000618/WC500033991.pdf.
126. Duong S LM. Should the concomitant use of erlotinib and acid-reducing agents be avoided? The drug interaction between erlotinib and acid-reducing agents. J Oncol Pharm Pract. 2011;17(4):448-52.
127. Carlert S, Palsson A, Hanisch G, von Corswant C, Nilsson C, Lindfors L, et al. Predicting intestinal precipitation--a case example for a basic BCS class II drug. Pharm Res. 2010 Oct;27(10):2119-30.
128. Miller WK MM, inventor Bend Research, Inc., assignee. SOLID DISPERSIONS OF LOW-WATER SOLUBILITY ACTIVES. US patent 20150374827. 2015.
129. Perez-Pitarch A, Nacher A, Merino V, Catalan-Latorre A, Jimenez-Torres NV, Merino-Sanjuan M. Impact of nutritional status on the pharmacokinetics of erlotinib in rats. Biopharm Drug Dispos. 2015 Mar 12. Vol. 36, Issue 6, pages 373–384.
130. Walker AD, C; Watkins, JB. Nutrition in Pediatrics: Basic Science and Clinical Application2016.
131. Wang S, Guo P, Wang X, Zhou Q, Gallo JM. Preclinical pharmacokinetic/pharmacodynamic models of gefitinib and the design of equivalent dosing regimens in EGFR wild-type and mutant tumor models. Mol Cancer Ther. 2008 Feb;7(2):407-17.
132. Savic RM, Jonker DM, Kerbusch T, Karlsson MO. Implementation of a transit compartment model for describing drug absorption in pharmacokinetic studies. J Pharmacokinet Pharmacodyn. 2007 Oct;34(5):711-26.
133. Jawhari DA, M; Ghannam, M; Al Halman, J. Bioequivalence of a New Generic Formulation of Erlotinib Hydrochloride 150 mg Tablets versus

Tarceva in Healthy Volunteers under Fasting Conditions. Journal of Bioequivalence & Bioavailability. 2014;6(4):119-23.

134. Hidalgo M, Bloedow D. Pharmacokinetics and pharmacodynamics: maximizing the clinical potential of Erlotinib (Tarceva). Semin Oncol. 2003 Jun;30(3 Suppl 7):25-33.
135. Swaisland HC, Smith RP, Laight A, Kerr DJ, Ranson M, Wilder-Smith CH, et al. Single-dose clinical pharmacokinetic studies of gefitinib. Clin Pharmacokinet. 2005;44(11):1165-77.
136. FDA. FDA Advisory Committee Meeting Briefing Document NDA 21-399 for the use of IRESSA for the treatment of patients with locally advanced or metastatic non-small cell lung cancer (NSCLC) who have previously received platinum-based chemotherapy. 2002.
137. Roy V, Gupta D, Gupta P, Sethi GR, Mishra TK. Pharmacokinetics of isoniazid in moderately malnourished children with tuberculosis. Int J Tuberc Lung Dis. 2010 Mar;14(3):374-6.

# 7 Appendices

## 7.1 Authorizations for animal studies

VNIVERSITAT
DE VALÈNCIA
Vicerectorat d'Investigació i Política Científica

**D. Enrique Font Bisier**, Profesor Titular de Zoología y Secretario del Comité Ético de Experimentación y Bienestar Animal de la Comisión de Ética en Investigación Experimental de la Universitat de València,

CERTIFICA:

Que, reunido el Comité Ético de Experimentación y Bienestar Animal de la Comisión de Ética de la Universitat de València el día 13 de febrero de 2012, acordó informar FAVORABLEMENTE la realización en sus instalaciones del protocolo de experimentación animal A1326906234491 titulado "Impacto del estado nutricional sobre los parámetros farmacocinéticos de fármacos antineoplásicos orales", cuya investigadora principal es Dña. Matilde Merino Sanjuan.

En Valencia, a 24 de mayo de 2013.

Correr. Blasco Ibáñez, 13
VALENCIA 46071
Teléfono (96) 386 41 09
Fax (96) 369 32 21
e-mail: vicerect.investigacion@uv.es

GENERALITAT VALENCIANA
CONSELLERIA DE AGRICULTURA, MEDIO AMBIENTE, CAMBIO CLIMATICO Y DESARROLLO RURAL
DIRECCIÓN GENERAL DE AGRICULTURA, GANADERÍA Y PESCA

Unión Europea

**AUTORIZACION PROCEDIMIENTO 2016/VSC/PEA/00101**

Vista la solicitud realizada en fecha **01/06/16** con nº reg. entrada **21695** por D/Dª. **Pilar Campins Falcó**, Vicerrectora de Investigación y Política Científica, centro usuario **ES460780001001**, para realizar el procedimiento:

***"Evaluación del impacto de la desnutrición sobre los parámetros farmacocinéticos de gefitinib y sunitinib en rata"***

Teniendo en cuenta la documentación aportada, según se indica en el artículo 33, punto 5 y 6, y puesto que dicho procedimiento se halla sujeto a autorización en virtud de lo dispuesto en el artículo 31 del Real Decreto 53/2013, de 1 de febrero,

Vista la propuesta del jefe del servicio de Ganadería y Sanidad y Bienestar Animal.

**AUTORIZO:**

la realización de dicho procedimiento al que se le asigna el código: **2016/VSC/PEA/00101** tipo **2,** de acuerdo con las características descritas en la propia documentación para el número de animales, especie y periodo de tiempo solicitado. Todo ello sin menoscabo de las autorizaciones pertinentes, por otras Administraciones y entidades, y llevándose a cabo en las siguientes condiciones:

Usuario: **Universitat de Valencia**

Responsable del proyecto: **Matilde Merino Sanjuan**

Establecimiento: **Sección de Producción Animal SCIE-Campus Burjassot**

Necesidad de evaluación restrospectiva:

Condiciones específicas:

Observaciones:

Valencia a, 27 de junio de 2016

El director general de Agricultura, Ganadería y Pesca

Rogelio Llanes Ribas

## 7.2 NONMEM control stream for erlotinib absorption model in proximal intestine (model 9013)

```
$PROBLEM PK model
$INPUT ID TIME AMT DV NUT EVID MDV LEVO WGT TRAM VIN VFI C
$DATA DATOS280815.csv IGNORE(C.EQ.C) IGNORE(TRAM.EQ.2)
$SUBROUTINES ADVAN6 TOL=3

$MODEL
COMP=(LUM, DEFDOSE,DEFOBS)

$PK
TVKA = THETA(1)
KA   = TVKA * EXP(ETA(1))
TVKM = THETA(2)+LEVO*THETA(6)
KM   = TVKM
TVVMAX = THETA(3)*(1+NUT*THETA(5))
VMAX   = TVVMAX * EXP(ETA(2))
F1=THETA(4)
S1 = F1

$DES
VT = VIN-(((VIN-VFI)/30)*T)
DADT(1) = - KA*(A(1))  +  ((VMAX*(A(1)/VT)) / (KM+(A(1)/VT)))

$THETA
(0, 0.159)          ; KA         1
(0) FIX             ; KM         2
(0, 0.209)          ; VMAX       3
(0, 0.861,1)        ; fr         4
(-0.634)            ; NUT-VMAX   5
(6.49)              ; LEVO-KM    6

$OMEGA
0.256               ; KA         1
0.213               ; VMAX       2

$SIGMA
0.0242
```

```
$ERROR
VTt=VIN-(((VIN-VFI)/30)*TIME)

IPRED = A(1)/VTt ;F
IRES = DV-IPRED
W = IPRED
IF (W.EQ.0) W = 1
IWRES = IRES/W
Y = (IPRED)*EXP(ERR(1))

$EST METHOD=1 MAXEVAL=9999 SIG=3 PRINT=5 NOABORT
$COV PRINT=E
```

## 7.3 NONMEM control stream for erlotinib absorption model in distal intestine (model 9913)

```
$PROBLEM PK model
$INPUT ID TIME AMT DV NUT EVID MDV LEVO WGT TRAM VIN VFI C
$DATA DATOS280815.csv IGNORE(C.EQ.C) IGNORE(TRAM.EQ.1)
$SUBROUTINES ADVAN6 TOL=3

$MODEL
COMP=(LUM, DEFDOSE,DEFOBS)

$PK
TVKA = THETA(1)
KA   = TVKA * EXP(ETA(1))
TVKM = THETA(2)+LEVO*THETA(6)
KM   = TVKM
TVVMAX = THETA(3)*(1+NUT*THETA(5))
VMAX   = TVVMAX * EXP(ETA(2))
F1=THETA(4)
S1 = F1

$DES
VT = VIN-(((VIN-VFI)/30)*T)
DADT(1) = - KA*(A(1))  +  ((VMAX*(A(1)/VT)) / (KM+(A(1)/VT)))

$THETA
(0, 0.138)          ; KA         1
(0) FIX             ; KM         2
(0, 0.423)          ; VMAX       3
(0, 0.978,1)        ; fr         4
(-0.715)            ; NUT-VMAX   5
(4.70)              ; LEVO-KM    6

$OMEGA
0.284               ; KA         1
0.116               ; VMAX       2

$SIGMA
0.0146
```

```
$ERROR
VTt=VIN-(((VIN-VFI)/30)*TIME)

IPRED = A(1)/VTt ;F
IRES = DV-IPRED
W = IPRED
IF (W.EQ.0) W = 1
IWRES = IRES/W
Y = (IPRED)*EXP(ERR(1))

$EST METHOD=1 MAXEVAL=9999 SIG=3 PRINT=5 NOABORT
$COV PRINT=E
```

## 7.4 NONMEM control stream for gefitinib absorption model in proximal and distal intestine (model 905)

```
$PROBLEM PK model

$INPUT ID TIME DV EVID MDV AMT TRAM NUT INH CIN VIN VFI CMT C

$DATA../Datasets/datosDolusNMsimult.csv IGNORE(C.EQ.C)

$SUBROUTINES ADVAN6 TOL=3

$MODEL
COMP=(PRO)   ; PROXIMAL INTESTINE
COMP=(DIS)   ; DISTAL INTESTINE

$PK
TVBETA1 = THETA(1)
BETA1   = TVBETA1 * EXP(ETA(1))
TVBETA2 = TVBETA1 * EXP(ETA(2))
BETA2   = TVBETA2
F1   = THETA(2)
IF(CIN.EQ.40) F1 = THETA(3)
F2   = THETA(4)
IF(CIN.EQ.40) F2 = THETA(5)
ALPHA  = THETA(6)

$DES
IF(CMT.EQ.1) VT=VIN-(((VIN-VFI)/0.5)*T)
IF(CMT.EQ.2) VT=VIN-(((VIN-VFI)/0.5)*T)

DADT(1) = - (ALPHA/BETA1)*VT*(A(1)/VT)
*((T+0.001)/ALPHA)**(BETA1-1)
DADT(2) = - (ALPHA/BETA2)*VT*(A(2)/VT)
*((T+0.001)/ALPHA)**(BETA2-1)

$THETA
(0, 0.78)           ; BETA1      1
(1)          FIX    ; F1 8       2
(0, 0.61,1)         ; F1 40      3
```

```
(1) FIX             ; F2 8       4
(0, 0.51,1)         ; F2 40      5
(0, 2.40)           ; ALPHA      6

$OMEGA
0.0069 ; KA1 1
0.0049 ; KA2 2

$SIGMA
0.051

$ERROR
VTO=VIN-(((VIN-VFI)/0.5)*TIME)
IPRED = F/VTO    ;
IRES = DV-IPRED
W = IPRED
IWRES = IRES/W
Y = (IPRED)*EXP(ERR(1))

$EST METHOD=1 MAXEVAL=9999 SIG=3 PRINT=5 NOABORT POSTHOC
$COV PRINT=E UNCONDITIONAL
```

## 7.5 NONMEM control stream for erlotinib pharmacokinetic model (model 054)

```
$PROB ERLOTINIB PK MODEL
$INPUT ID TIME AMT MDV DV CMT GRUP NUT WGT ALB MEDI VIA C
$DATA Erlotinib_IV_oral.csv
IGNORE(C.EQ.C)

$SUBROUTINES  ADVAN6 TOL=5

$MODEL
COMP=(CP, DEFOBS)
COMP=(PERI)
COMP=(OR)

$PK

TVCL = THETA(1) * (1+NUT*THETA(5)) * ((PESF/1000)/70) ** 0.75
CL   = TVCL *EXP(ETA(1))
TVV  = THETA(2)*((PESF/1000)/70)**1
VC   = TVV
TVVP = THETA(3)*((PESF/1000)/70)**1
VP   = TVVP*EXP(ETA(2))
TVQ  = THETA(4)*((PESF/1000)/70)**0.75
Q    = TVQ
TVKA = THETA(6)
IF(GRUP.EQ.3) TVKA = THETA(7)
IF(GRUP.GE.4) TVKA = THETA(8)

KA   = TVKA*EXP(ETA(3))

K12 = Q/VC
K21 = Q/VP
KE=CL/VC

S1=VC*1000
F3 = THETA(9)
IF(GRUP.EQ.5) F3 = THETA(10)
```

```
$DES
DADT(1) = - KE*A(1) - K12*A(1) + K21*A(2) + KA*A(3)
DADT(2) =             K12*A(1) - K21*A(2)
DADT(3) =                                - KA*A(3)

$THETA
(0.1, 9.9)          ;      CL
(0.001, 21.6)       ;      VC
(0.1, 108.0)        ;      VP
(0.001, 36.4)       ;      Q
(-0.0511)           ;      FCL
(0.001, 0.147)      ;      KA
(0.001, 0.417)      ;      KA
(0.001, 0.200)      ;      KA
(0,1) FIX           ;      F
(0, 0.872,1)        ;      F

$OMEGA
0.0.148      ;      CL
1.21         ;      VP
0.254        ;      CVKA

$ERROR
DEL=0
IF (F.LE.0.00001) DEL=1
W=F+DEL
IPRE=F
IRES=DV-F
WIRE=IRES/W
Y=F*EXP(EPS(1))

$SIGMA 0.145

$EST METHOD=1 MAXEVAL=20000 NOABORT SIG=3 PRINT=1
$COV
```

## 7.6 NONMEM control stream for gefitinib pharmacokinetic model (model 513)

```
$PROBLEM GEFITINIB PK MODEL

$INPUT ID TIME EVID AMT DV VIA CMT NUT WGT DOSE ALB C

$DATA ../Datasets/FinalDS.csv
IGNORE=(C.EQ.C)

$SUBROUTINES ADVAN6 TOL=5

$MODEL
COMP=(ABS)
COMP=(CENTRAL,DEFOBS)
COMP=(PERIF)
COMP=(TRANSI)

$PK
TVCL = THETA(1) * ((WGT/1000)/70)**0.75
CL   = TVCL * EXP(ETA(1))
TVV  = THETA(2) * (1+NUT*THETA(6)) *((WGT/1000)/70)**1
V    = TVV
KEL  = CL/V
TVVP = THETA(4) *((WGT/1000)/70)**1
VP     = TVVP
Q    = THETA(5) * ((WGT/1000)/70)**0.75
K12  = Q/V
K21  = Q/VP
KA   = THETA(3) * EXP(ETA(2))
S2   = V/1000
F1   = THETA(7)
IF(NUT.EQ.1) F1= THETA(8)

$DES
DADT(1) = -KA*A(1)
DADT(2) =  KA*A(4) - KEL*A(2) - K12*A(2) + K21*A(3)
DADT(3) =  K12*A(2) - K21*A(3)
DADT(4) =  KA*A(1) - KA*A(4)
```

```
$ERROR
IPRED = F
W = IPRED
Y = IPRED *EXP(EPS(1))
IRES = DV-IPRED
IWRES = IRES/W

$THETA
(0, 14.1)           ; CL               1
(0, 22.8)           ; V                2
(0, 0.198)          ; KA               3
(0, 366)            ; VP               4
(0, 19.5)           ; Q                5
(0.321)             ; NUT on V2        6
(0,0.446,1)         ; F1 NN            7
(0,0.681,1)         ; F1 UN            8

$OMEGA
(0.168)             ; IIV CL           1
(0.442)             ; IIV KA           3

$SIGMA
0.163               ; Residual error   1

$EST METHOD=1 MAXEVAL=20000 NOABORT SIG=3 PRINT=1
$COV PRINT=E
```